

NASA Technical Paper 1498

Low-Speed Aerodynamic Characteristics
of a 13-Percent-Thick Medium-Speed
Airfoil Designed for General
Aviation Applications

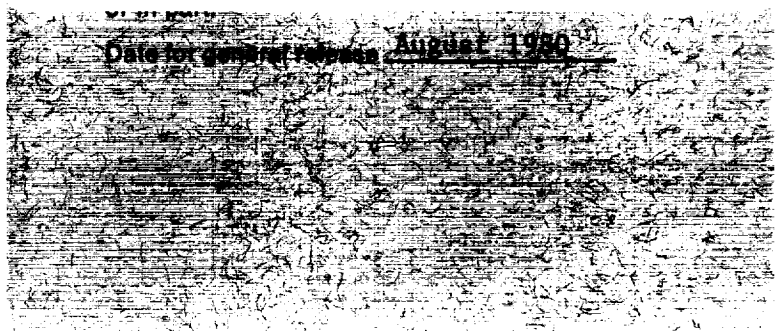
Robert J. McGhee and William D. Beasley

**CASE FILE
COPY**

FOR EARLY DOMESTIC DISSEMINATION

AUGUST 1979

NASA



100

100

100

100

100

100

100

100

100

100

100

100

100

100

100

100

100

100

100

NASA Technical Paper 1498

Low-Speed Aerodynamic Characteristics
of a 13-Percent-Thick Medium-Speed
Airfoil Designed for General
Aviation Applications

Robert J. McGhee and William D. Beasley
Langley Research Center
Hampton, Virginia

NASA

National Aeronautics
and Space Administration

**Scientific and Technical
Information Branch**

1979

SUMMARY

An investigation was conducted in the Langley low-turbulence pressure tunnel to determine the low-speed two-dimensional aerodynamic characteristics of a 13-percent-thick medium-speed airfoil designed for general aviation applications. The results are compared with data for the 13-percent-thick low-speed airfoil section. Also, theoretical predictions of the drag-rise characteristics of the medium-speed airfoil are provided. The tests were conducted over a Mach number range from 0.10 to 0.32, a chord Reynolds number range from 2.0×10^6 to 12.0×10^6 , and an angle-of-attack range from about -8° to 20° .

The results of the investigation indicate that the objective of retaining good high-lift low-speed characteristics for an airfoil designed to have good medium-speed cruise performance was achieved. Maximum section lift coefficients at a Mach number of 0.15 increased from about 1.70 to 2.06 as the Reynolds number increased from about 2.0×10^6 to 12.0×10^6 . Stall characteristics were of the trailing-edge type and were docile at the lower Reynolds numbers. The application of a roughness strip near the leading edge of the airfoil resulted in only small effects on maximum section lift coefficients. Increasing the Mach number from 0.10 to 0.32 at a constant Reynolds number of 6.0×10^6 decreased the maximum section lift coefficient about 0.08. The magnitude of the quarter-chord pitching-moment coefficient was decreased about 25 percent for the medium-speed airfoil compared with the low-speed airfoil.

INTRODUCTION

Research on advanced-aerodynamic-technology airfoils for general aviation applications has been conducted over the last several years at the Langley Research Center and reported in references 1 to 6. This research effort was initially generated to develop advanced airfoils for low-speed applications. Emphasis was placed on designing airfoils with largely turbulent boundary layers that had the following performance requirements: low cruise drag, high lift-drag ratios during climb, high maximum lift, and docile stall behavior. More recently the general aviation industry indicated a requirement for airfoils which provide higher cruise Mach numbers than the low-speed airfoils and which still retain good high-lift low-speed characteristics. These medium-speed airfoils have been designed to fill the gap between the low-speed airfoils and the supercritical airfoils for application on light executive-type aircraft. The status of NASA low- and medium-speed airfoil research is reported in reference 7.

The present investigation was conducted to determine the low-speed aerodynamic characteristics of a 13-percent-thick medium-speed airfoil designed for a lift coefficient of 0.30, a Reynolds number of 14.0×10^6 , and a Mach number of 0.72. This new airfoil is designated as MS(1)-0313. In addition, the results are compared with the 13-percent-thick low-speed airfoil, LS(1)-0413.

Theoretical predictions of the drag-rise characteristics of this medium-speed airfoil are also provided.

The investigation was performed in the Langley low-turbulence pressure tunnel over a Mach number range from 0.10 to 0.32. The Reynolds number, based on the airfoil chord, varied from about 2.0×10^6 to 12.0×10^6 , and the geometric angle of attack varied from about -8° to 20° .

SYMBOLS

Values are given in both SI and U.S. Customary Units. The measurements and calculations were made in U.S. Customary Units.

C_p	pressure coefficient, $\frac{p_\ell - p_\infty}{q_\infty}$
c	airfoil chord, cm (in.)
C_C	section chord-force coefficient, $\oint C_p d\left(\frac{z}{c}\right)$
C_d	section profile-drag coefficient, $\int_{\text{wake}} C_d' d\left(\frac{h}{c}\right)$
C_d'	point drag coefficient
C_l	section lift coefficient, $C_n \cos \alpha - C_c \sin \alpha$
C_m	section pitching-moment coefficient about quarter-chord point, $-\oint C_p \left(\frac{x}{c} - 0.25\right) d\left(\frac{x}{c}\right) + \oint C_p \frac{z}{c} d\left(\frac{z}{c}\right)$
C_n	section normal-force coefficient, $-\oint C_p d\left(\frac{x}{c}\right)$
h	vertical distance in wake profile, cm (in.)
M	free-stream Mach number
p	static pressure, Pa (lb/ft ²)
q	dynamic pressure, Pa (lb/ft ²)
R	Reynolds number based on free-stream conditions and airfoil chord
x	airfoil abscissa, cm (in.)
z	airfoil ordinate, cm (in.)

z_c mean line ordinate, cm (in.)
 z_t mean thickness, cm (in.)
 α geometric angle of attack, deg

Subscripts:

l local point on airfoil
max maximum
 ∞ free-stream conditions

AIRFOIL DESIGNATION

Sketches of the low- and medium-speed airfoils are shown in figure 1. The airfoils are designated in the form LS(1)-xxxx or MS(1)-xxxx. LS(1) indicates low speed (first series) and MS(1) indicates medium speed (first series). The next two digits designate the airfoil-design lift coefficient in tenths, and the last two digits designate the airfoil thickness in percent chord.

AIRFOIL DEVELOPMENT

The intention of the medium-speed airfoil development was to combine the best features of low-speed and supercritical airfoil technology. In order to expedite the airfoil development, the computer program of reference 8 was used to predict the results of various design modifications. The medium-speed airfoil is 13 percent thick with a blunt nose and a cusped lower surface near the trailing edge. The design objective of the airfoil was to increase the cruise Mach number of the 13-percent-thick low-speed airfoil but retain good high-lift low-speed characteristics. This type of airfoil is intended to fill the gap between the low-speed airfoils and the supercritical airfoils for application on light executive-type aircraft. The airfoil was designed for a lift coefficient of 0.30, a Reynolds number of 14.0×10^6 , and a Mach number of 0.72.

The medium-speed airfoil was obtained by reshaping the 13-percent-thick low-speed airfoil as indicated by figure 1. The calculated pressure distributions (fig. 2(a)) indicate that increasing the Mach number to 0.72 for the low-speed airfoil at a lift coefficient of 0.30 results in a region of high induced velocities near the midchord on the upper surface of the airfoil. Note also that the low-speed airfoil is highly aft loaded and actually carries a small negative load in the forward region. Further increases in Mach number or lift coefficient would result in a shock wave developing on the airfoil upper surface near the midchord. This airfoil has been reshaped to decrease the velocities near the midchord and increase the velocities in the forward region on the airfoil upper surface. In addition, the camber of the medium-speed airfoil was decreased about 25 percent compared with the low-speed airfoil. Comparison of the experimental low-speed ($M = 0.15$) pressure data for both airfoils at $\alpha = 0^\circ$ is shown in figure 2(b). The thickness distributions and camber lines

for both airfoils are compared in figure 3. Table I presents the design coordinates for the medium-speed airfoil.

MODEL, APPARATUS, AND PROCEDURE

Model

The airfoil model was constructed with a metal core around which plastic fill and two thin layers of fiberglass were used to form the contour of the airfoil. The model had a chord of 61 cm (24 in.) and a span of 91 cm (36 in.). The model was equipped with both upper- and lower-surface orifices located 5 cm (2 in.) off the midspan. The airfoil surface was sanded in the chordwise direction with No. 400 dry silicon carbide paper to provide a smooth aerodynamic finish. The model contour accuracy was generally within ± 0.100 mm (0.004 in.).

Wind Tunnel

The Langley low-turbulence pressure tunnel (ref. 9) is a closed-throat, single-return tunnel which can be operated at stagnation pressures from 1.0 to 10.0 atm (1 atm = 101.3 kPa) with tunnel-empty test-section Mach numbers up to 0.42 and 0.22, respectively. The maximum Reynolds number is about 49×10^6 per meter (15×10^6 per foot) at a Mach number of about 0.22. The tunnel test section is 91 cm (3 ft) wide and 229 cm (7.5 ft) high.

Hydraulically actuated circular plates provided positioning and attachment for the two-dimensional model. The plates are 102 cm (40 in.) in diameter, rotate with the airfoil, and are flush with the tunnel wall. The airfoil ends were attached to rectangular model-attachment plates (fig. 4) and the airfoil was mounted so that the center of rotation of the circular plates was at 0.25c on the model reference line. The air gaps in the tunnel walls between the rectangular plates and the circular plates were sealed with metal seals.

Wake Survey Rake

A fixed wake survey rake (fig. 5) at the model midspan was mounted from the tunnel sidewall and located 1 chord length behind the trailing edge of the airfoil. The wake rake utilized 0.15-cm (0.06-in.) diameter total-pressure tubes and 0.32-cm (0.125-in.) diameter static-pressure tubes. The total-pressure tubes were flattened to 0.10 cm (0.04 in.) for 0.61 cm (0.24 in.) from the tip of the tube. The static-pressure tubes each had four flush orifices drilled 90° apart and located 8 tube diameters from the tip of the tube and in the plane of measurement of the total-pressure tubes.

Instrumentation

Measurements of the static pressures on the airfoil surfaces and the wake-rake pressures were made by an automatic pressure-scanning system utilizing

variable-capacitance-type precision transducers. Basic tunnel pressures were measured with precision quartz manometers. Angle of attack was measured with a calibrated digital shaft encoder operated by a pinion gear and rack attached to the circular model-attachment plates. Data were obtained by a high-speed acquisition system and recorded on magnetic tape.

TESTS AND METHODS

The airfoil was tested at Mach numbers from 0.10 to 0.32 over an angle-of-attack range from about -8° to 20° . Reynolds number based on the airfoil chord was varied from about 2.0×10^6 to 12.0×10^6 . The airfoil was tested both in the smooth condition (natural transition) and with roughness located on both upper and lower surfaces at 0.075c. The roughness was sized for each Reynolds number according to the technique in reference 10. The roughness was sparsely distributed and consisted of granular-type strips 0.13-cm (0.05-in.) wide which were attached to the surfaces with clear lacquer.

The static-pressure measurements at the airfoil surface were reduced to standard pressure coefficients and machine integrated to obtain section normal-force and section chord-force coefficients as well as section pitching-moment coefficients about the quarter chord. Section profile-drag coefficients were computed from the wake-rake total and static pressures by the method reported in reference 11.

An estimate of the standard low-speed wind-tunnel boundary corrections (ref. 12) amounted to a maximum of about 2 percent of the measured coefficients and these corrections have not been applied to the data. An estimate of the total-pressure tube displacement effects on the values of c_d showed these effects to be negligible (ref. 11).

PRESENTATION OF RESULTS

The test conditions are summarized in table II. The results of this investigation have been reduced to coefficient form and are presented in the following figures:

	Figure
Section characteristics for MS(1)-0313 airfoil	6,7
Effect of roughness on section characteristics	8
Effect of Reynolds number on section characteristics. Model smooth; M = 0.15	9
Effect of Reynolds number on section characteristics. Roughness on; M = 0.15	10
Effect of Mach number on section characteristics. Roughness on; R = 6.0×10^6	11
Comparison of section characteristics for LS(1)-0413 and MS(1)-0313 airfoils. Roughness on; M = 0.15	12
Effect of angle of attack and Reynolds number on chordwise pressure distributions for MS(1)-0313 airfoil. Roughness on; M = 0.15	13

Comparison of chordwise pressure distributions for LS(1)-0413 and MS(1)-0313 airfoils. Roughness on; $M = 0.15$	14
Variation of maximum lift coefficient with Reynolds number for LS(1)-0413 and MS(1)-0313 airfoils. $M = 0.15$	15
Variation of maximum lift coefficient with Mach number for LS(1)-0413 and MS(1)-0313 airfoils. Roughness on; $R = 6.0 \times 10^6$	16
Calculated drag-rise characteristics for LS(1)-0413 and MS(1)-0313 airfoils. $R = 14.0 \times 10^6$	17

DISCUSSION OF RESULTS

Section Characteristics

Lift.- Figure 9(a) shows that the lift-curve slope for the medium-speed airfoil in a smooth condition (natural boundary-layer transition) varied from about 0.11 to 0.12 per degree for the Reynolds numbers investigated ($M = 0.15$). The angle of attack for zero lift coefficient was about -3° . Maximum lift coefficients increased from about 1.70 to 2.06 as the Reynolds number was increased from about 2.0×10^6 to 12.0×10^6 , with the greatest increase occurring between Reynolds numbers of 2.0×10^6 and 4.0×10^6 . The stall characteristics of the airfoil are of the trailing-edge type, as shown by the lift data of figure 9(a) and the pressure data of figure 13. The nature of the stall is docile at Reynolds numbers of 2.0×10^6 and 4.0×10^6 .

The addition of a roughness strip at 0.075c (fig. 8) resulted in the expected decambering effect because of the increase in boundary-layer thickness. For example, at $R = 2.0 \times 10^6$ (fig. 8(a)) the angle of attack for zero lift coefficient changed from about -3° to -2.7° . No measurable change in lift-curve slope was indicated, and the lift coefficient at $\alpha = 0^\circ$ decreased from about 0.35 to 0.31. These effects on the lift characteristics decreased as the Reynolds number was increased and were essentially eliminated at $R = 12.0 \times 10^6$ (fig. 8(e)). The roughness strip had only minor effects on the $c_{l,max}$ performance of the airfoil for the Reynolds number range tested.

The effects of Mach number on the airfoil lift characteristics at a Reynolds number of 6.0×10^6 with a roughness strip located at 0.075c are shown in figure 11(a). The expected Prandtl-Glauert increase in lift-curve slope is indicated for increases in Mach number from 0.10 to 0.32. This same Mach number increase, however, resulted in a decrease of about 2.5° in the angle of attack for stall and a decrease in $c_{l,max}$ of about 0.08.

Comparisons of the lift data for the 13-percent-thick low- and medium-speed airfoils are shown in figure 12 for Reynolds numbers from 2.0×10^6 to 9.0×10^6 and summarized in figures 15 and 16. The design lift coefficients for the low-speed and medium-speed airfoils were 0.40 and 0.30, respectively. Figure 12(a), $R = 2.0 \times 10^6$, shows that the lift characteristics are similar for both airfoils and that the medium-speed airfoil, with a lower design lift coefficient, develops the same $c_{l,max}$ as the low-speed airfoil. This result is attributed to reduced upper-surface boundary-layer separation for the medium-

speed airfoil, as illustrated by the pressure-data comparison of figure 14(e). At the higher Reynolds numbers (fig. 15) a decrease in $c_{l,max}$ of about 0.06 is shown for the medium-speed airfoil compared with the low-speed airfoil. This decrease in $c_{l,max}$ is as expected for an airfoil with a decrease in design lift coefficient of about 0.10. The effects of Mach number on $c_{l,max}$ for both airfoils are shown in figure 16 for a Reynolds number of 6.0×10^6 . The medium-speed airfoil generally shows smaller decreases in $c_{l,max}$ above a Mach number of about 0.28 compared with the low-speed airfoil.

Pitching moment.- The pitching-moment-coefficient data of figures 8, 9, and 10 illustrate the expected positive increments in c_m due to decreasing the Reynolds number or the addition of roughness at a constant Reynolds number. This is typical of the decambering effect associated with boundary-layer thickening for aft-loaded airfoils. At a Reynolds number of 6.0×10^6 , increasing the Mach number from 0.10 to 0.32 (fig. 11(c)) showed no effects on the pitching-moment data up to about $\alpha = 8^\circ$. At the higher angles of attack a positive increment in c_m is shown.

Comparisons of the pitching-moment data for the low- and medium-speed airfoils are shown in figure 12. A reduction in the magnitude of c_m of about 25 percent throughout the c_l range is indicated for the medium-speed airfoil. This result is important because of the expected reduced trim penalties for the medium-speed airfoil at cruise conditions.

Drag.- The design pressure distribution for the medium-speed airfoil (fig. 2(a)) shows that a favorable pressure gradient exists only back to about 0.10c on the upper surface and 0.05c on the lower surface at a Mach number of 0.72. The low-speed ($M = 0.15$) pressure data (fig. 14(a)) show that a pressure peak develops at about 0.06c on the upper surface of the airfoil. Thus, the pressure distributions are not conducive to long runs of laminar flow. Therefore, the discussion of drag is limited to data obtained with fixed transition at 0.075c to ensure turbulent flow over most of the airfoil chord.

The profile-drag coefficient at design lift ($c_l = 0.30$) decreased from about 0.0102 at $R = 2.0 \times 10^6$ to about 0.0083 at $R = 12.0 \times 10^6$ (fig. 10(b)). This drag reduction is associated with the related decrease in boundary-layer thickness and accompanying reduction in skin-friction drag. There are only small effects of Mach number on c_d (fig. 11(b)) over a Mach number range from 0.10 to 0.32.

Comparisons of the drag data for the low- and medium-speed airfoils are shown in figure 12 for Reynolds numbers from 2.0×10^6 to 9.0×10^6 with fixed transition at 0.075c. At a Reynolds number of 2.0×10^6 (fig. 12(a)), a decrease in c_d for lift coefficients greater than about 1.0 is shown for the medium-speed airfoil. The drag polars are essentially the same at the higher Reynolds numbers for the two airfoils.

Drag-rise characteristics calculated by using the theory of reference 8 are shown in figure 17 for the low- and medium-speed airfoils at $R = 14.0 \times 10^6$. Boundary-layer transition was specified at $x/c = 0.04$ for the calculations to ensure a turbulent boundary-layer development on the air-

foils. At lift coefficients of 0.30 or 0.40 the theory indicates an increase in drag-rise Mach number of about 0.02 for the medium-speed airfoil.

Pressure Distributions

The chordwise pressure data of figure 13 illustrate the effects of angle of attack for several Reynolds numbers. For a Reynolds number of 2.0×10^6 (fig. 13(a)), the data at $\alpha = 0^\circ$ ($c_l = 0.31$) indicate an upper-surface pressure peak at about $x/c = 0.06$, followed by approximately constant values of C_p to about $x/c = 0.55$. On the lower surface, approximately constant values of C_p are shown from about $x/c = 0.04$ to $x/c = 0.50$. The pressure coefficient at the airfoil trailing edge is slightly positive. Upper-surface trailing-edge separation is first indicated at an angle of attack of about 8° by the constant-pressure region on the airfoil and is also indicated by the nonlinear lift curves above this angle of attack (fig. 8(a)). Increases in angle of attack above 8° resulted in this constant-pressure region moving forward along the airfoil, and at maximum lift ($\alpha = 16.2^\circ$) trailing-edge separation was present from about $x/c = 0.70$ to $x/c = 1.0$. The airfoil stall is of the trailing-edge type, as indicated by figure 13(a) ($\alpha = 17.1^\circ$). The stall characteristics are more abrupt at the higher Reynolds numbers, as illustrated by figures 8 and 13.

Comparisons of the pressure data for the low- and medium-speed airfoils at several test conditions are illustrated in figure 14. The reduction in design lift coefficient of 0.10 for the medium-speed airfoil is illustrated by the decrease in the magnitude of the pressure differences between the upper and lower surfaces compared with the low-speed airfoil (fig. 14(b)). Note also the increase in suction ($-C_p$) on the upper surface at about $x/c = 0.06$ for the medium-speed airfoil. At typical climb lift coefficients ($c_l = 1.0$), both airfoils are separation free, as illustrated by the pressure-data comparisons of figure 14(c). For a Reynolds number of 2.0×10^6 and at higher lift coefficients (figs. 14(d) and 14(e)), the medium-speed airfoil exhibits less trailing-edge separation than the low-speed airfoil. Separation is indicated by the constant-pressure region on the aft upper surface of the airfoils.

CONCLUDING REMARKS

Wind-tunnel tests have been conducted to determine the low-speed two-dimensional aerodynamic characteristics of a 13-percent-thick medium-speed airfoil designed for general aviation applications. The results were compared with the 13-percent-thick low-speed airfoil. Also, theoretical predictions of the drag-rise characteristics of this airfoil are provided. The tests were conducted over a Mach number range from 0.10 to 0.32. The chord Reynolds number was varied from about 2.0×10^6 to 12.0×10^6 . The following results were determined from this investigation:

1. The objective of retaining good high-lift low-speed characteristics for an airfoil designed to have good medium-speed cruise performance has been achieved.

2. Maximum section lift coefficients at a Mach number of 0.15 increased from about 1.70 to 2.06 as the Reynolds number was increased from about 2.0×10^6 to 12.0×10^6 .

3. Stall characteristics were of the trailing-edge type and were docile at the lower Reynolds numbers.

4. The application of a roughness strip near the leading edge of the airfoil resulted in only small effects on maximum section lift coefficients.

5. Increasing the Mach number from 0.10 to 0.32 at a constant Reynolds number of about 6.0×10^6 decreased the maximum section lift coefficient about 0.08.

6. The magnitude of the quarter-chord pitching-moment coefficient was decreased about 25 percent for the medium-speed airfoil compared with the low-speed airfoil.

Langley Research Center
National Aeronautics and Space Administration
Hampton, VA 23665
June 27, 1979

REFERENCES

1. McGhee, Robert J.; and Beasley, William D.: Low-Speed Aerodynamic Characteristics of a 17-Percent-Thick Airfoil Section Designed for General Aviation Applications. NASA TN D-7428, 1973.
2. McGhee, Robert J.; Beasley, William D.; and Somers, Dan M.: Low-Speed Aerodynamic Characteristics of a 13-Percent-Thick Airfoil Section Designed for General Aviation Applications. NASA TM X-72697, 1975.
3. McGhee, Robert J.; and Beasley, William D.: Effects of Thickness on the Aerodynamic Characteristics of an Initial Low-Speed Family of Airfoils for General Aviation Applications. NASA TM X-72843, 1976.
4. McGhee, Robert J.; and Beasley, William D.: Low-Speed Wind-Tunnel Results for a Modified 13-Percent-Thick Airfoil. NASA TM X-74018, 1977.
5. McGhee, Robert J.; and Beasley, William D.: Wind-Tunnel Results for an Improved 21-Percent-Thick Low-Speed Airfoil Section. NASA TM-78650, 1978.
6. Barnwell, Richard W.; Noonan, Kevin W.; and McGhee, Robert J.: Low-Speed Aerodynamic Characteristics of a 16-Percent-Thick Variable-Geometry Airfoil Designed for General Aviation Applications. NASA TP-1324, 1978.
7. McGhee, Robert J.; Beasley, William D.; and Whitcomb, Richard T.: NASA Low- and Medium-Speed Airfoil Development. NASA TM-78709, 1979.
8. Bauer, Frances; Garabedian, Paul; Korn, David; and Jameson, Antony: Supercritical Wing Sections II. Volume 108 of Lecture Notes in Economics and Mathematical Systems, Springer-Verlag, 1975.
9. Von Doenhoff, Albert E.; and Abbott, Frank T., Jr.: The Langley Two-Dimensional Low-Turbulence Pressure Tunnel. NACA TN 1283, 1947.
10. Braslow, Albert L.; and Knox, Eugene C.: Simplified Method for Determination of Critical Height of Distributed Roughness Particles for Boundary-Layer Transition at Mach Numbers From 0 to 5. NACA TN 4363, 1958.
11. Pankhurst, R. C.; and Holder, D. W.: Wind-Tunnel Technique. Sir Isaac Pitman & Sons, Ltd. (London), 1965.
12. Pope, Alan; and Harper, John J.: Low-Speed Wind Tunnel Testing. John Wiley & Sons, Inc., c.1966.

TABLE I.- MS(1)-0313 AIRFOIL COORDINATES

x/c	z/c, upper surface	z/c, lower surface
0.000000	0.000986	0.000986
.002000	.009475	-.006272
.005000	.015120	-.009977
.012500	.024286	-.015246
.025000	.034450	-.020594
.037500	.041872	-.024404
.050000	.047433	-.027454
.075000	.055169	-.032278
.100000	.060608	-.036076
.125000	.064805	-.039204
.150000	.068189	-.041819
.175000	.070963	-.044001
.200000	.073274	-.045806
.225000	.075199	-.047282
.250000	.076777	-.048471
.275000	.078033	-.049410
.300000	.078991	-.050129
.325000	.079678	-.050645
.350000	.080119	-.050960
.375000	.080324	-.051059
.400000	.080293	-.050919
.425000	.080026	-.050512
.450000	.079517	-.049814
.475000	.078763	-.048812
.500000	.077753	-.047511
.525000	.076464	-.045918
.550000	.074868	-.044024
.575000	.072934	-.041812
.600000	.070636	-.039274
.625000	.067958	-.036426
.650000	.064903	-.033315
.675000	.061488	-.030007
.700000	.057745	-.026571
.725000	.053710	-.023071
.750000	.049418	-.019568
.775000	.044899	-.016140
.800000	.040179	-.012881
.825000	.035288	-.009897
.850000	.030259	-.007286
.875000	.025177	-.005135
.900000	.020079	-.003535
.925000	.014950	-.002607
.950000	.009822	-.002523
.975000	.004699	-.003540
1.000000	-.000471	-.006054

TABLE II.- TEST CONDITIONS

M	R					Configuration
	2×10^6	4×10^6	6×10^6	9×10^6	12×10^6	
0.15	x	x	x	x	x	Smooth
.10			x			Roughness on
.15	x	x	x	x	x	Roughness on
.20			x			Roughness on
.28			x			Roughness on
.32			x			Roughness on

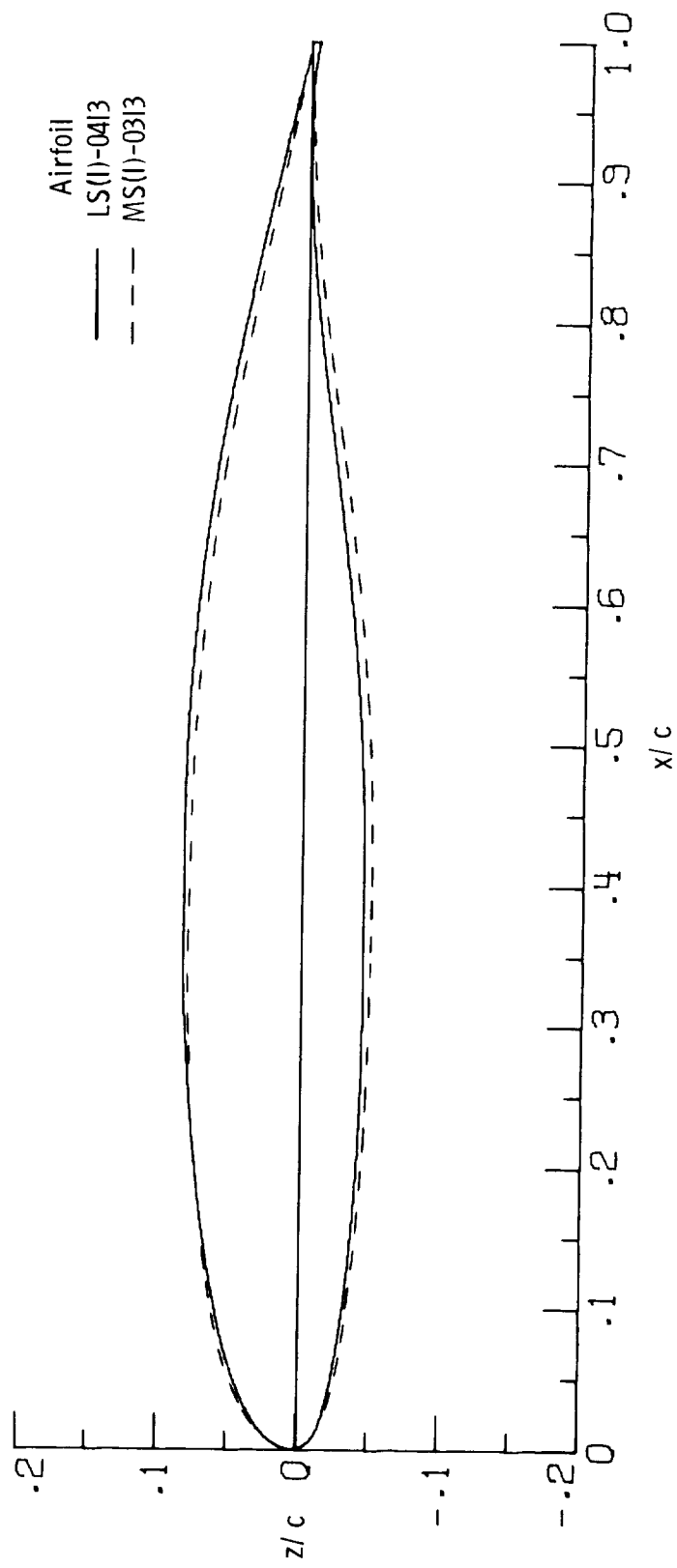
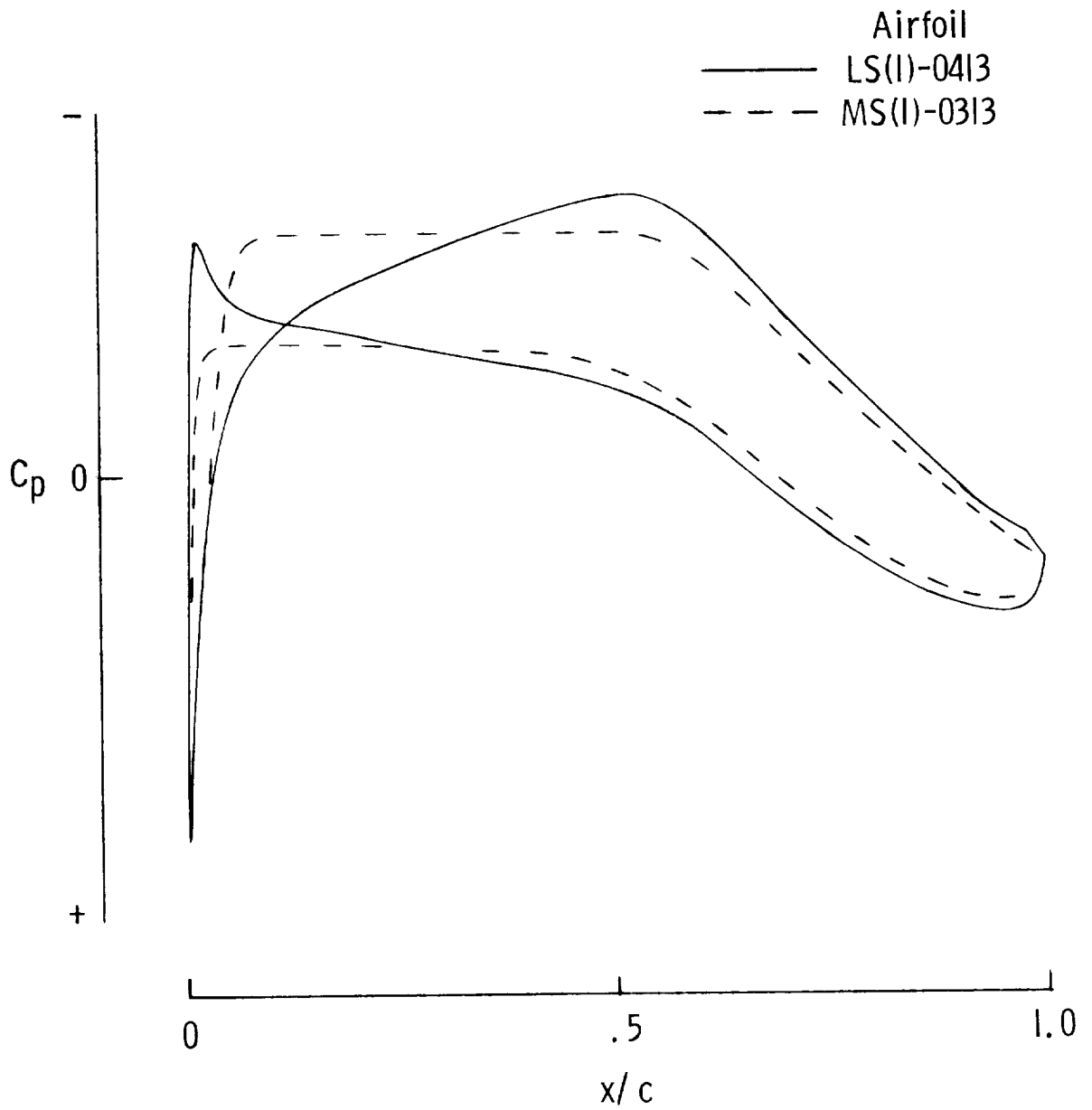


Figure 1.- Comparison of section shapes for LS(1)-0413 and MS(1)-0313 airfoils.

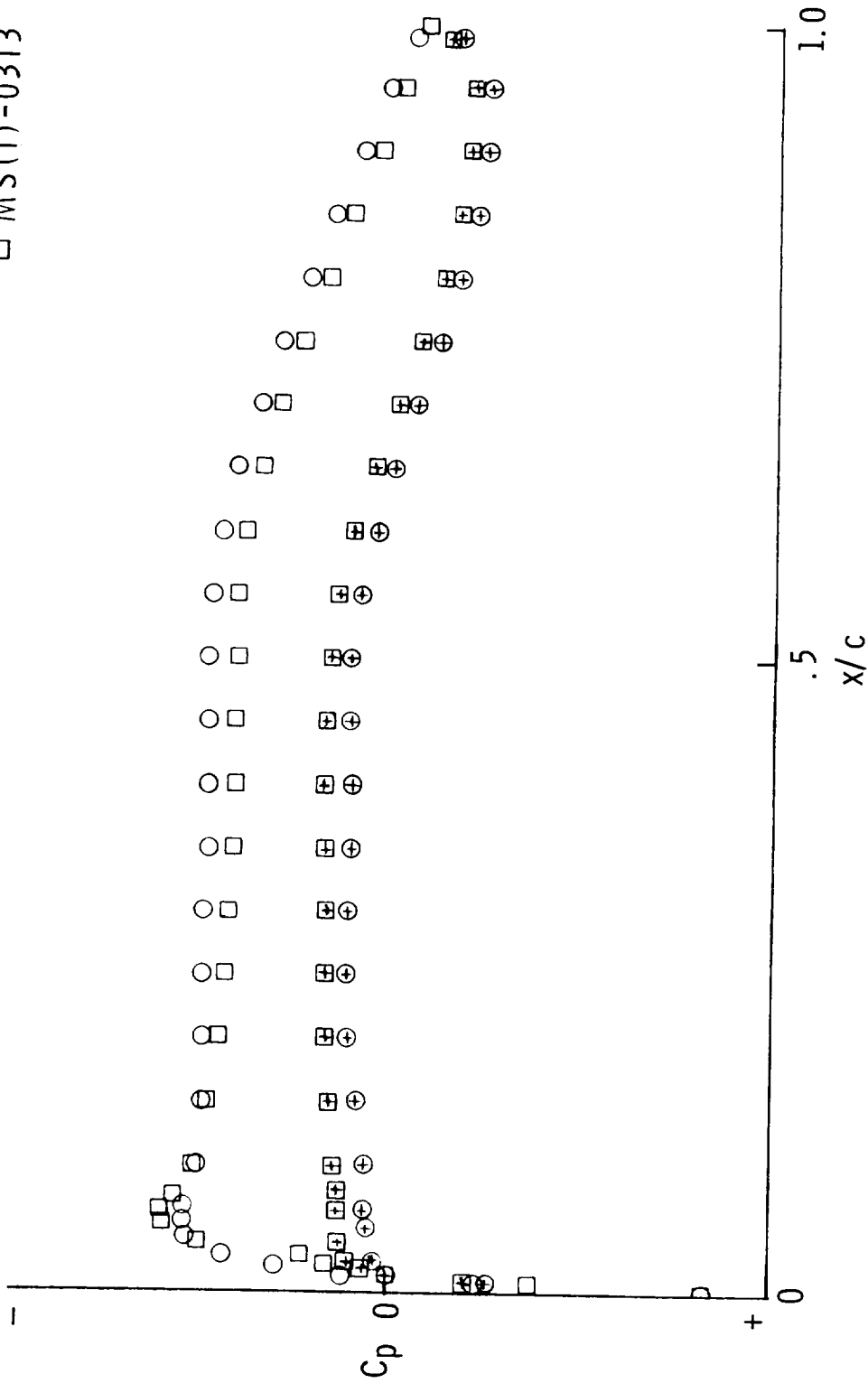


(a) Calculated. $M = 0.72$; $R = 14.0 \times 10^6$; $c_l = 0.30$.

Figure 2.- Chordwise pressure distributions for LS(1)-0413 and MS(1)-0313 airfoils.

Airfoil

- LS(1)-0413
- MS(1)-0313



(b) Experimental. $M = 0.15$; $R = 4.0 \times 10^6$; $\alpha = 0^\circ$. (Symbols with + inside designate lower surface.)

Figure 2.- Concluded.

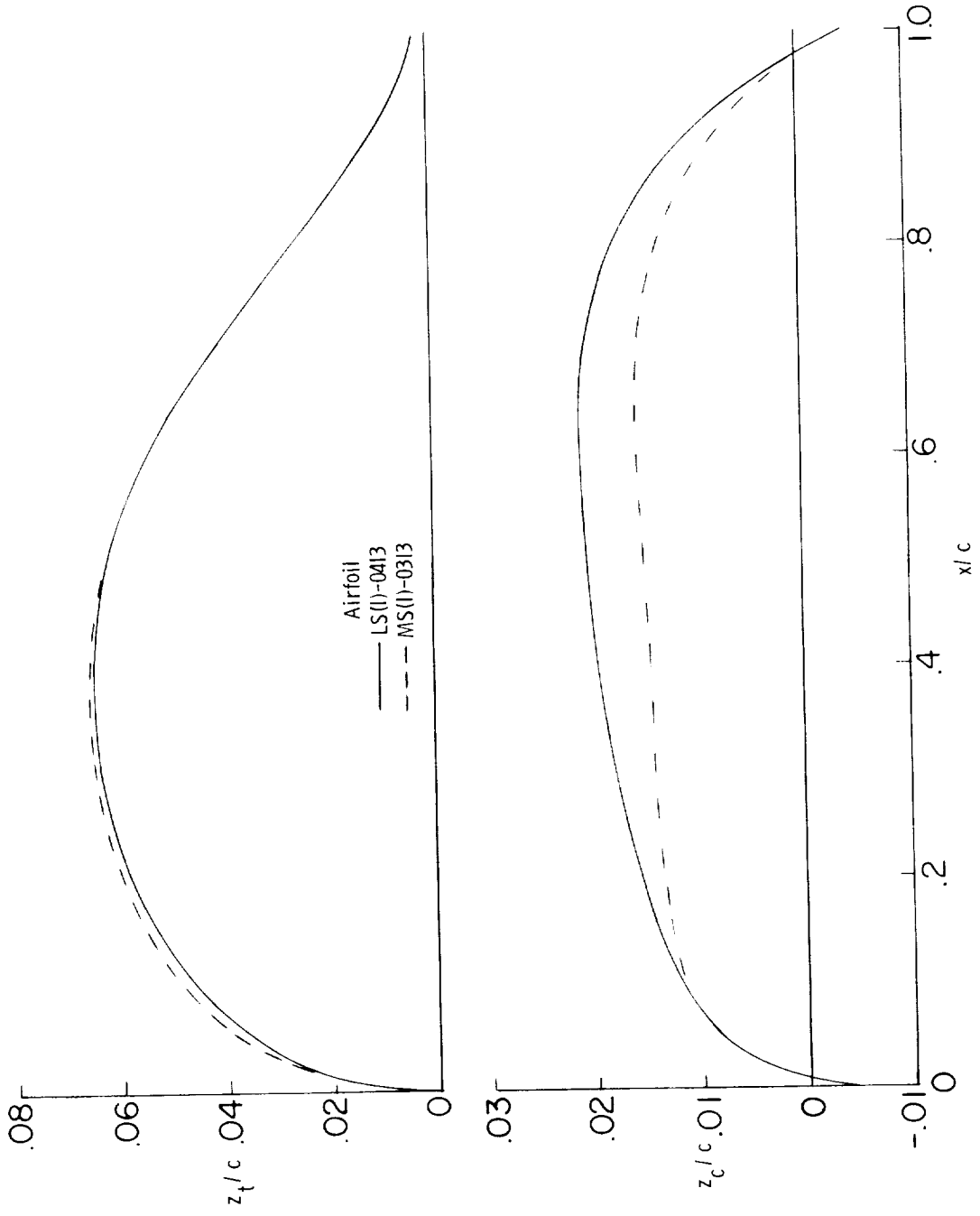


Figure 3.- Comparison of thickness distributions and camber lines for LS(1)-0413 and MS(1)-0313 airfoils.

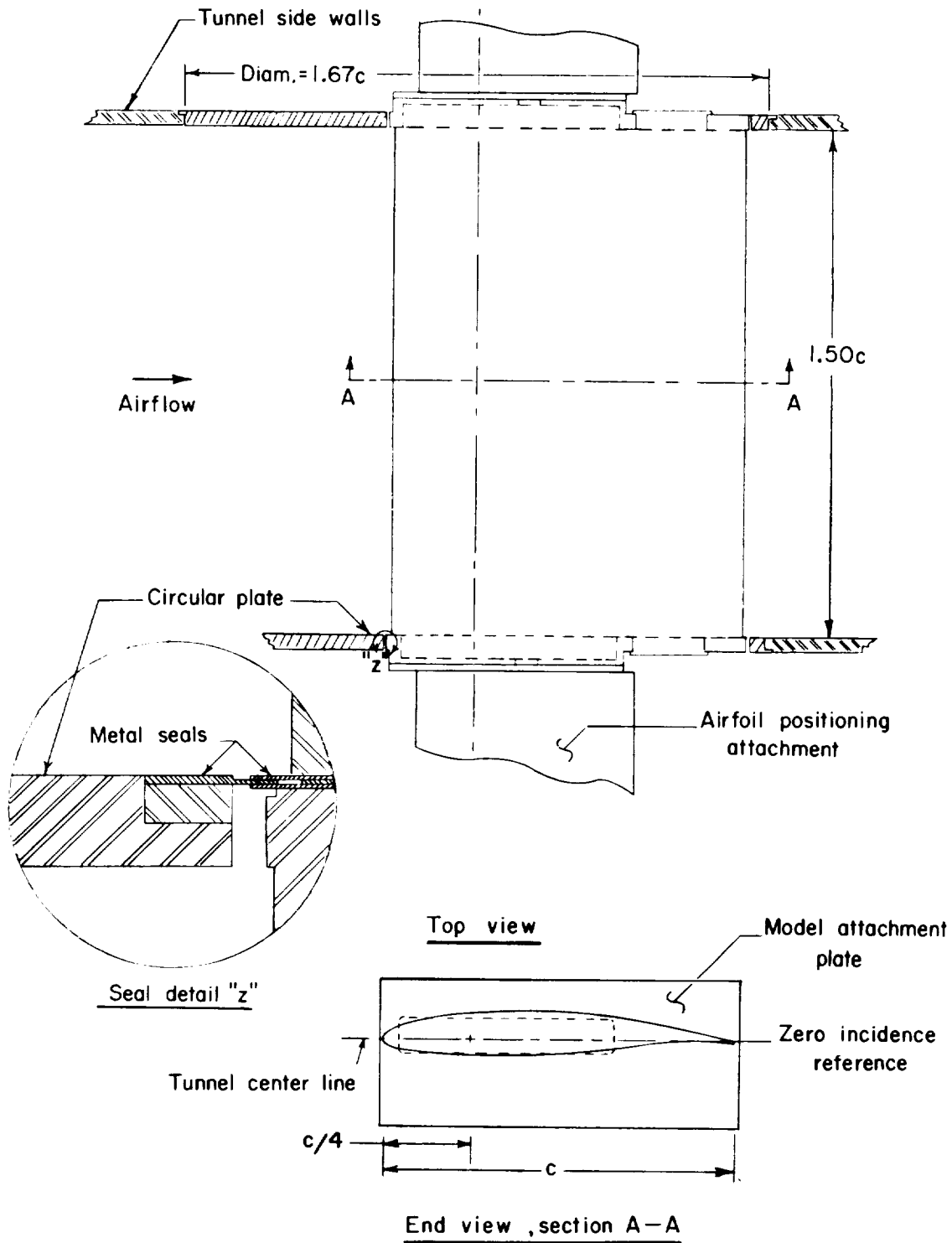


Figure 4.- Typical airfoil model mounted in wind tunnel. $c = 61 \text{ cm (24 in.)}$.

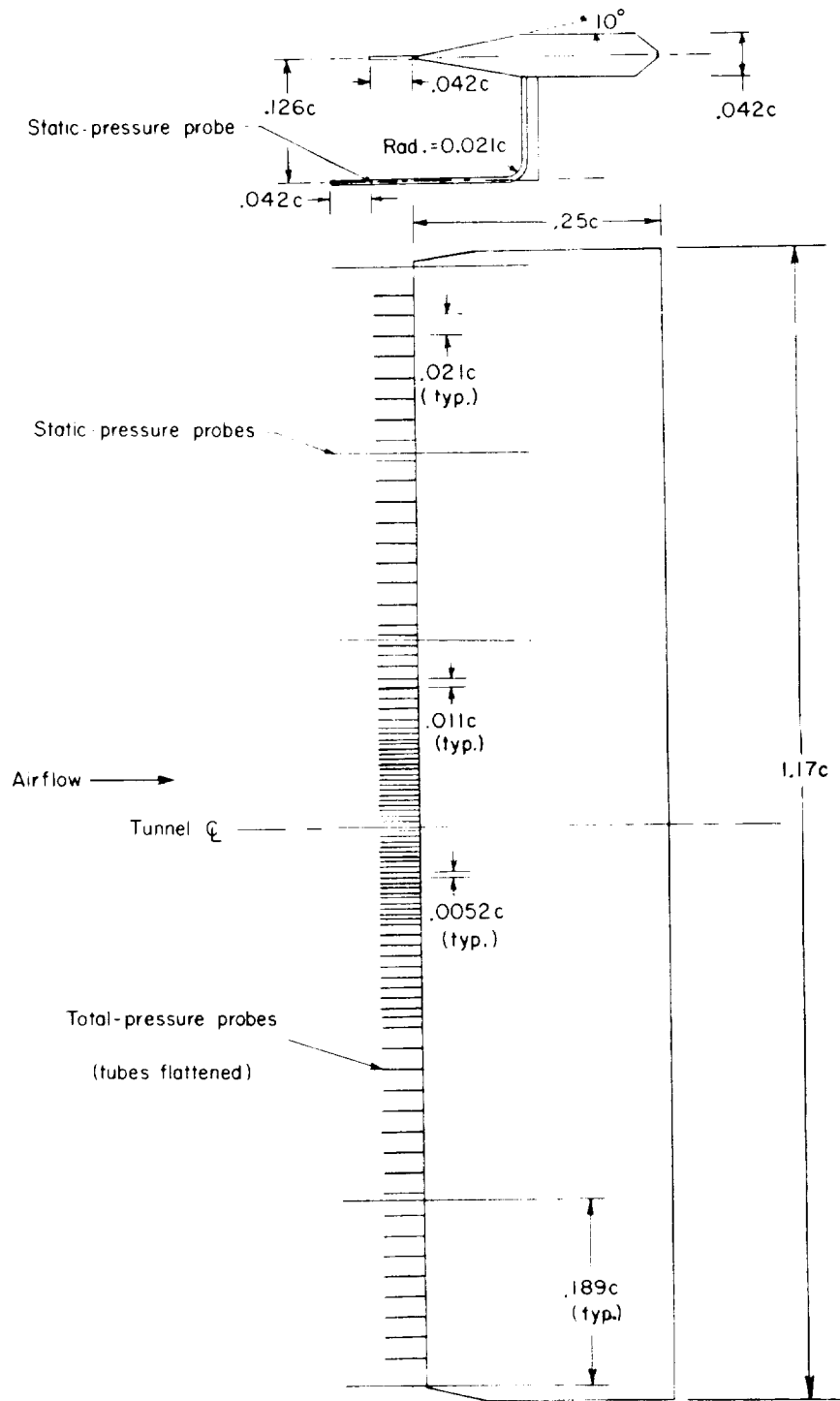
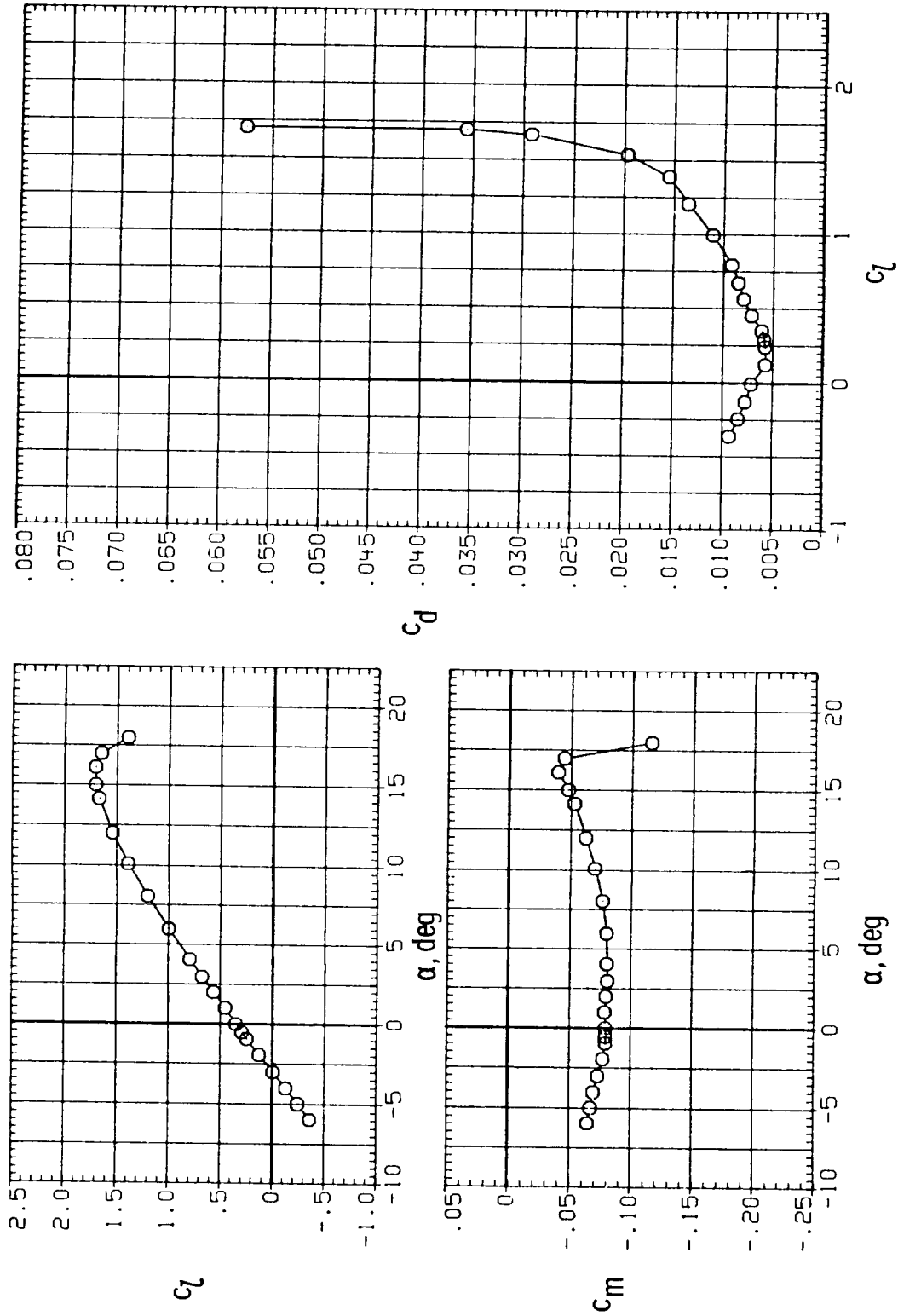
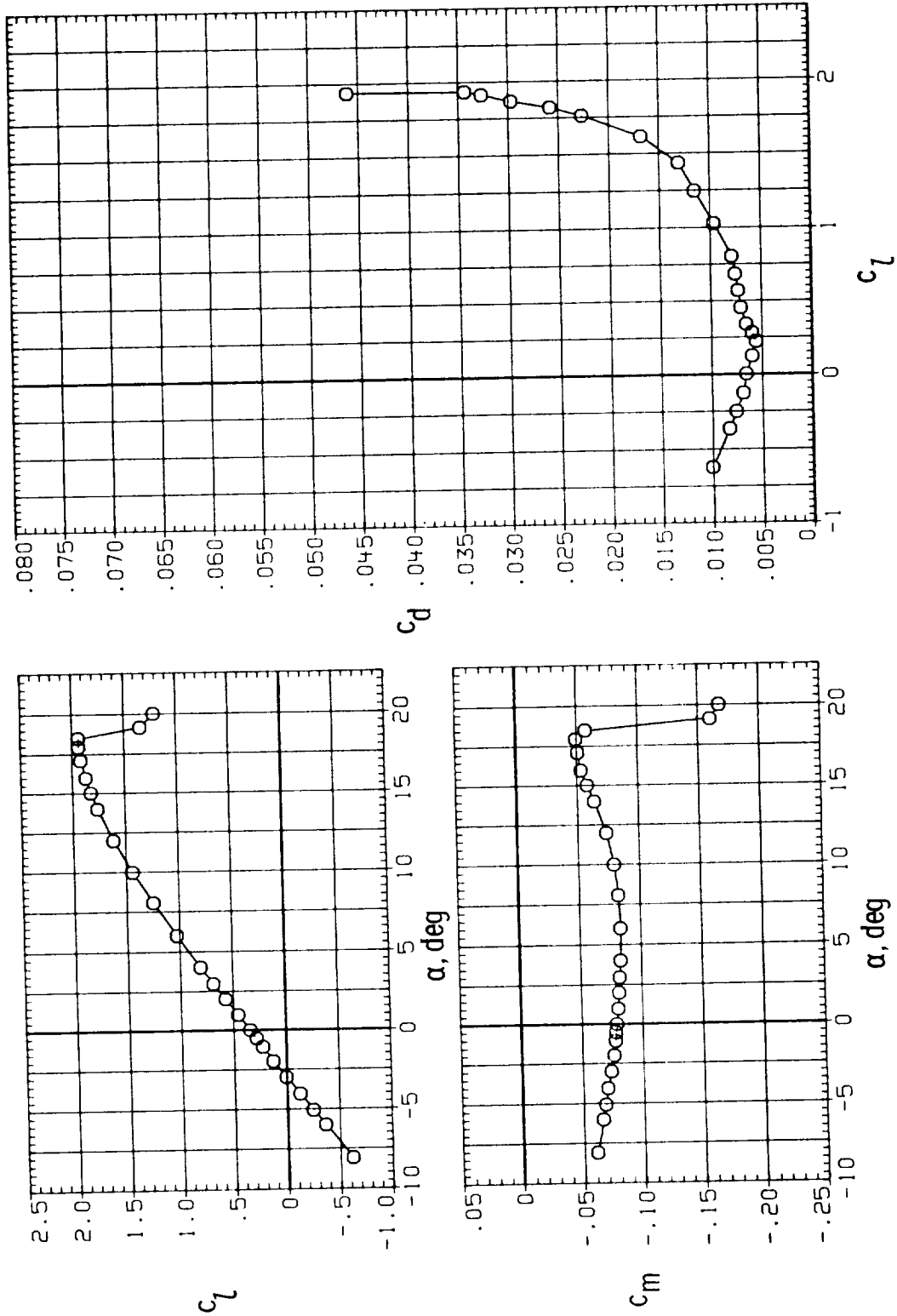


Figure 5.- Wake survey rake. $c = 61 \text{ cm (24 in.)}$.



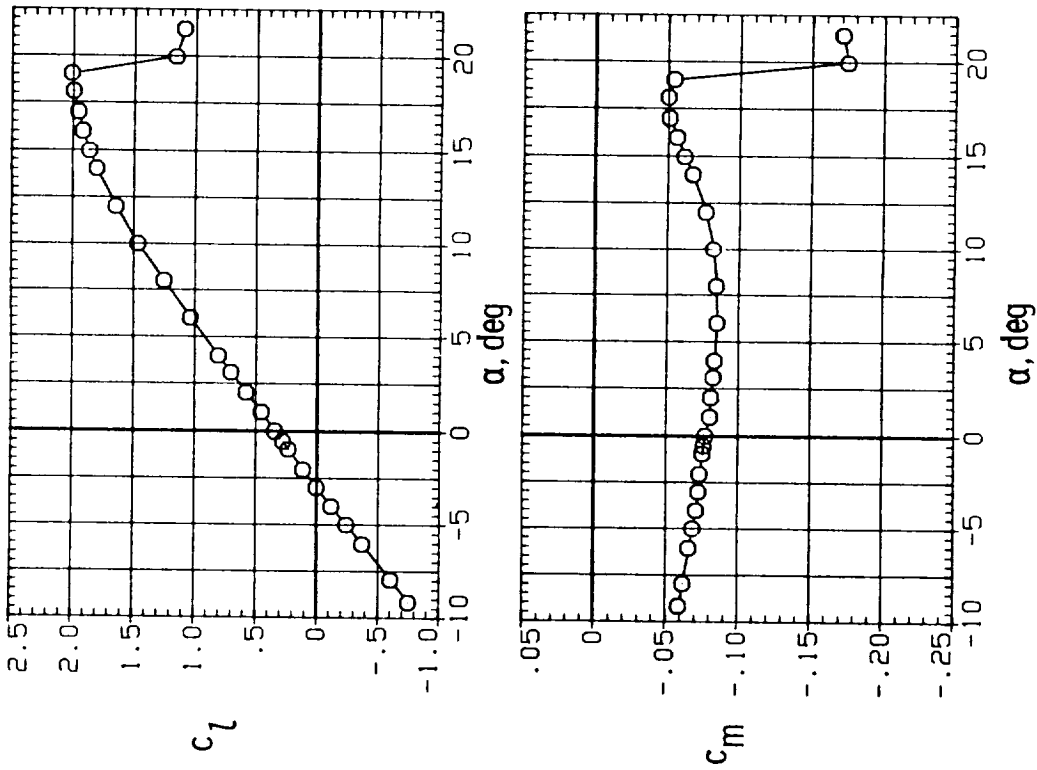
(a) $R = 2.1 \times 10^6$.

Figure 6.- Section characteristics for MS(1)-0313 airfoil. Model smooth; $M = 0.15$.



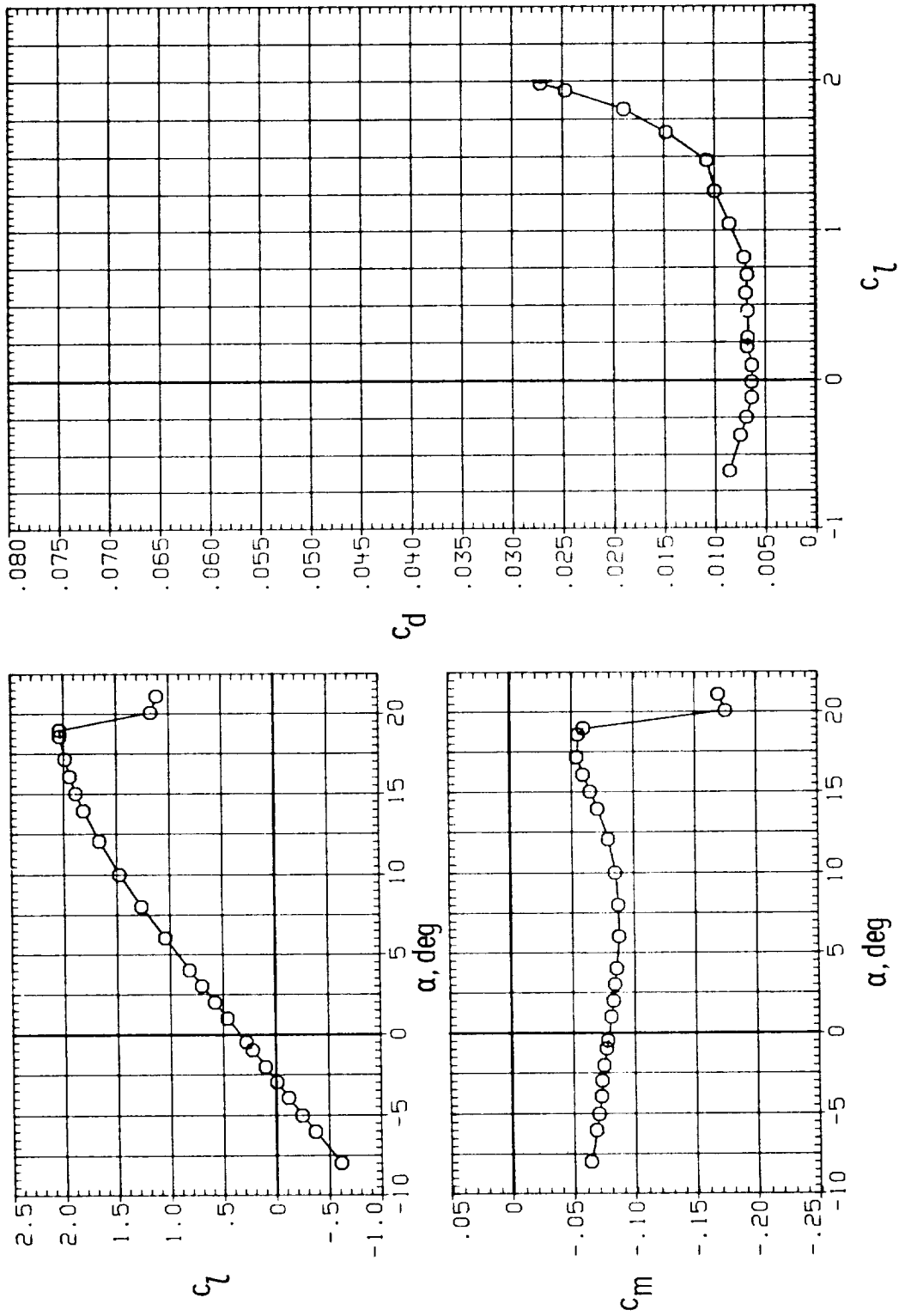
(b) $R = 4.0 \times 10^6$.

Figure 6.- Continued.



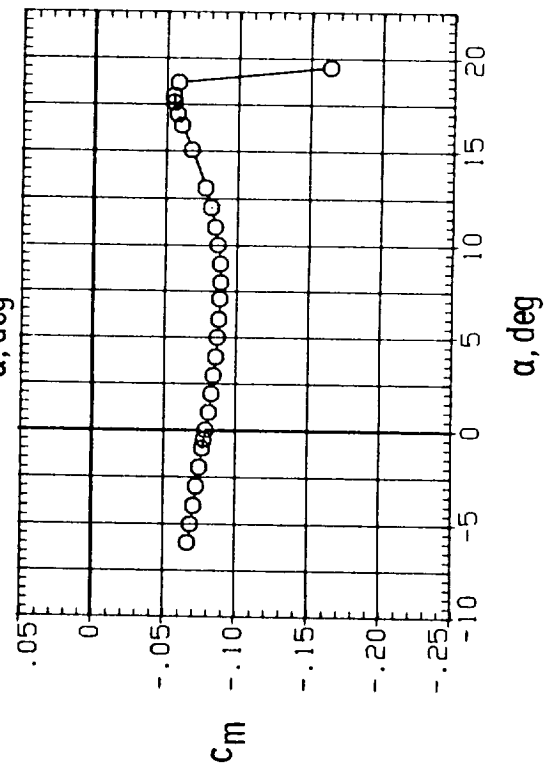
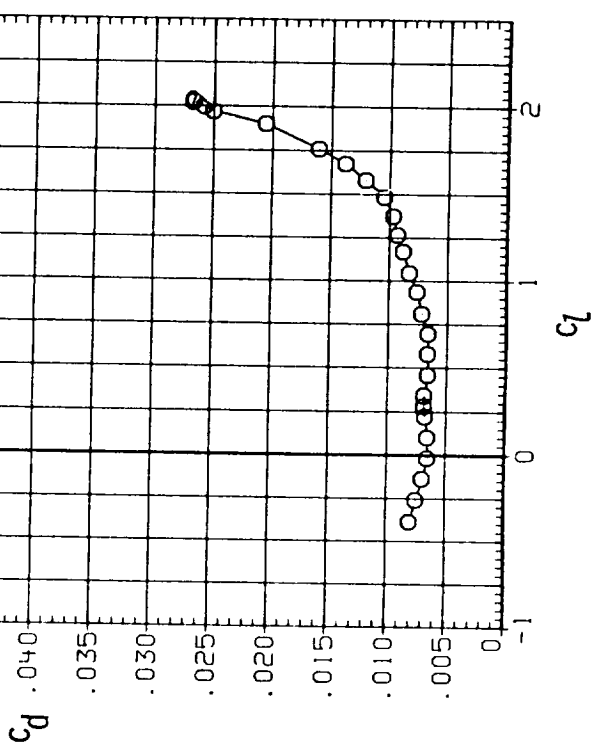
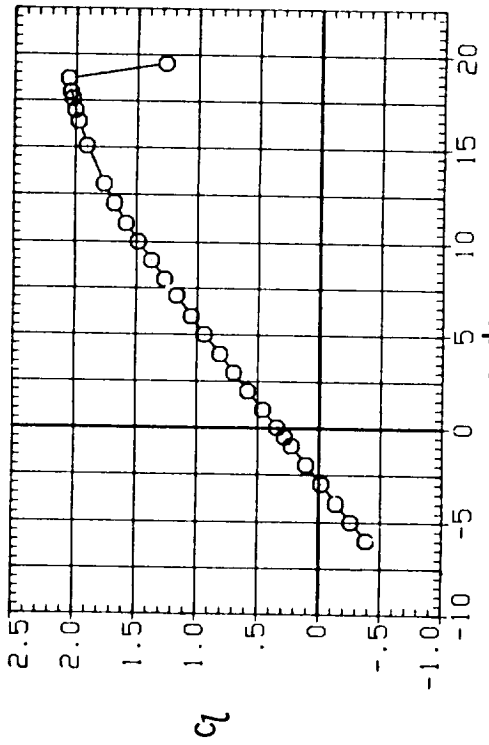
(c) $R = 6.0 \times 10^6$.

Figure 6.- Continued.



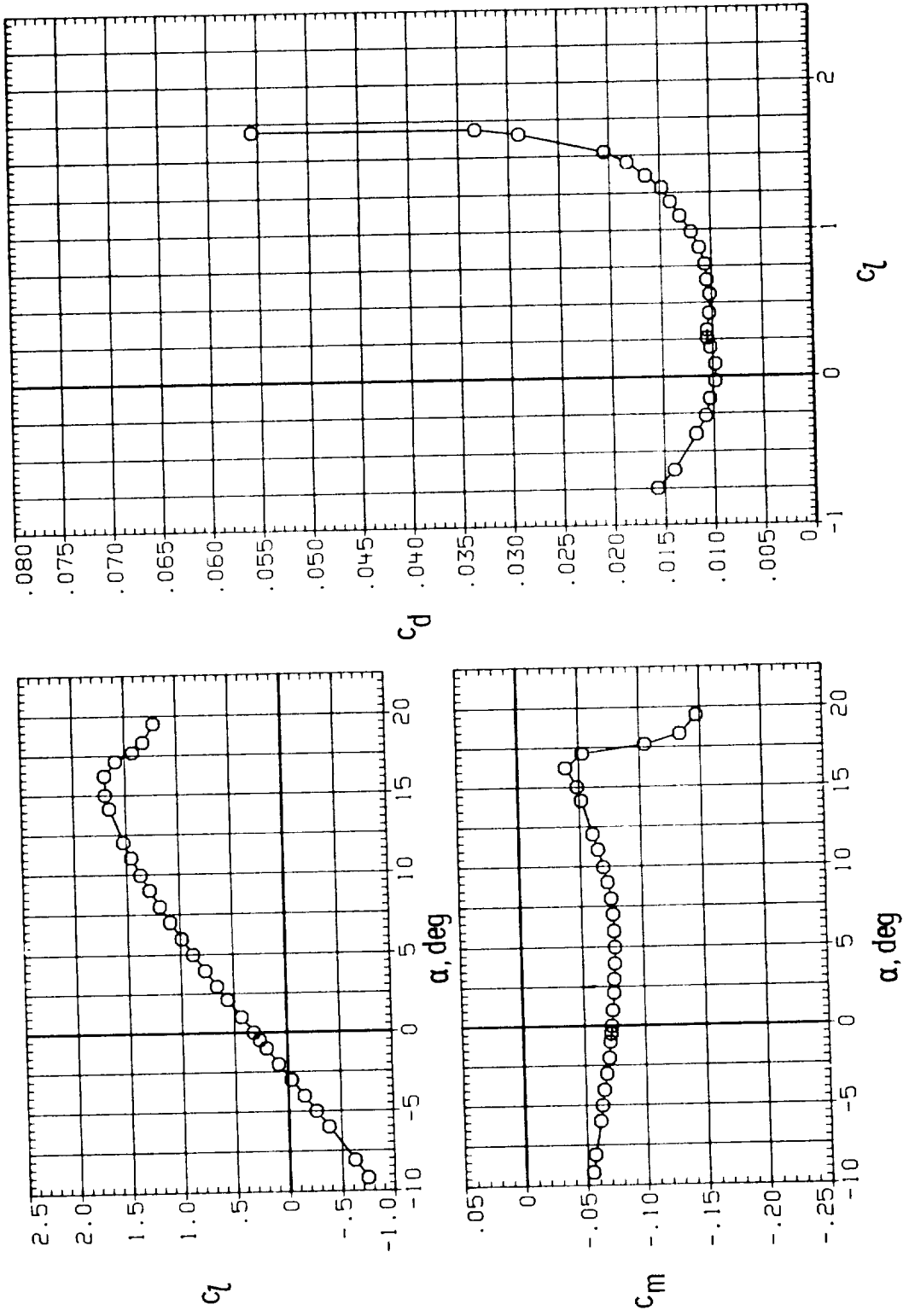
(d) $R = 9.0 \times 10^6$.

Figure 6.- Continued.



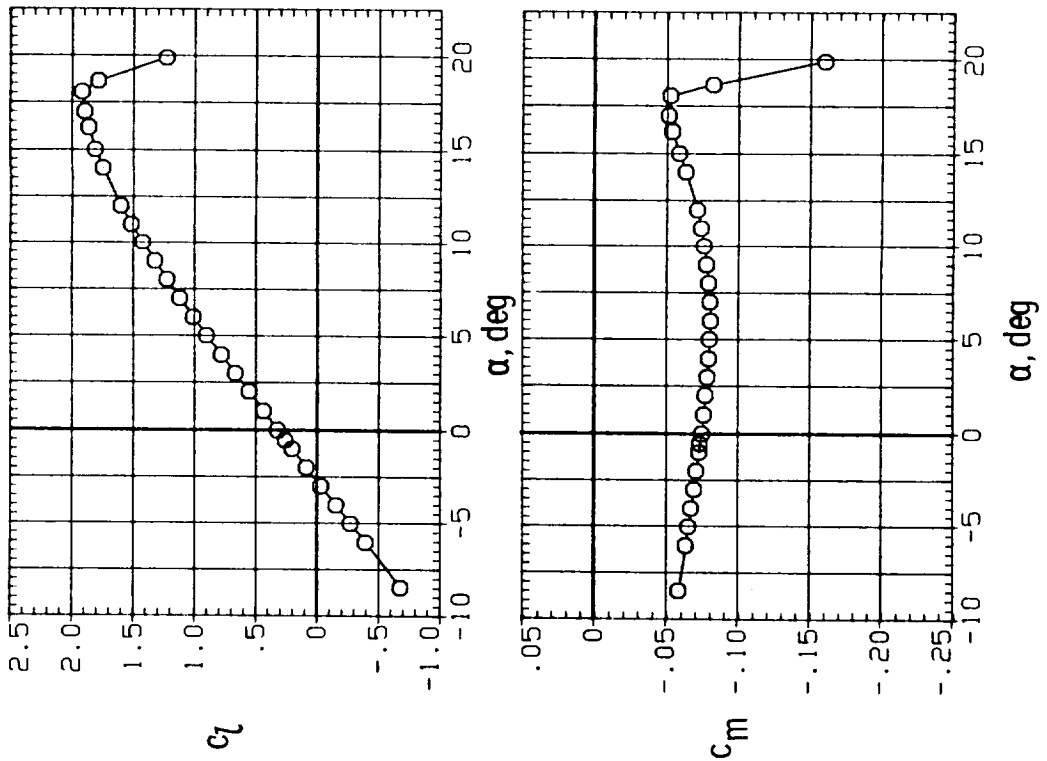
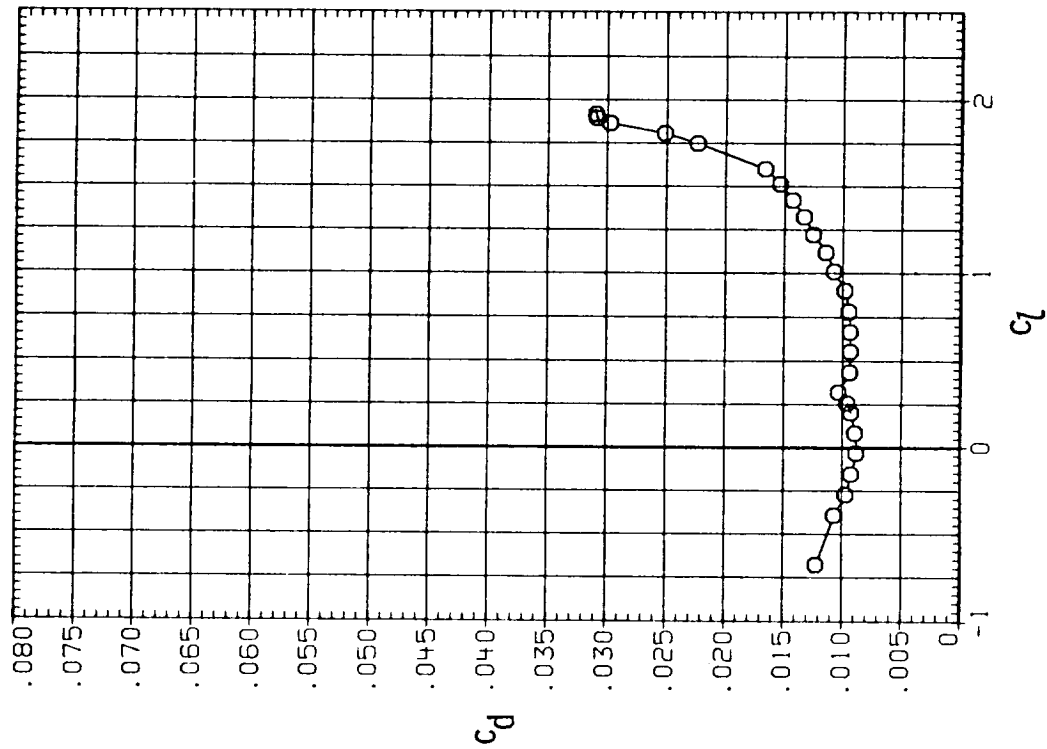
(e) $R = 12.0 \times 10^6$.

Figure 6.- Concluded.



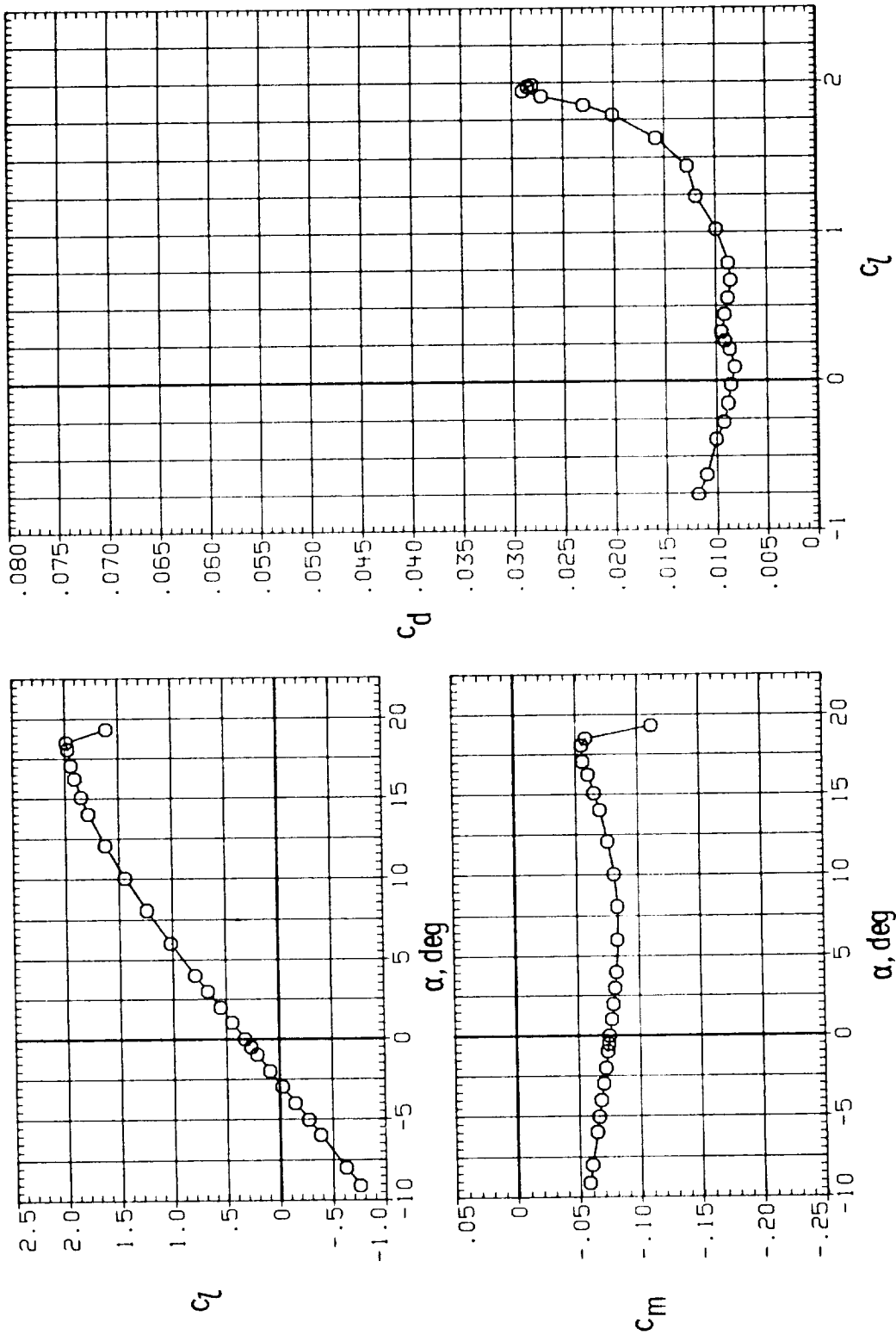
(a) $M = 0.15$; $R = 2.0 \times 10^6$.

Figure 7.- Section characteristics for MS(1)-0313 airfoil. Roughness located at 0.075c.



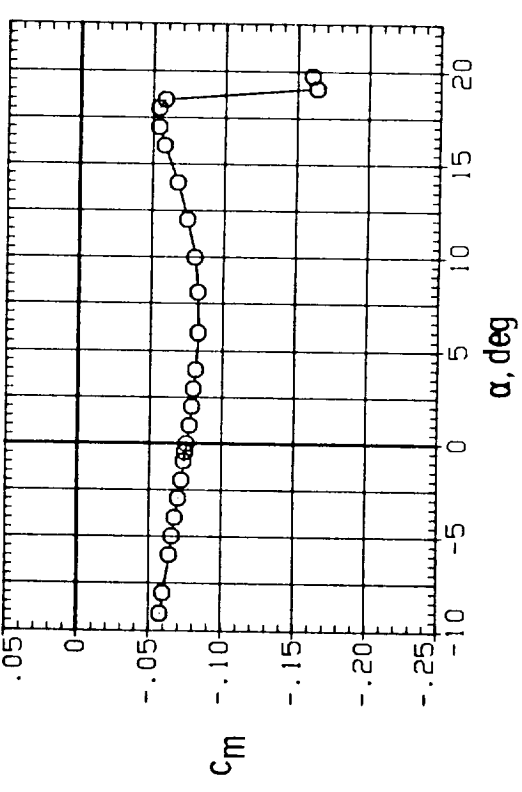
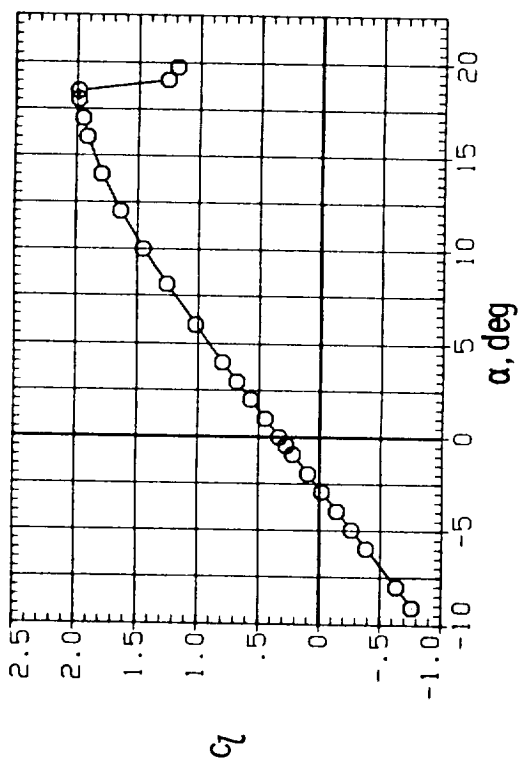
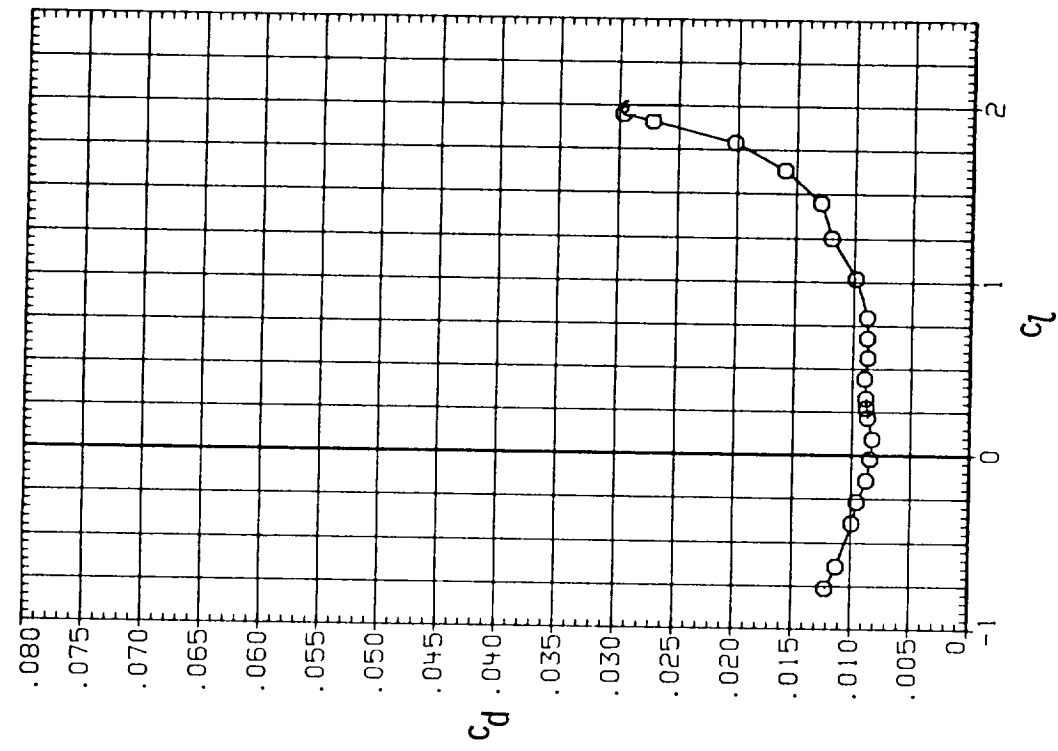
(b) $M = 0.15$; $R = 4.0 \times 10^6$.

Figure 7.- Continued.



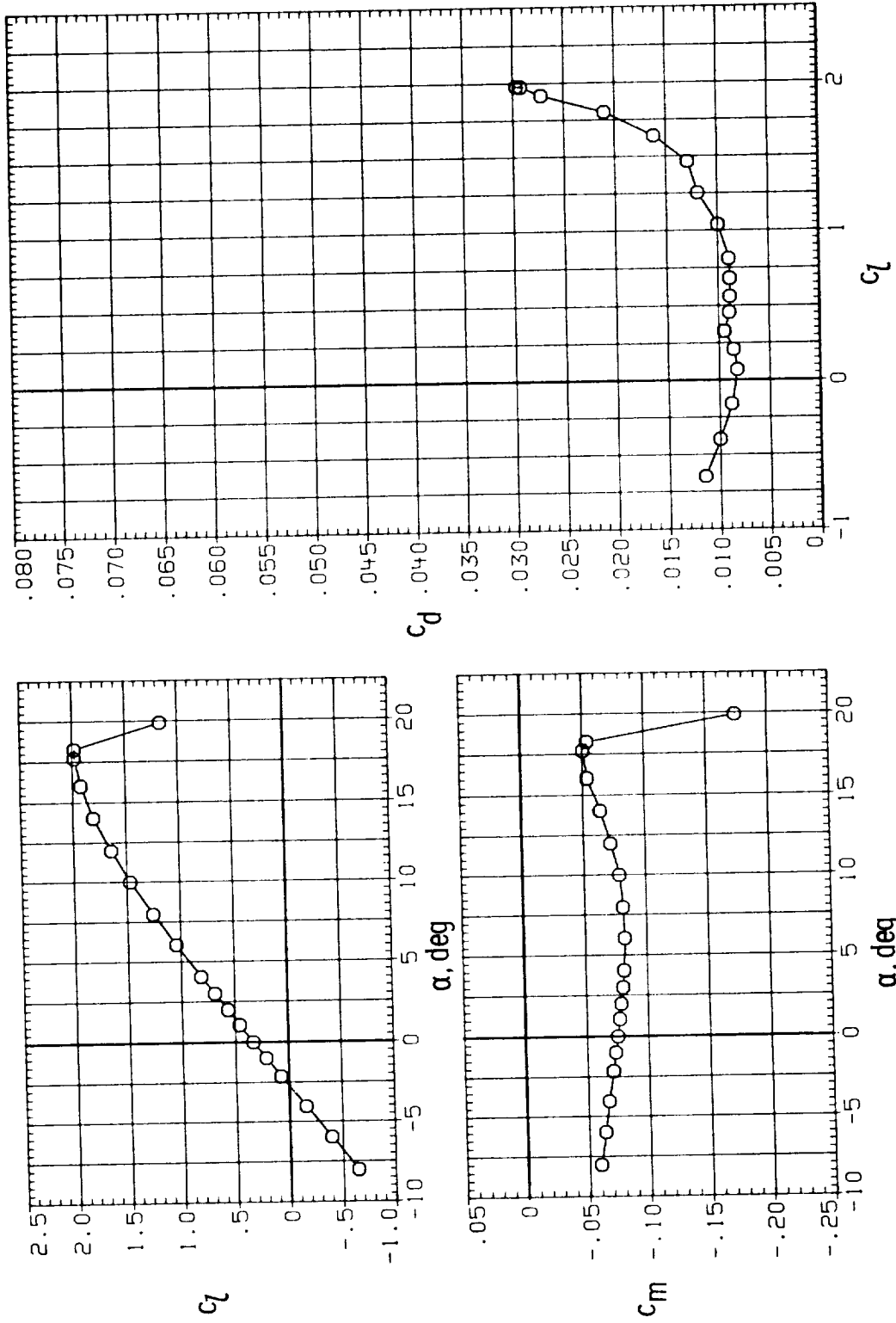
(c) $M = 0.10$; $R = 6.0 \times 10^6$.

Figure 7.- Continued.



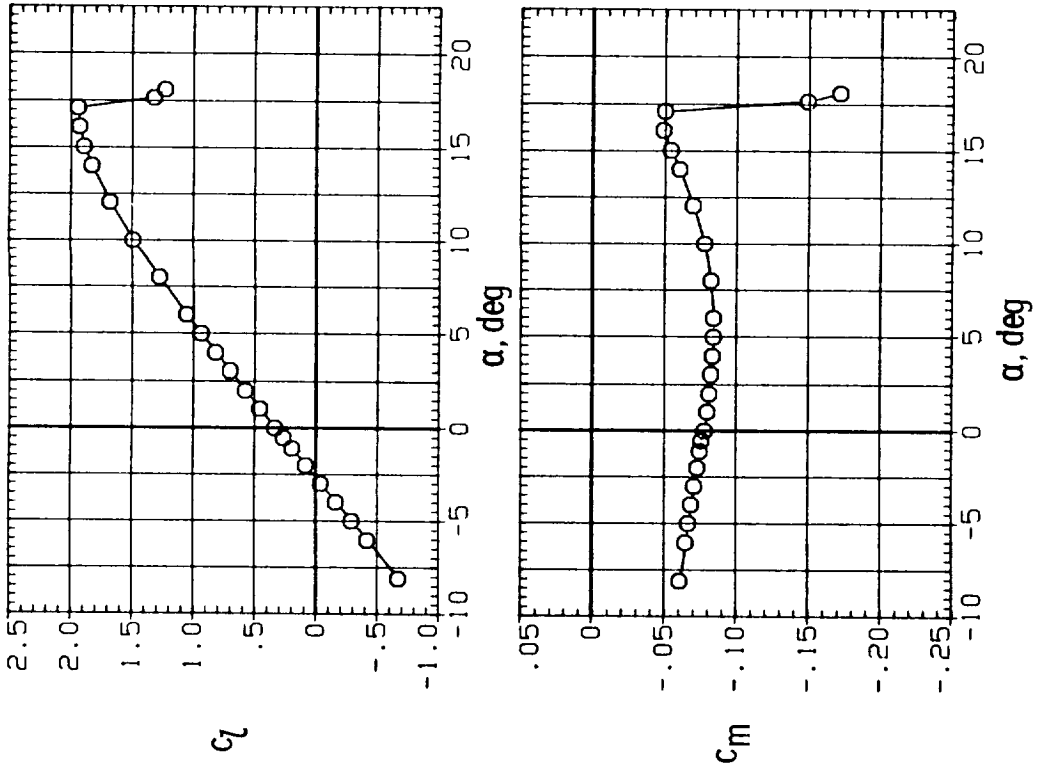
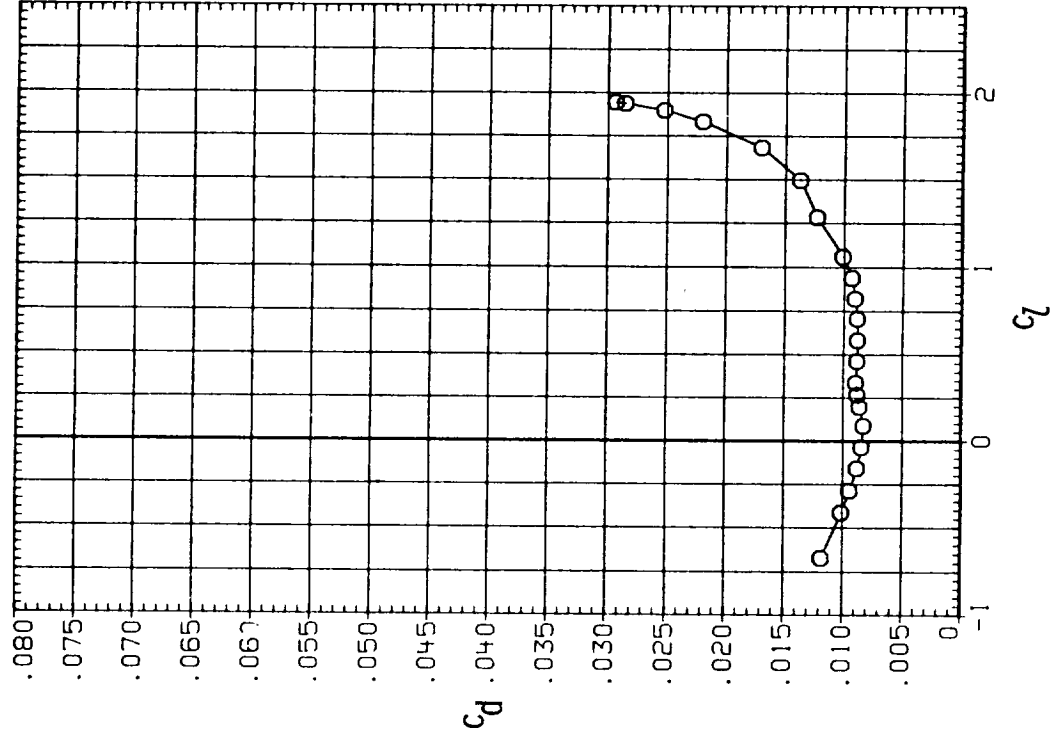
(d) $M = 0.15$; $R = 6.0 \times 10^6$.

Figure 7.- Continued.



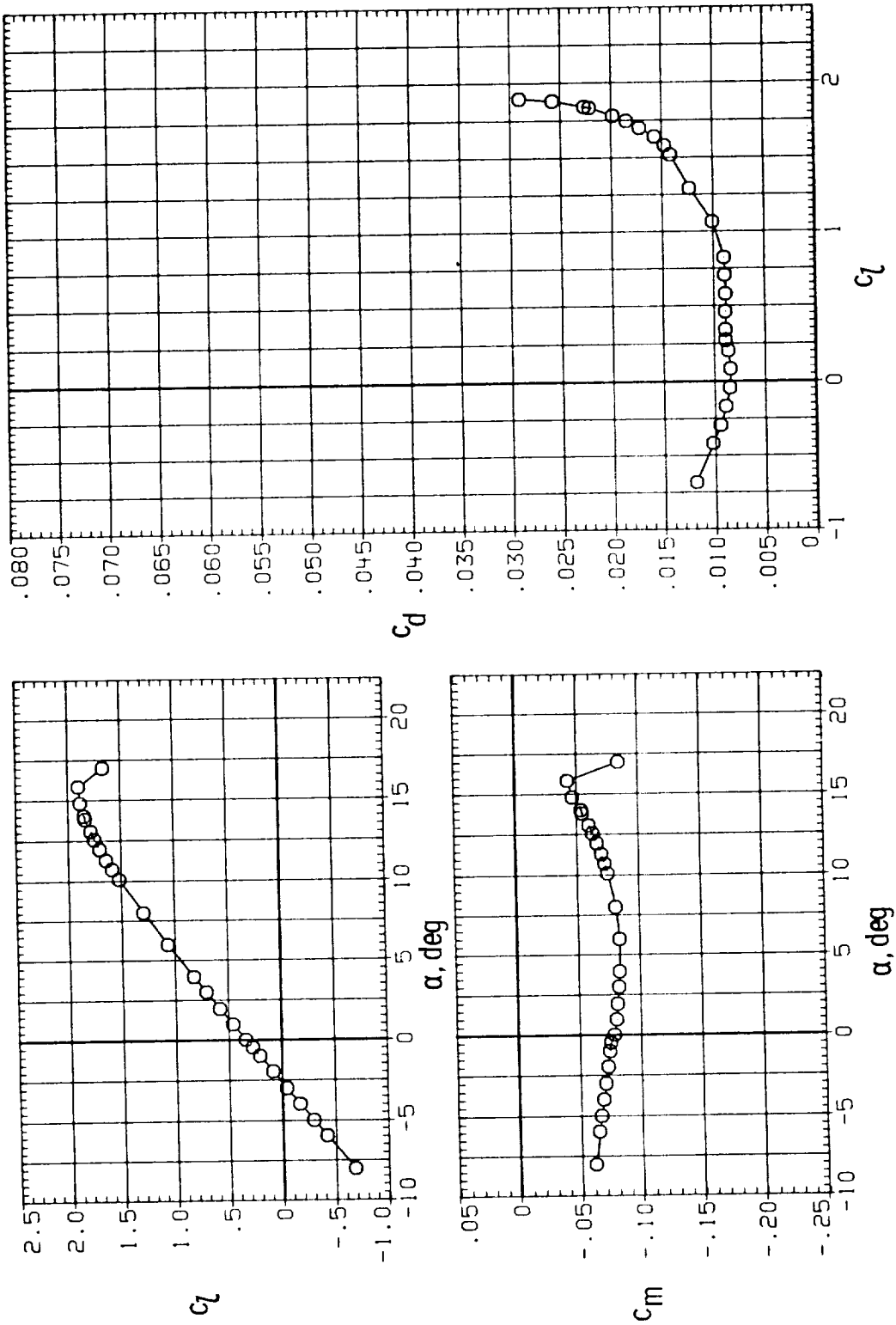
(e) $M = 0.20$; $R = 6.0 \times 10^6$.

Figure 7.- Continued.



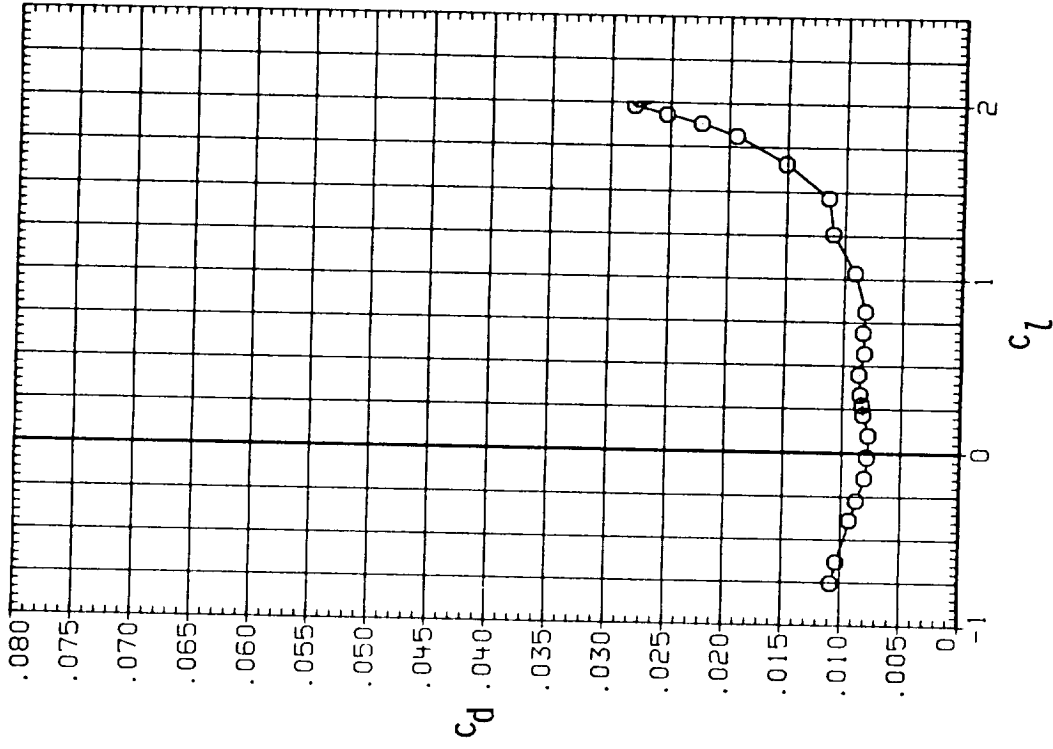
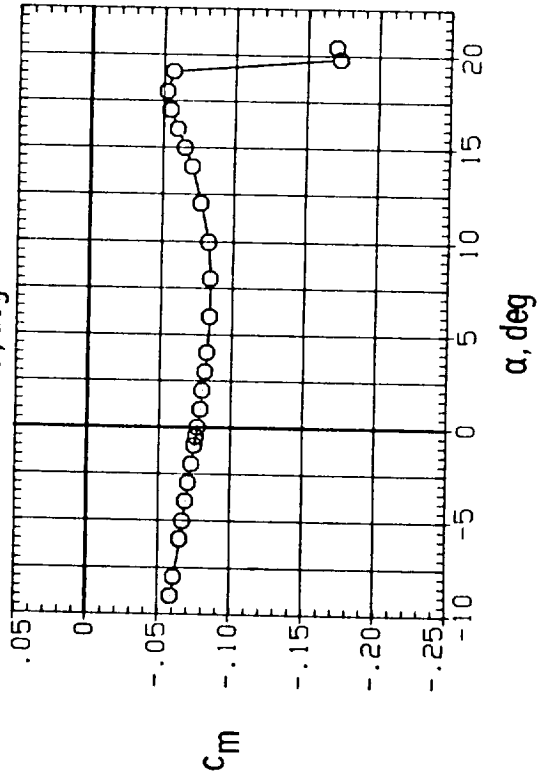
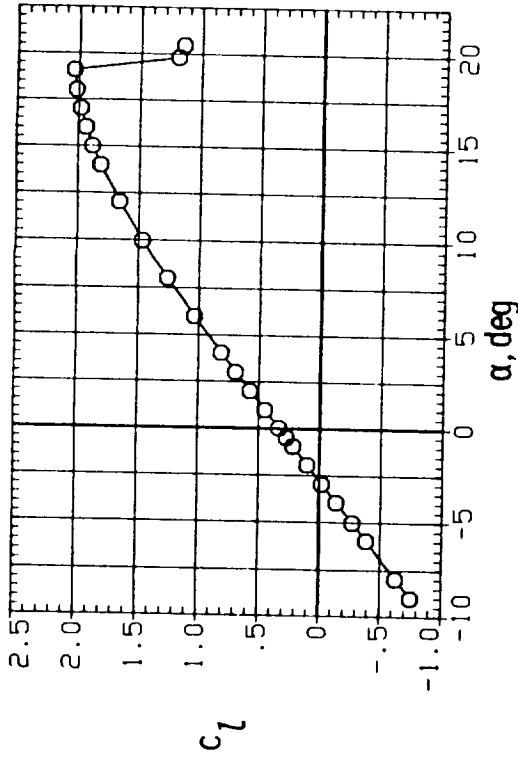
(F) $M = 0.28$; $R = 6.0 \times 10^6$.

Figure 7.- Continued.



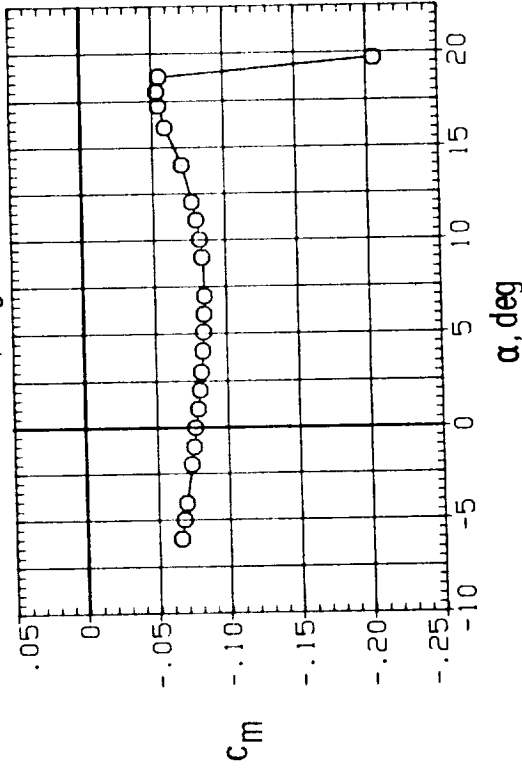
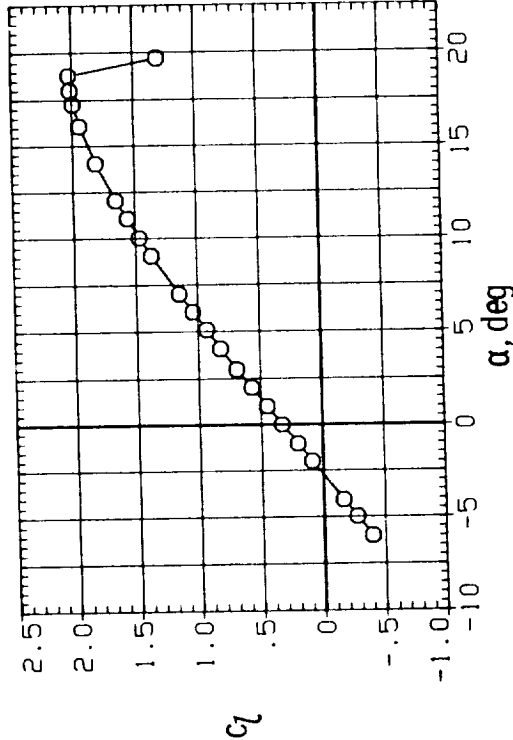
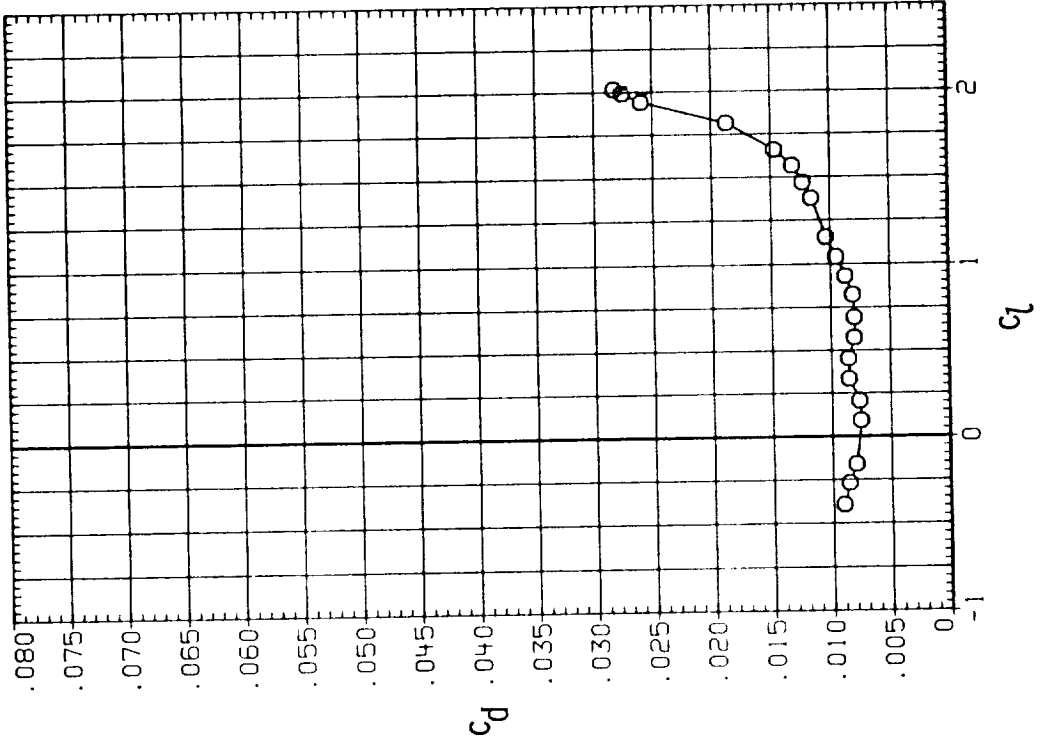
(g) $M = 0.32$; $R = 6.0 \times 10^6$.

Figure 7.- Continued.



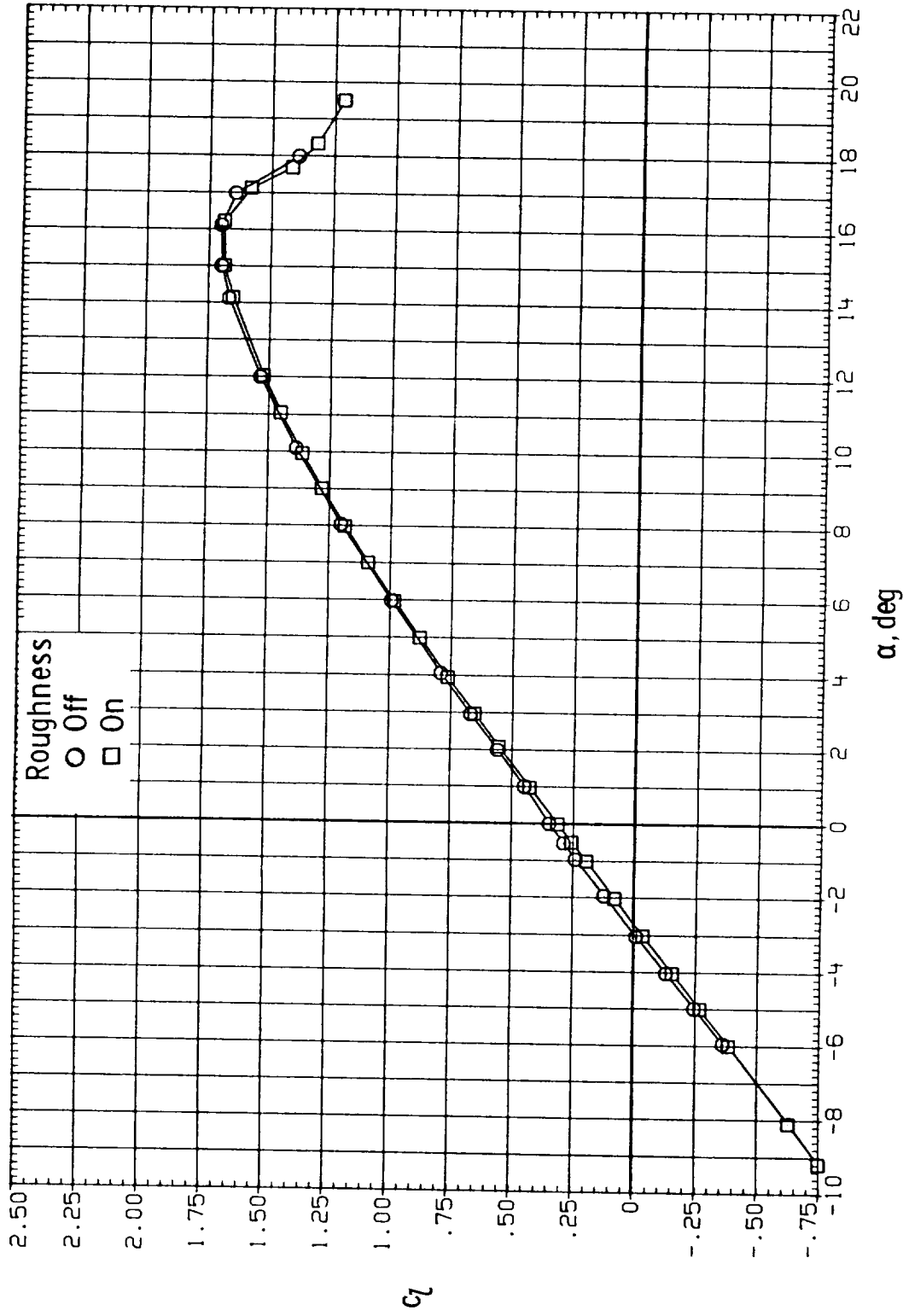
(h) $M = 0.15$; $R = 9.0 \times 10^6$.

Figure 7.- Continued.



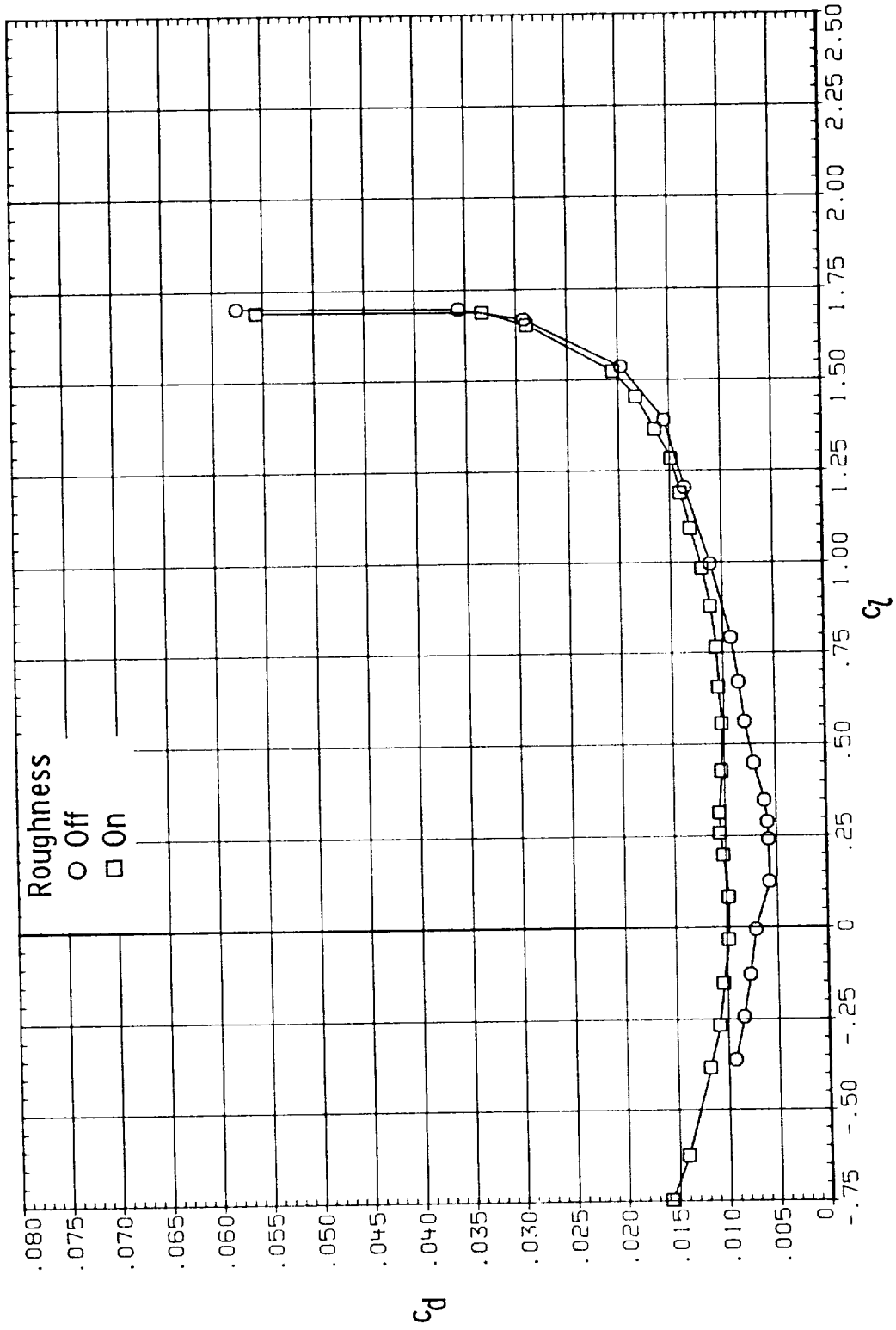
(i) $M = 0.15$; $R = 12.0 \times 10^6$.

Figure 7.- Concluded.



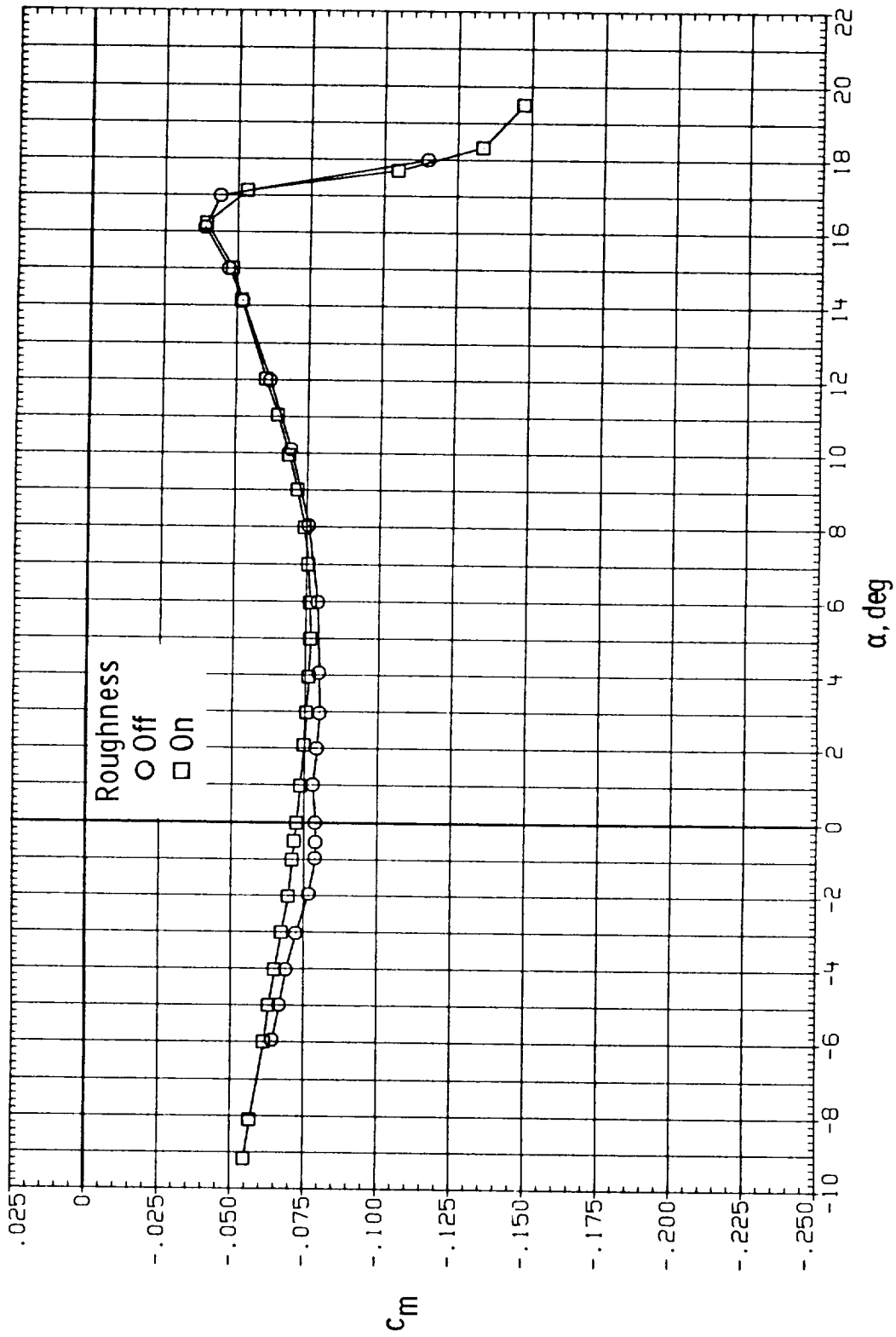
(a) $R = 2.0 \times 10^6$.

Figure 8.- Effect of roughness on section characteristics. $M = 0.15$.



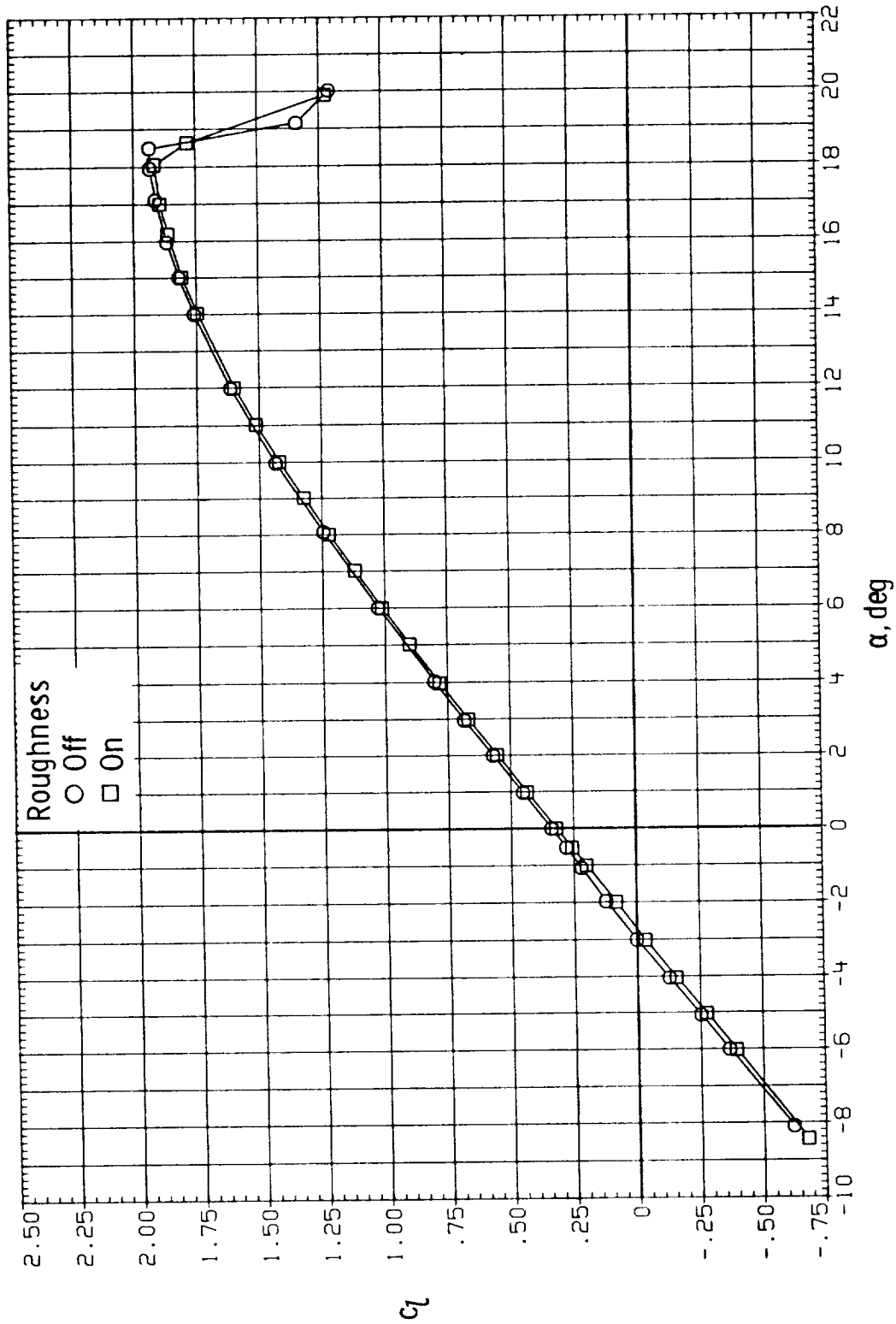
(a) $R = 2.0 \times 10^6$. Continued.

Figure 8.- Continued.



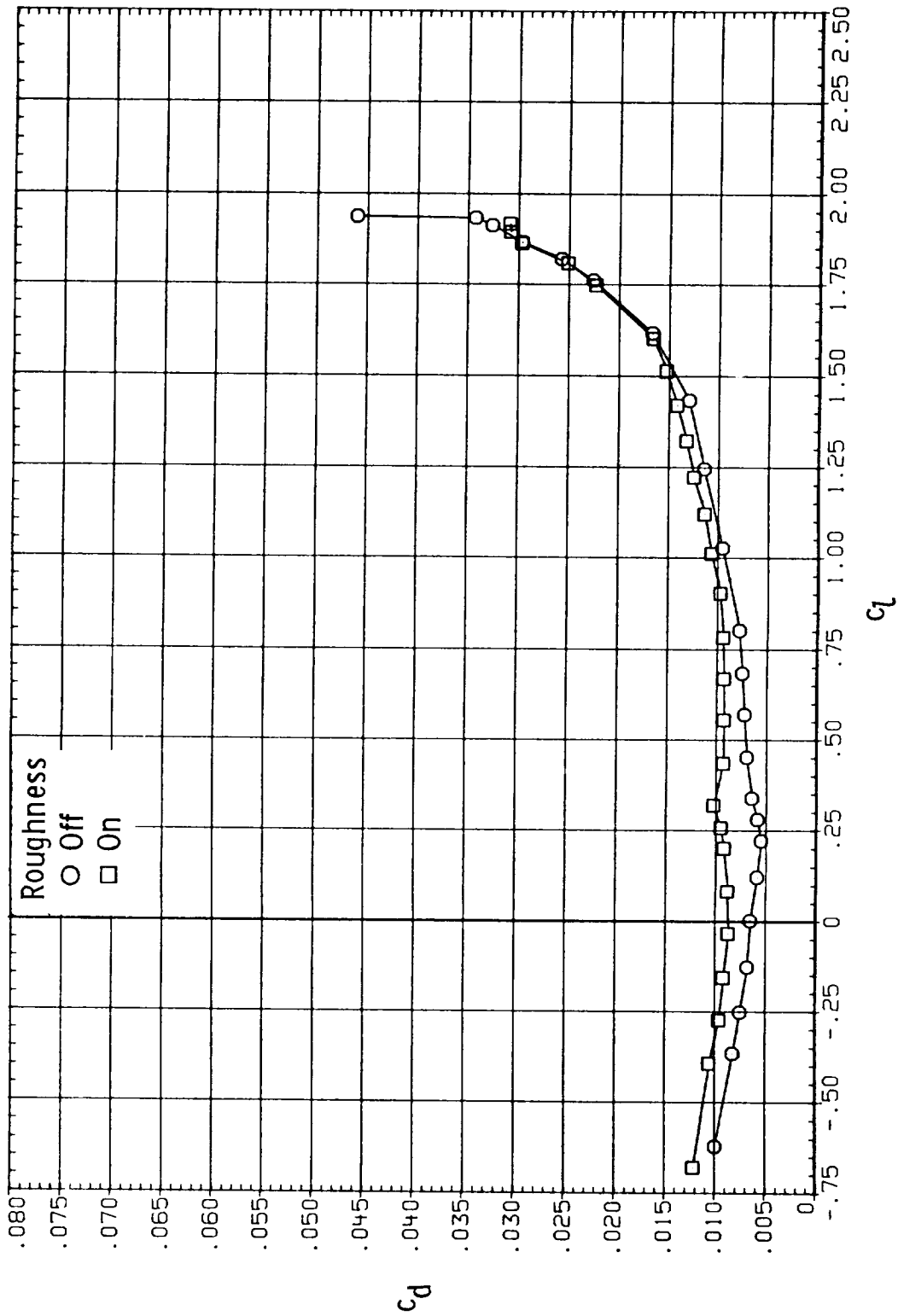
(a) $R = 2.0 \times 10^6$. Concluded.

Figure 8.- Continued.



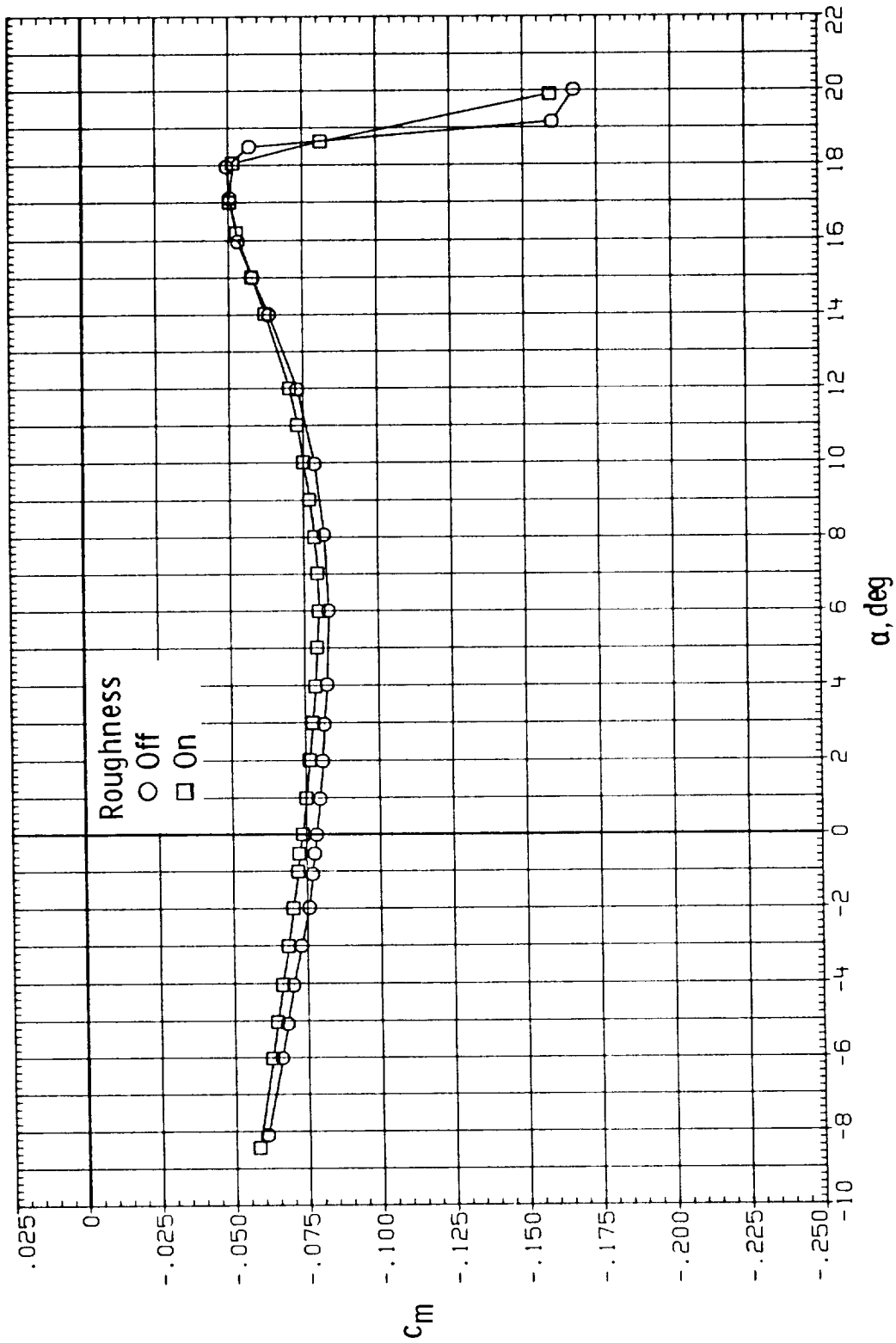
(b) $R = 4.0 \times 10^6$.

Figure 8.- Continued.



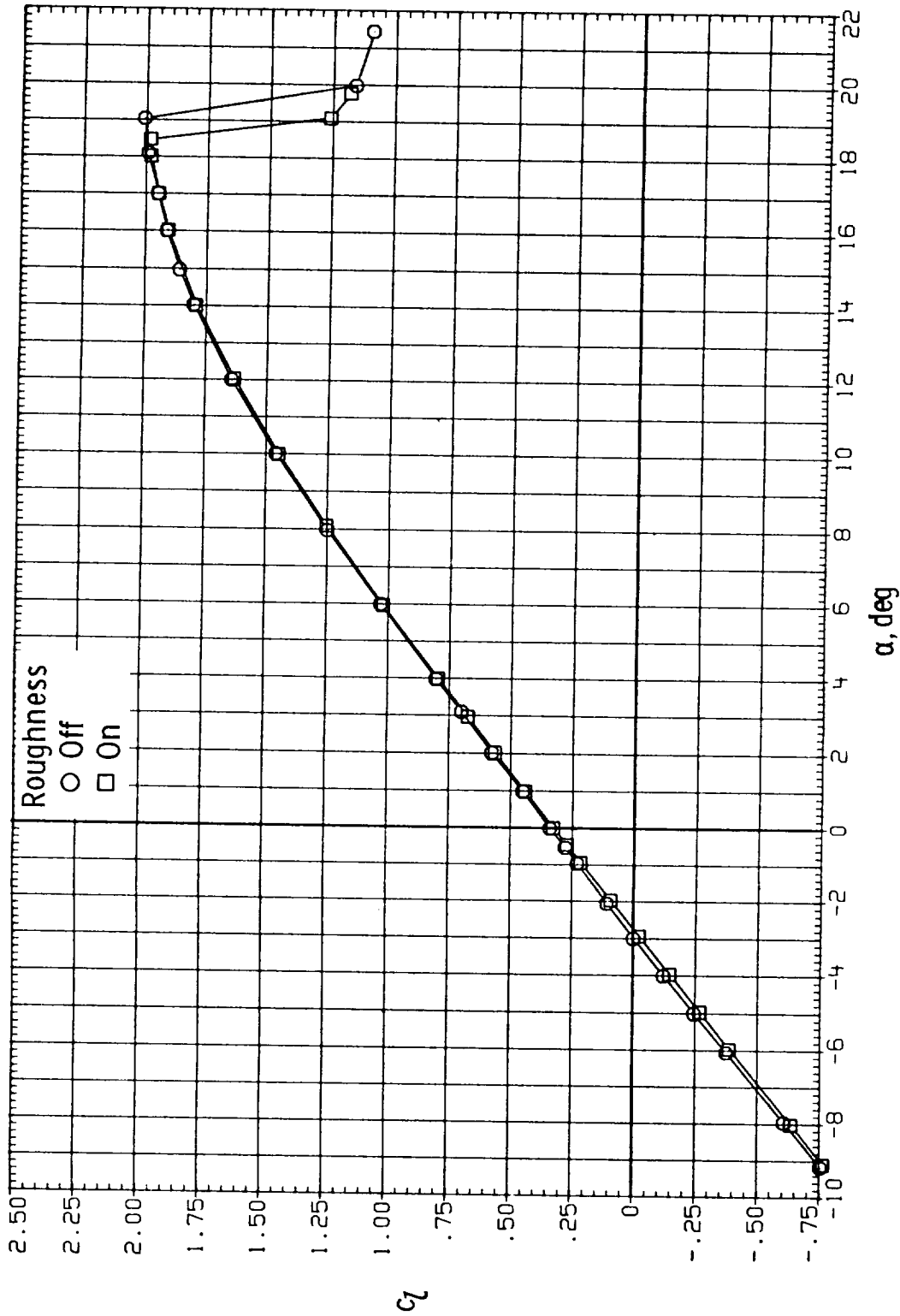
(b) $R = 4.0 \times 10^6$. Continued.

Figure 8.- Continued.



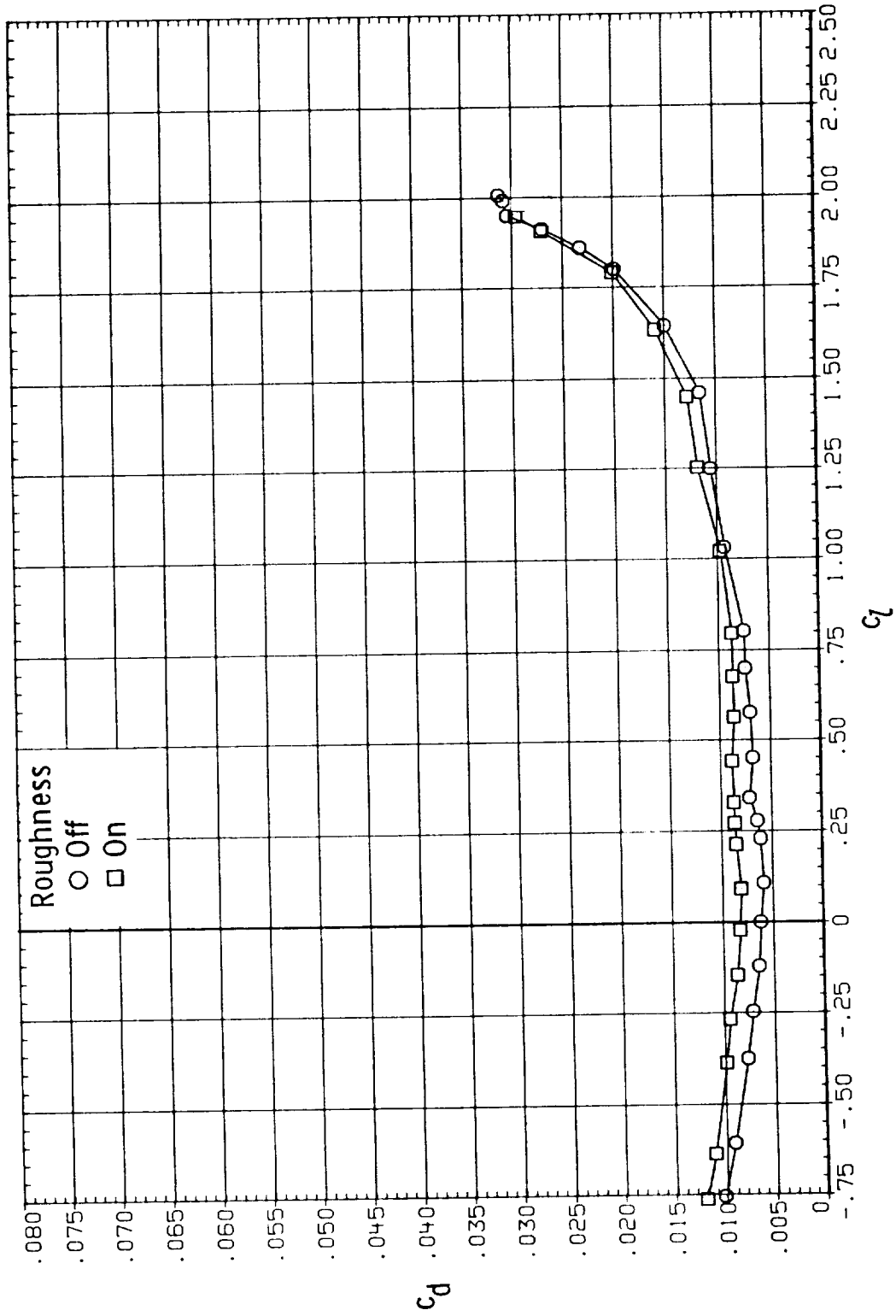
(b) $R = 4.0 \times 10^6$. Concluded.

Figure 8.- Continued.



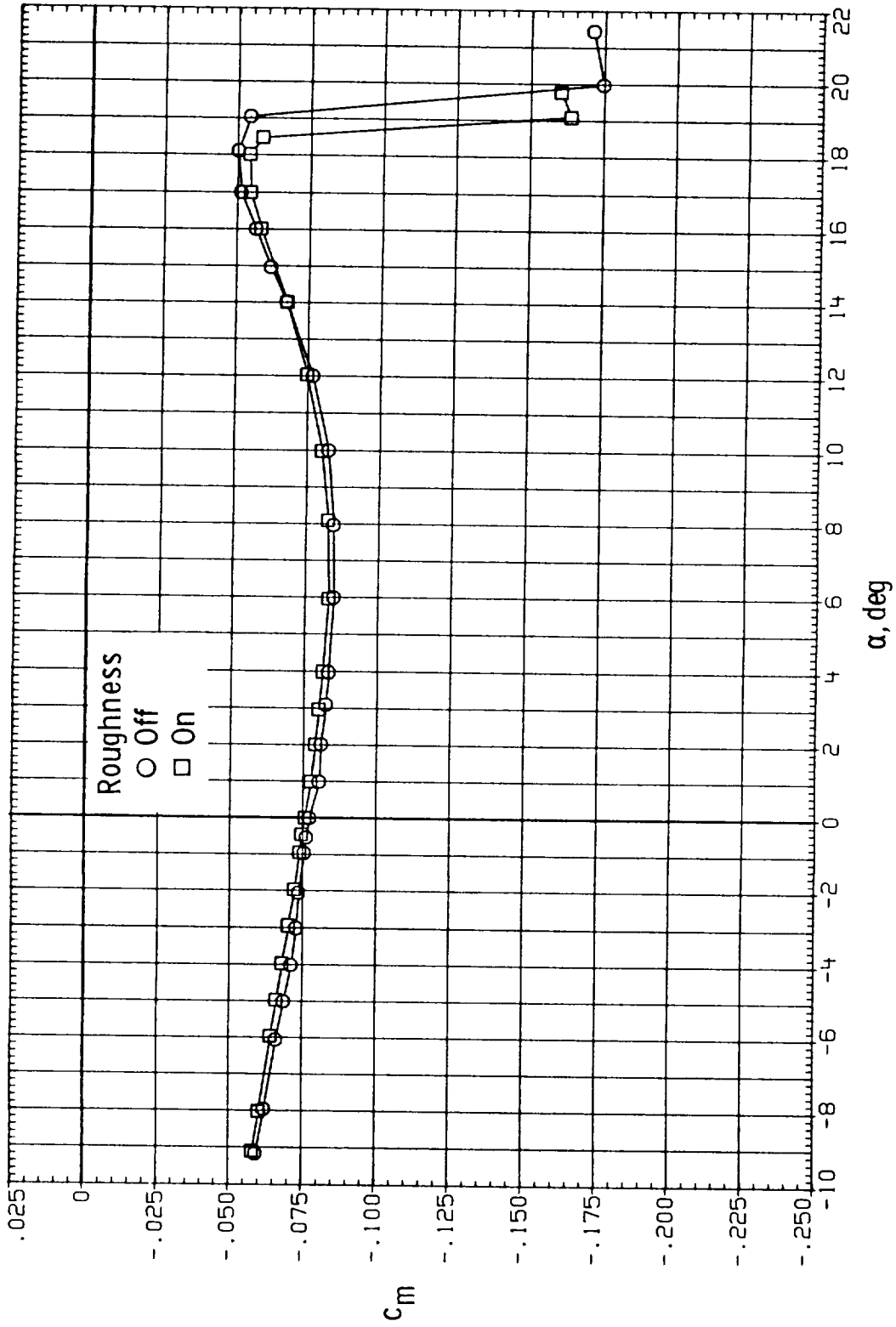
(c) $R = 6.0 \times 10^6$.

Figure 8.- Continued.



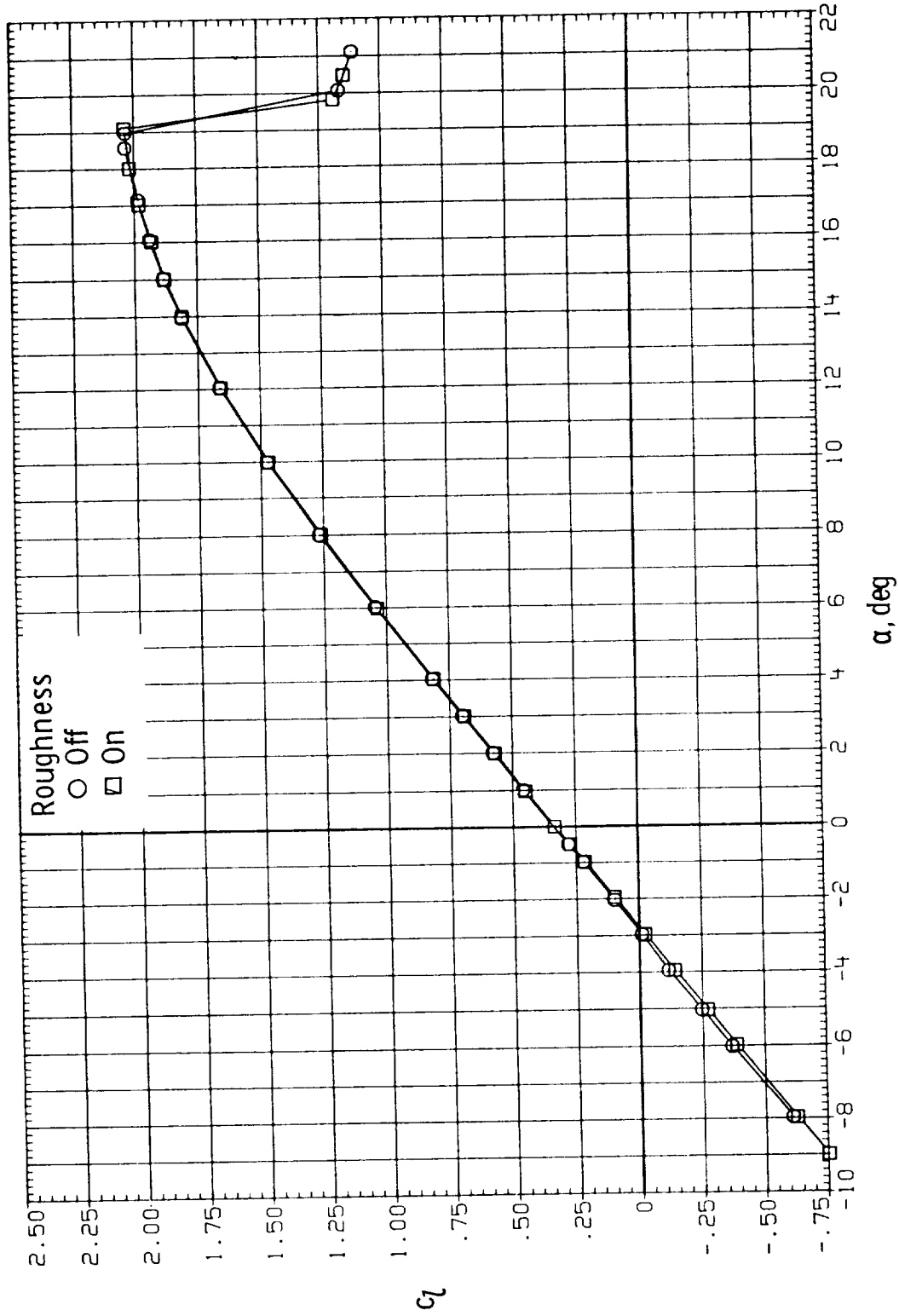
(c) $R = 6.0 \times 10^6$. Continued.

Figure 8.- Continued.



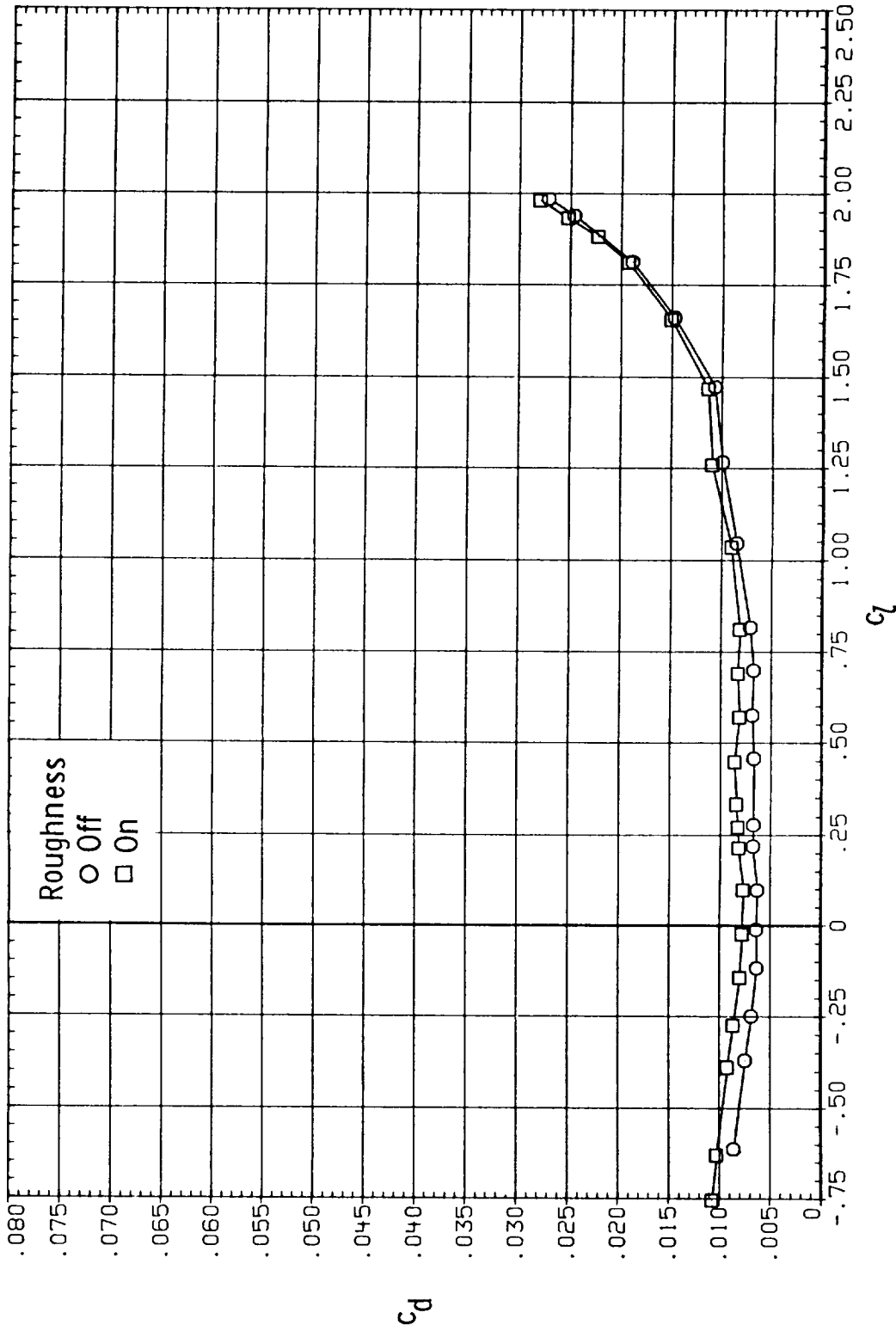
(c) $R = 6.0 \times 10^6$. Concluded.

Figure 8.- Continued.



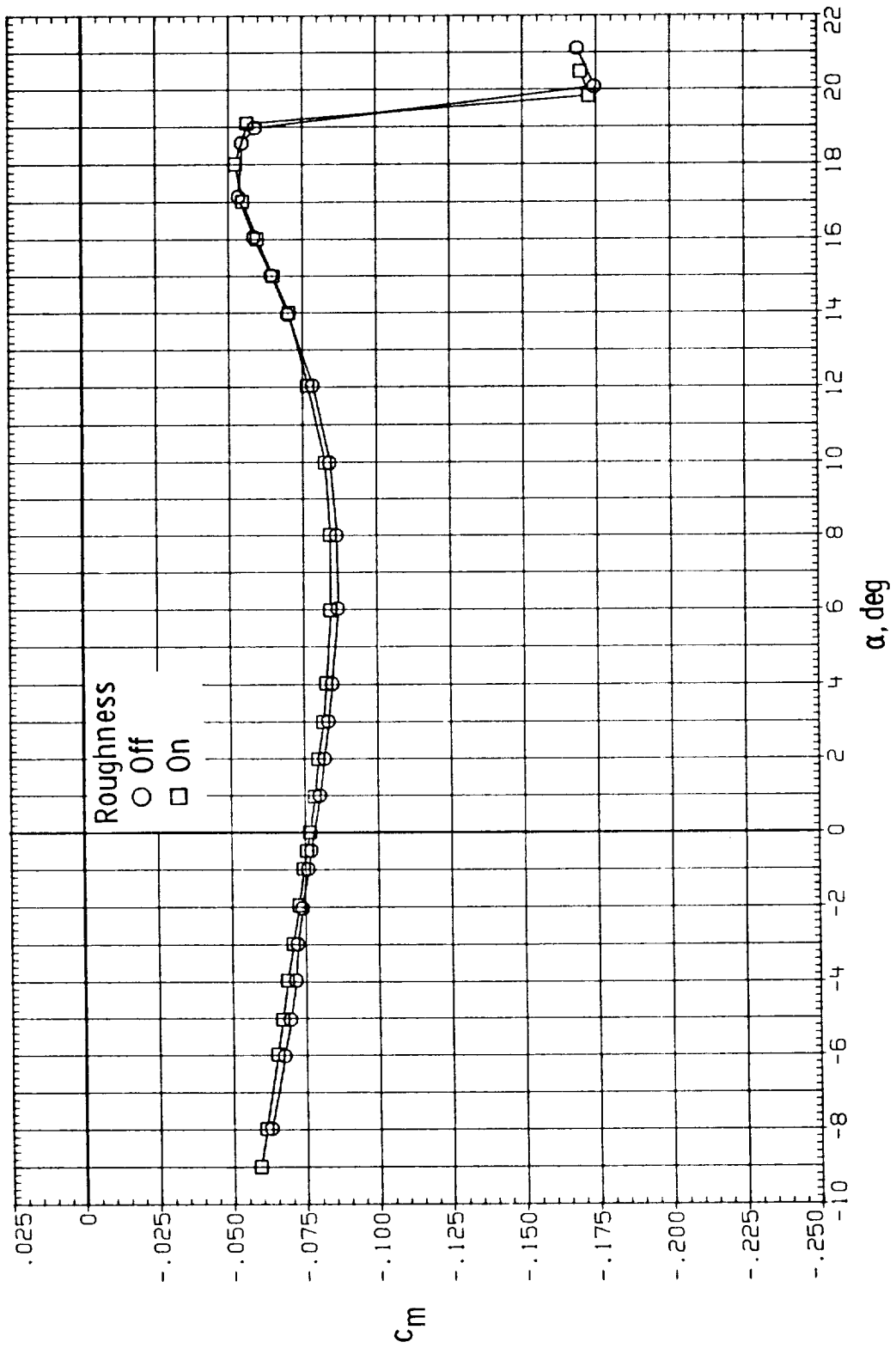
(d) $R = 9.0 \times 10^6$.

Figure 8.- Continued.



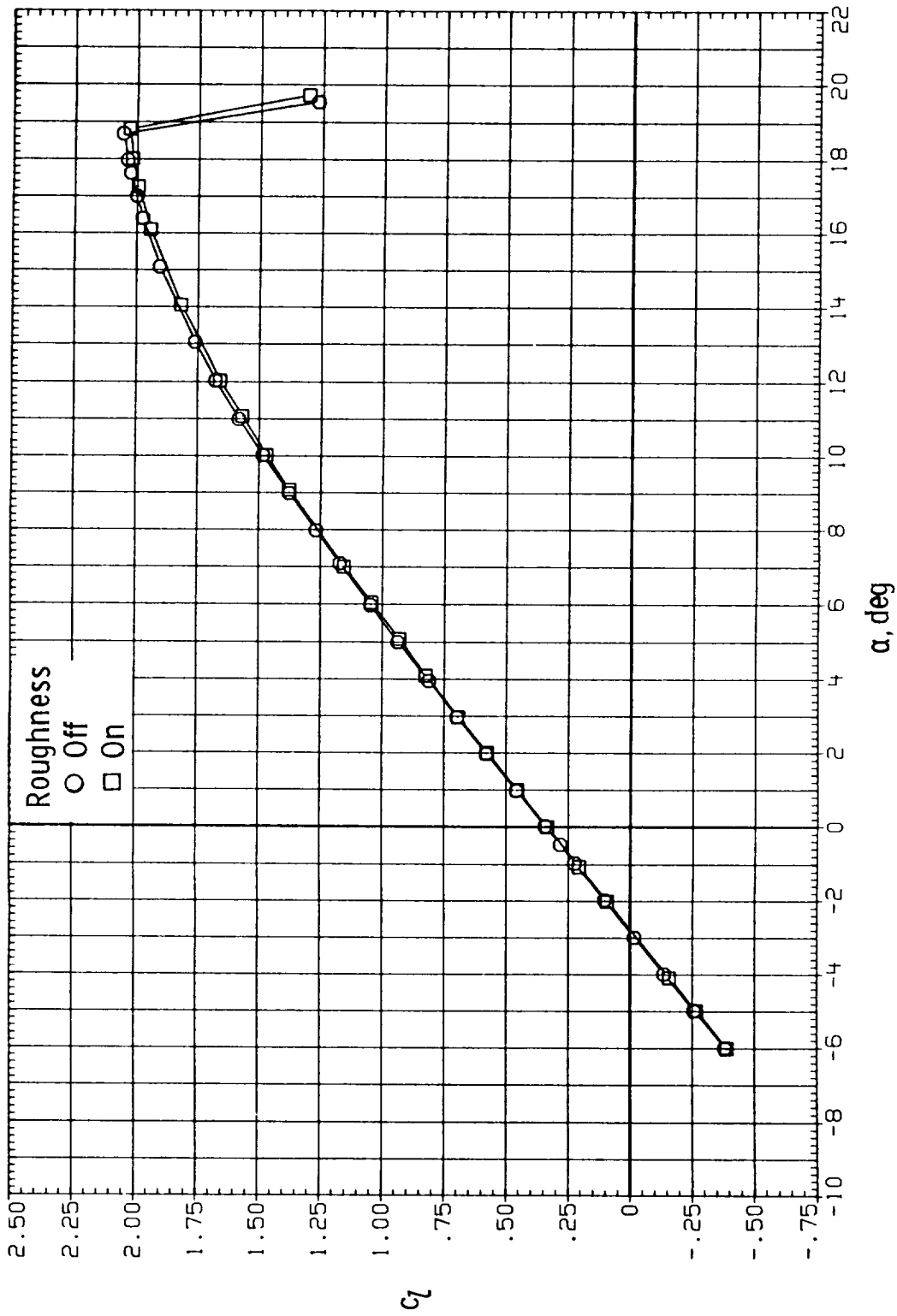
(d) $R = 9.0 \times 10^6$. Continued.

Figure 8.- Continued.



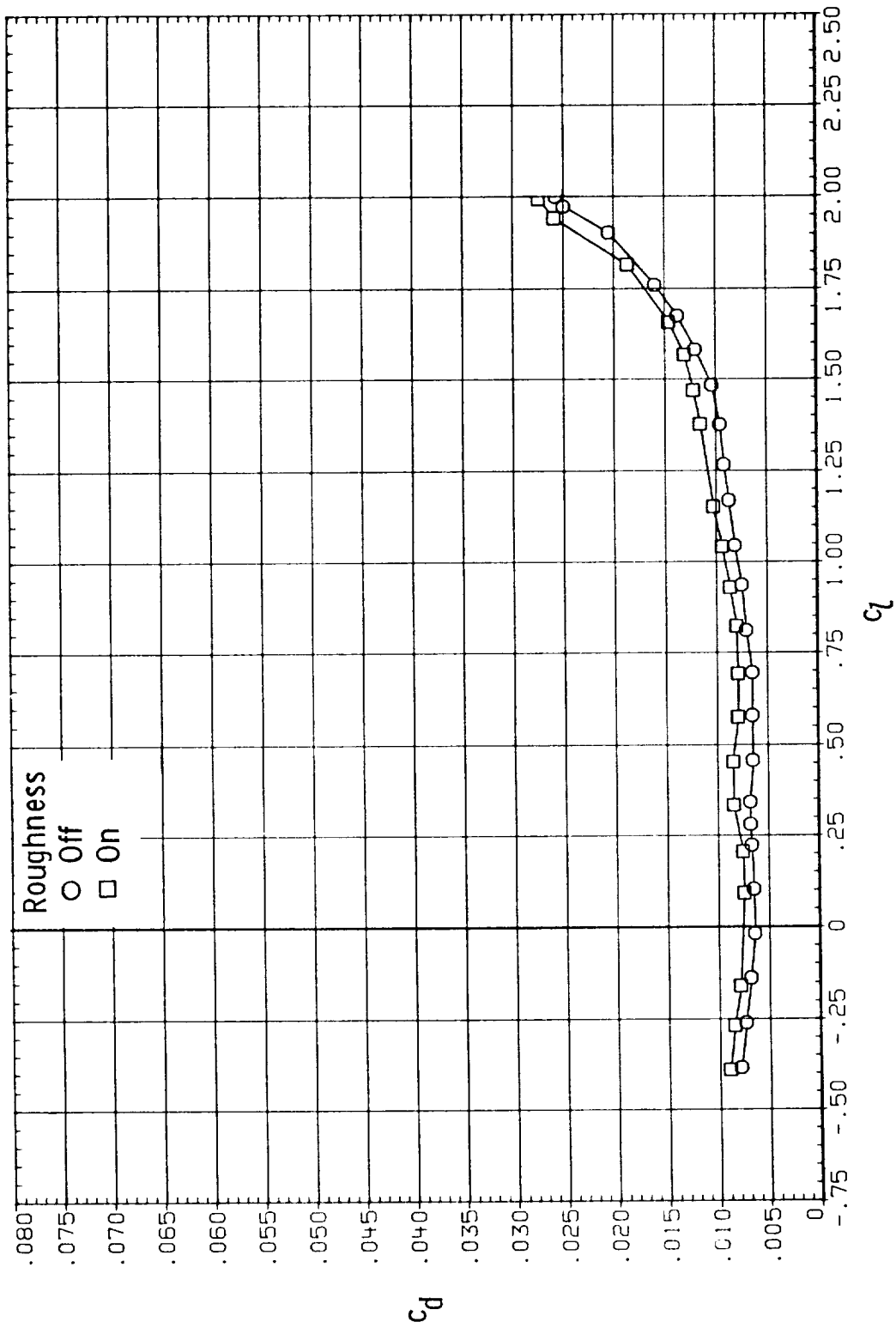
(d) $R = 9.0 \times 10^6$. Concluded.

Figure 8.- Continued.



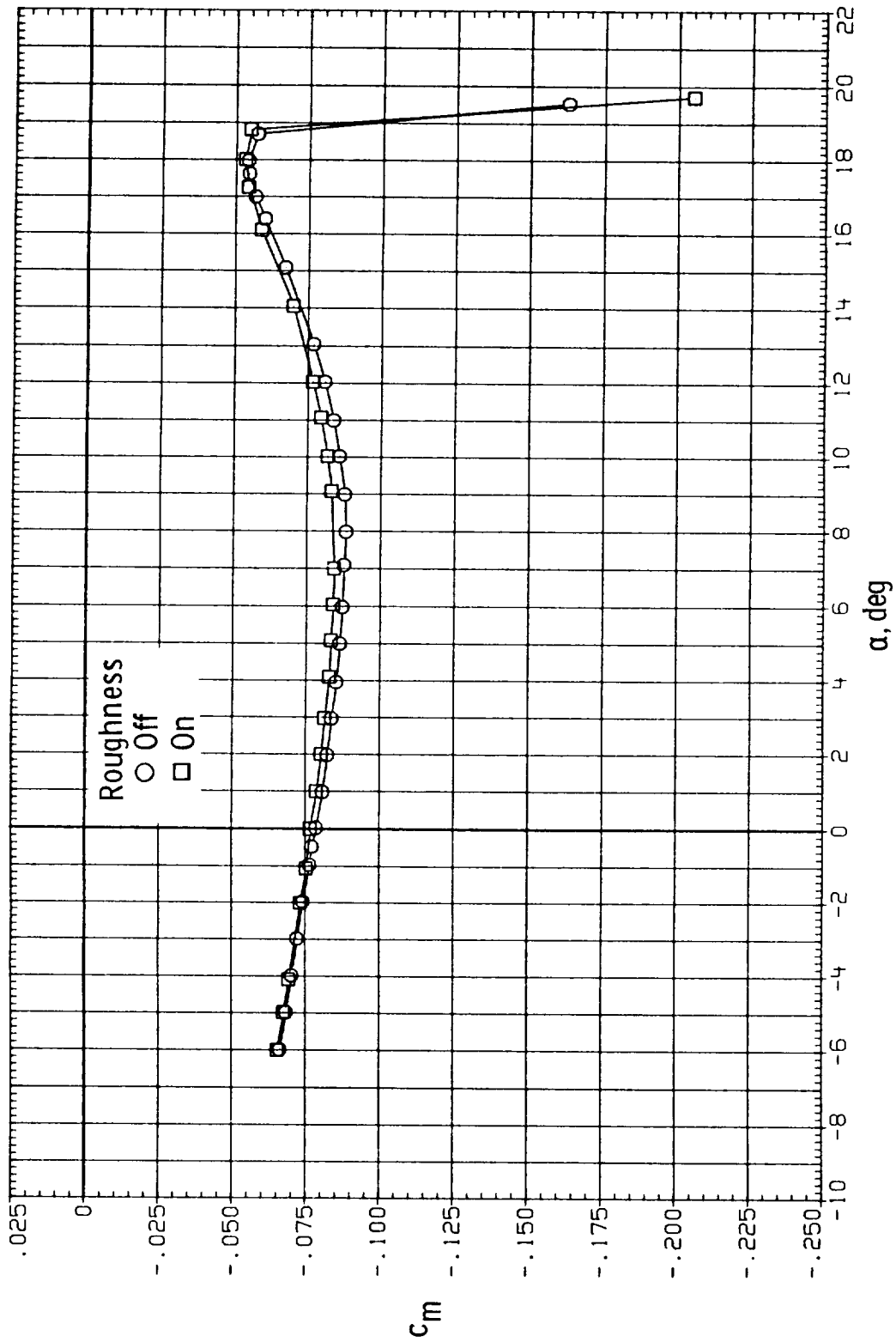
(e) $R = 12.0 \times 10^6$.

Figure 8.- Continued.



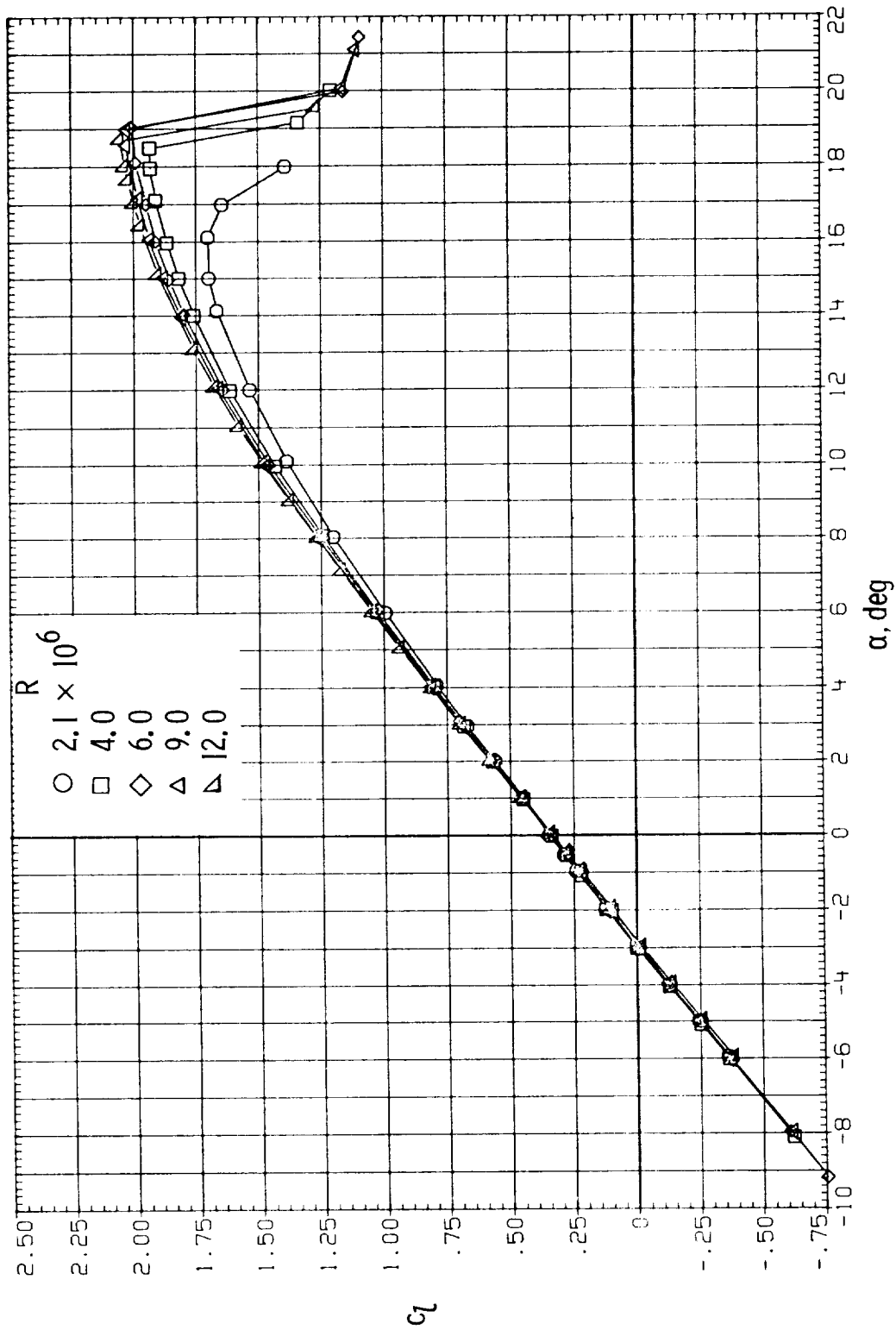
(e) $R = 12.0 \times 10^6$. Continued.

Figure 8.- Continued.



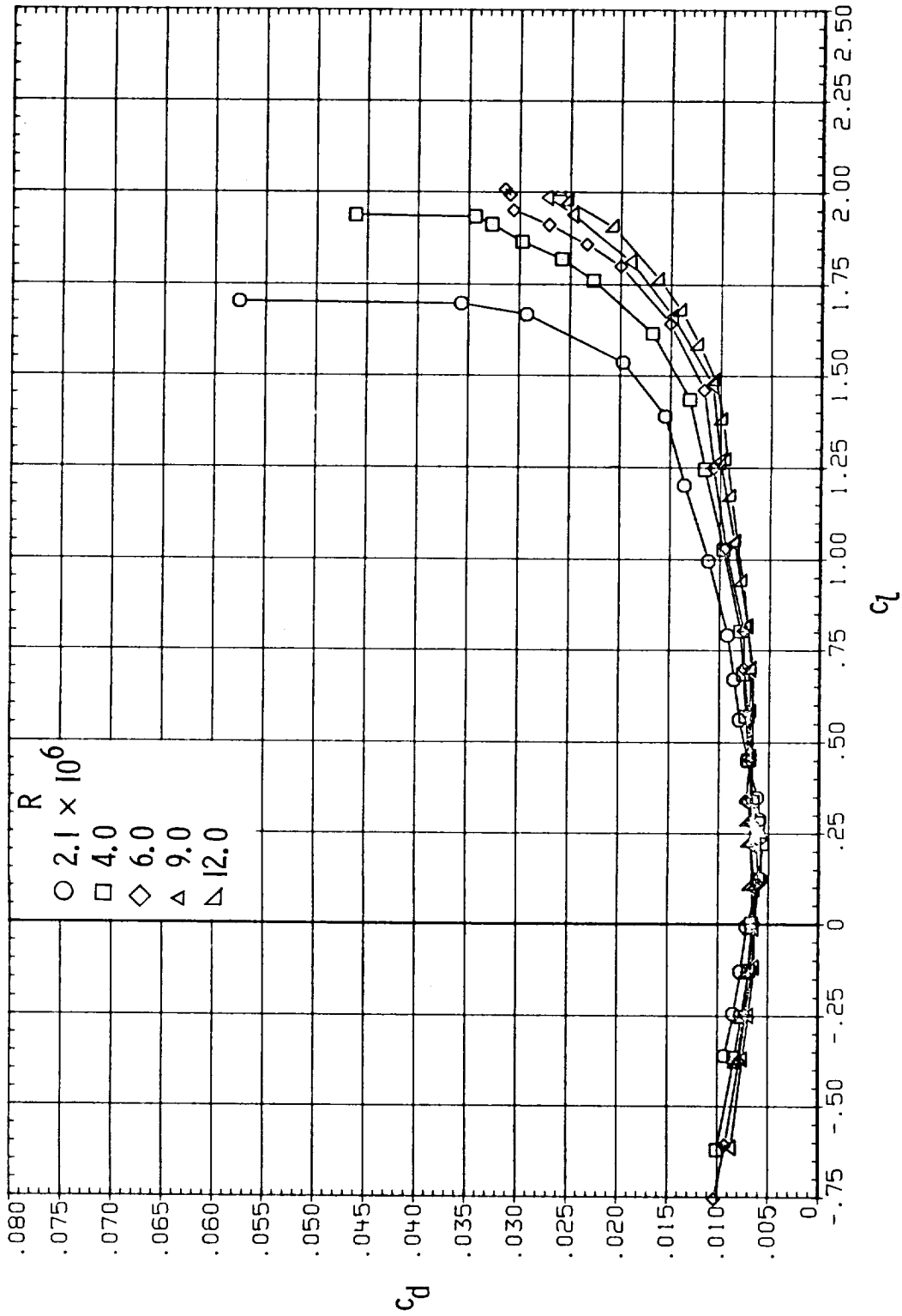
(e) $R = 12.0 \times 10^6$. Concluded.

Figure 8.- Concluded.



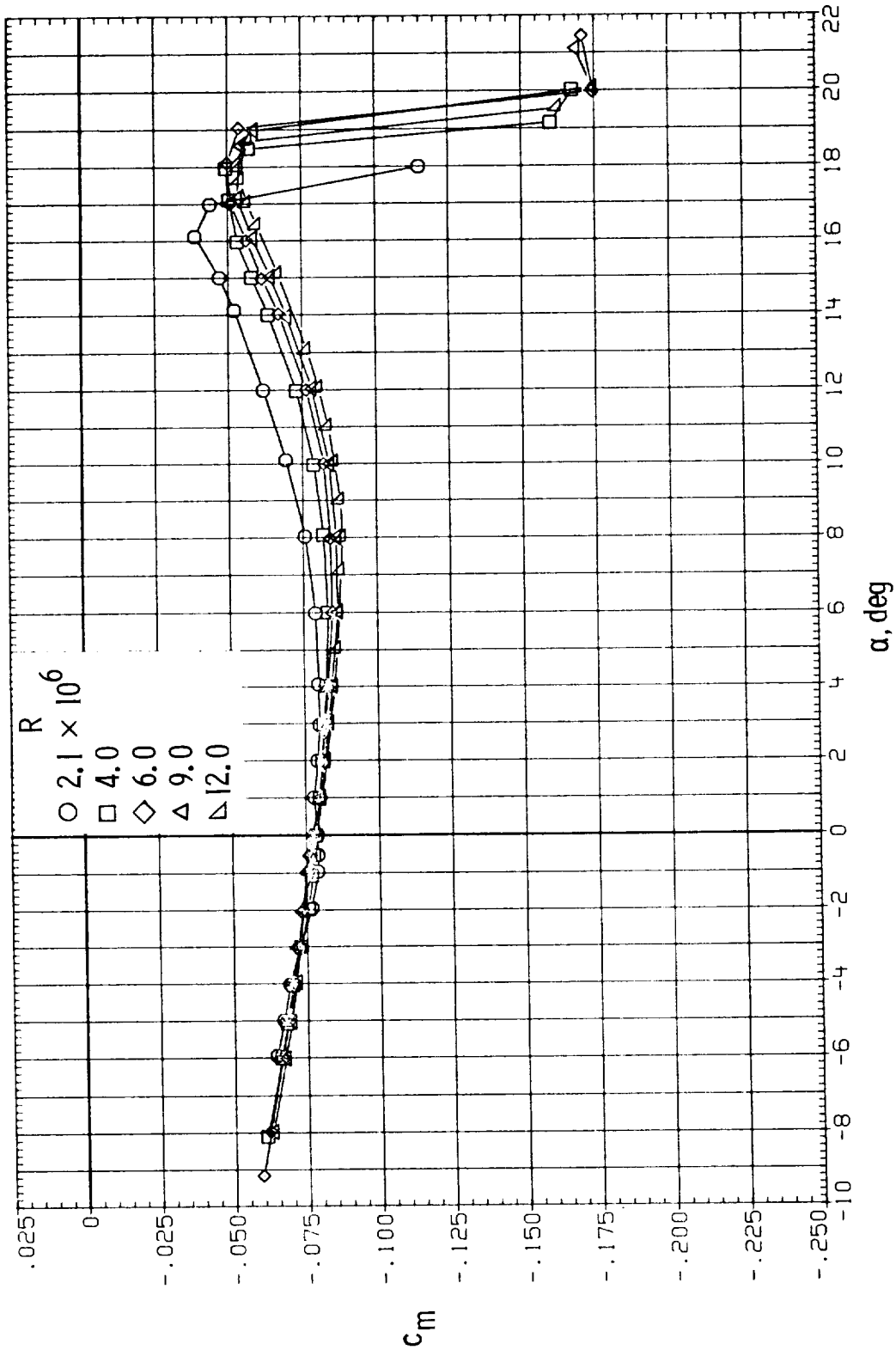
(a) Lift.

Figure 9.- Effect of Reynolds number on section characteristics. Model smooth; $M = 0.15$.



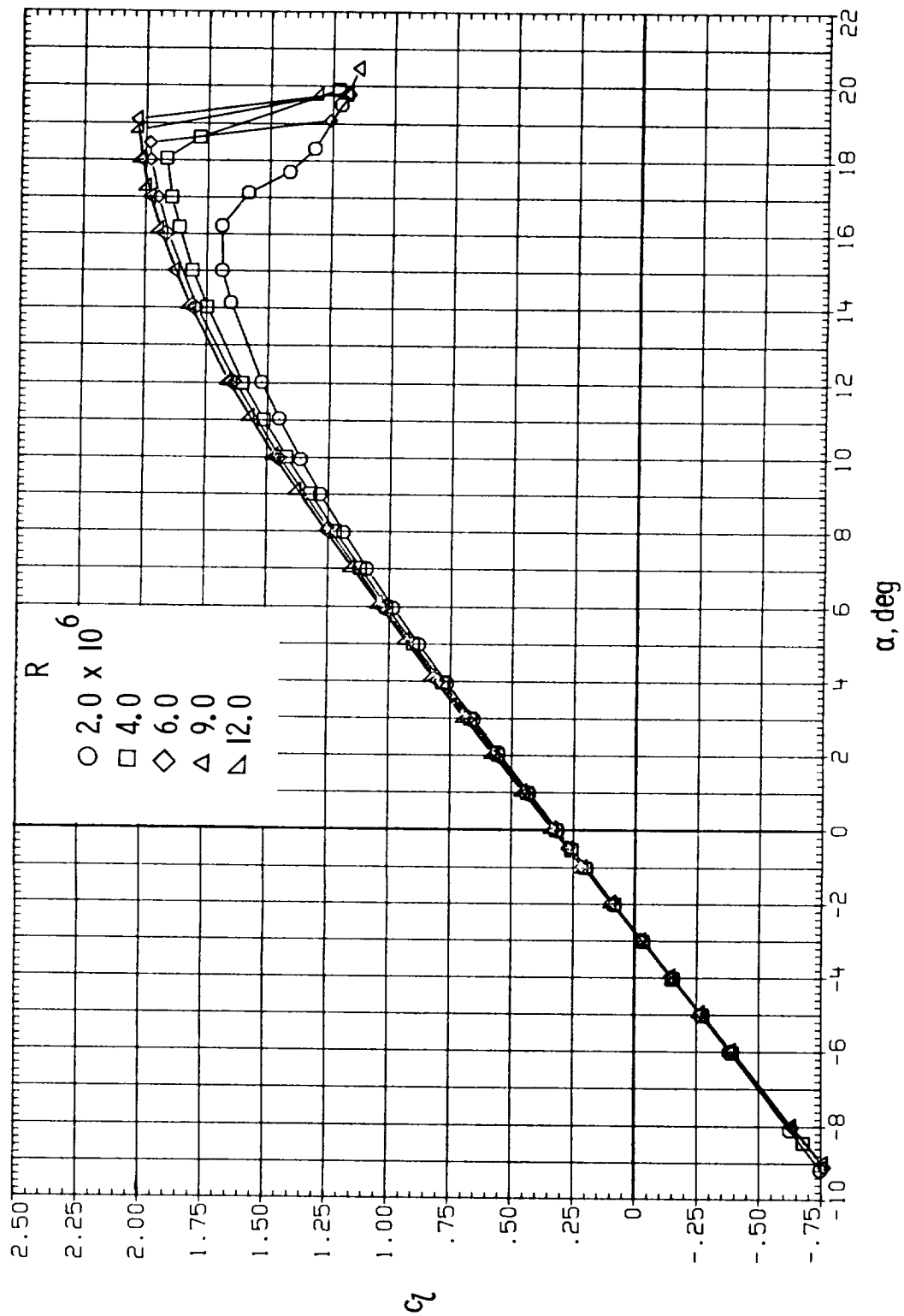
(b) Drag.

Figure 9.- Continued.



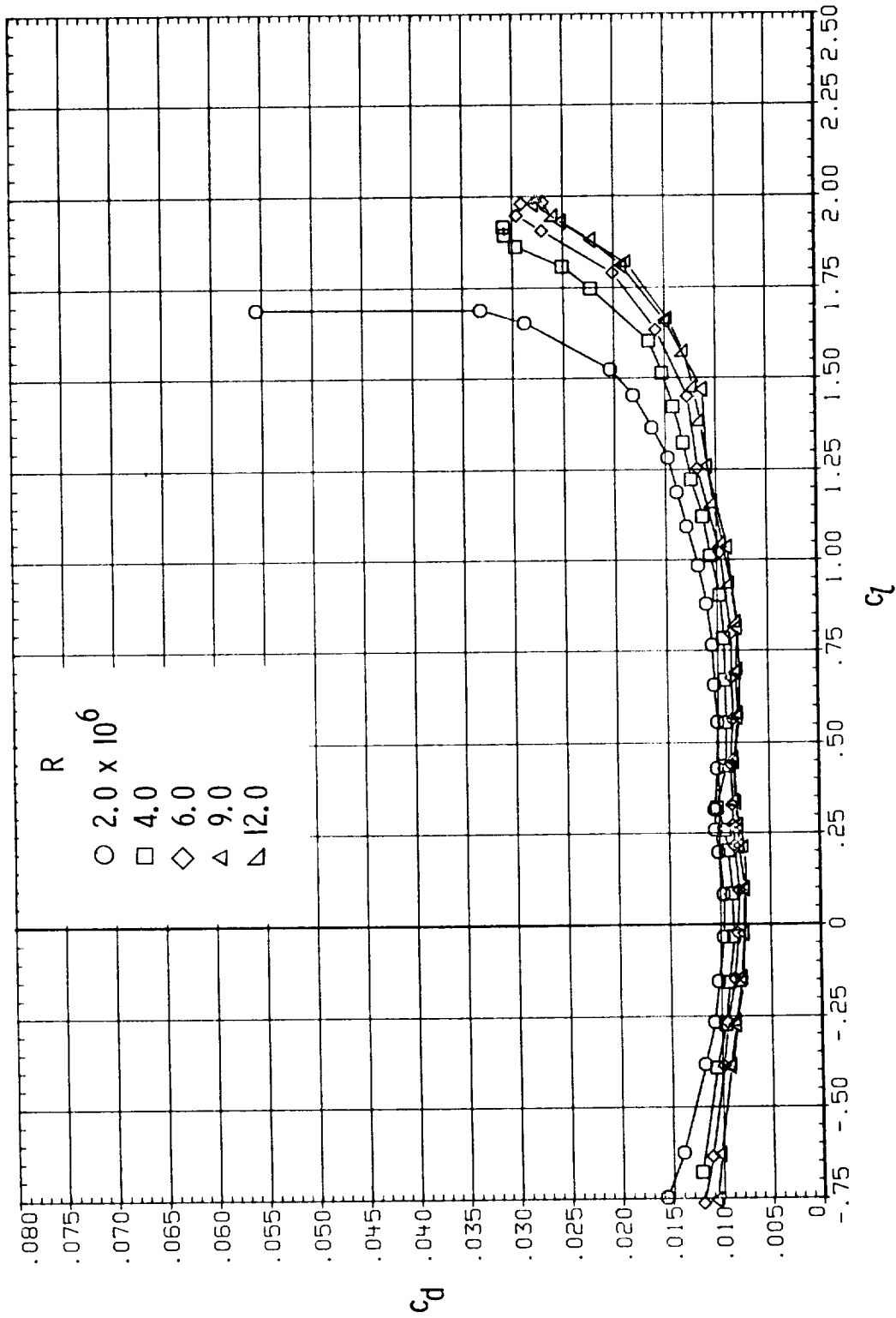
(c) Pitching moment.

Figure 9.- Concluded.



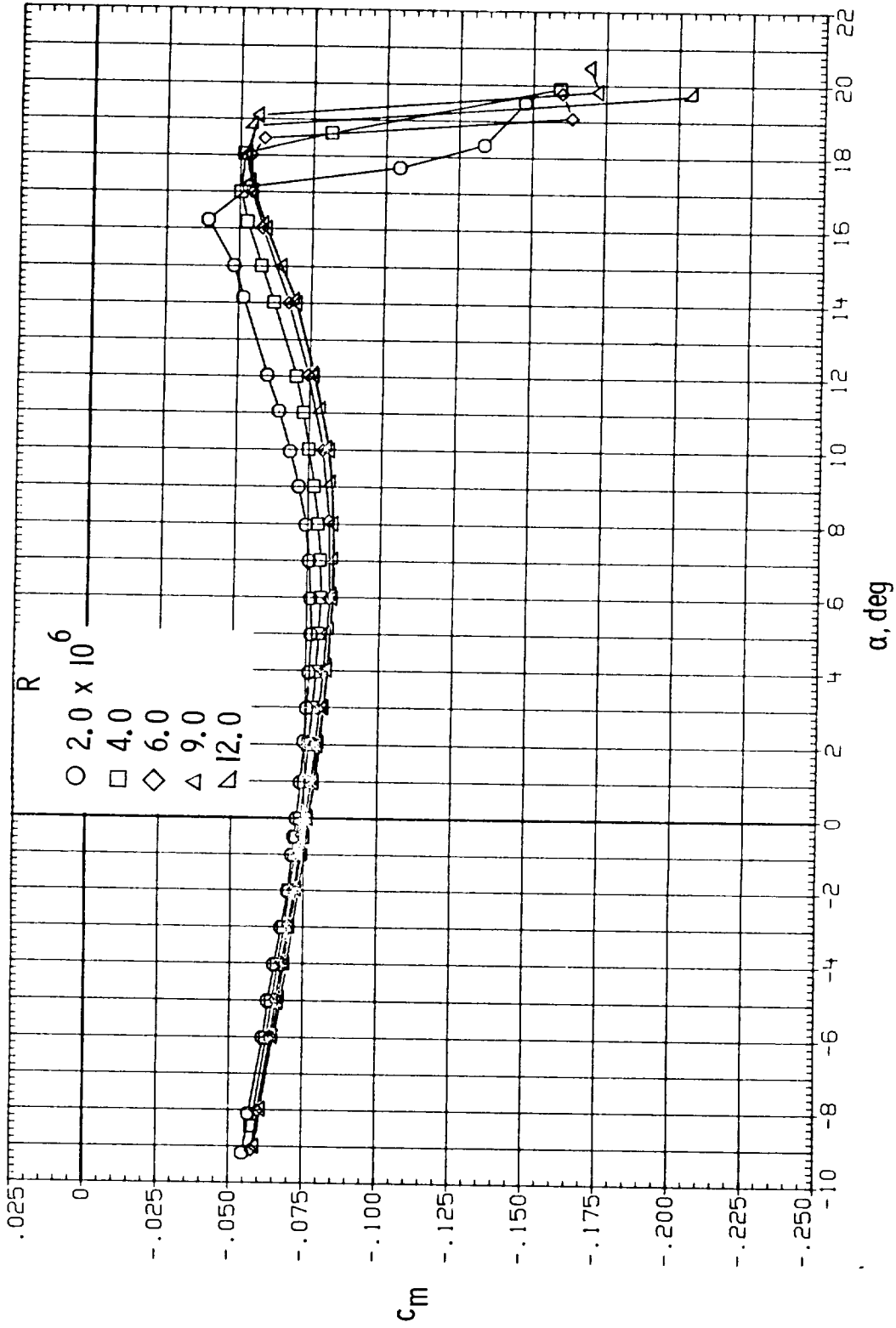
(a) Lift.

Figure 10.- Effect of Reynolds number on section characteristics. Roughness located at 0.075c; $M = 0.15$.



(b) Drag.

Figure 10.- Continued.



(c) Pitching moment.

Figure 10.- Concluded.

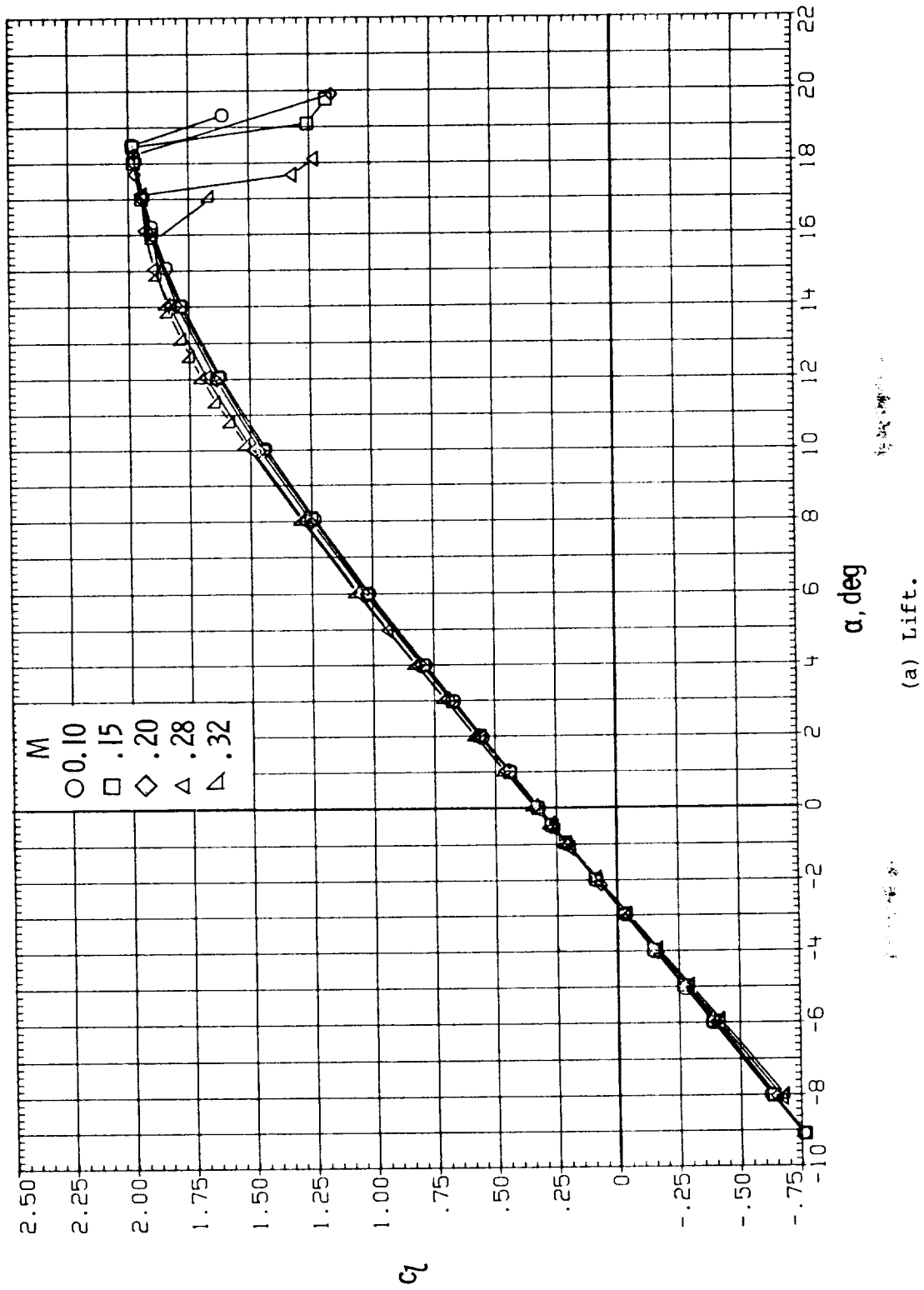
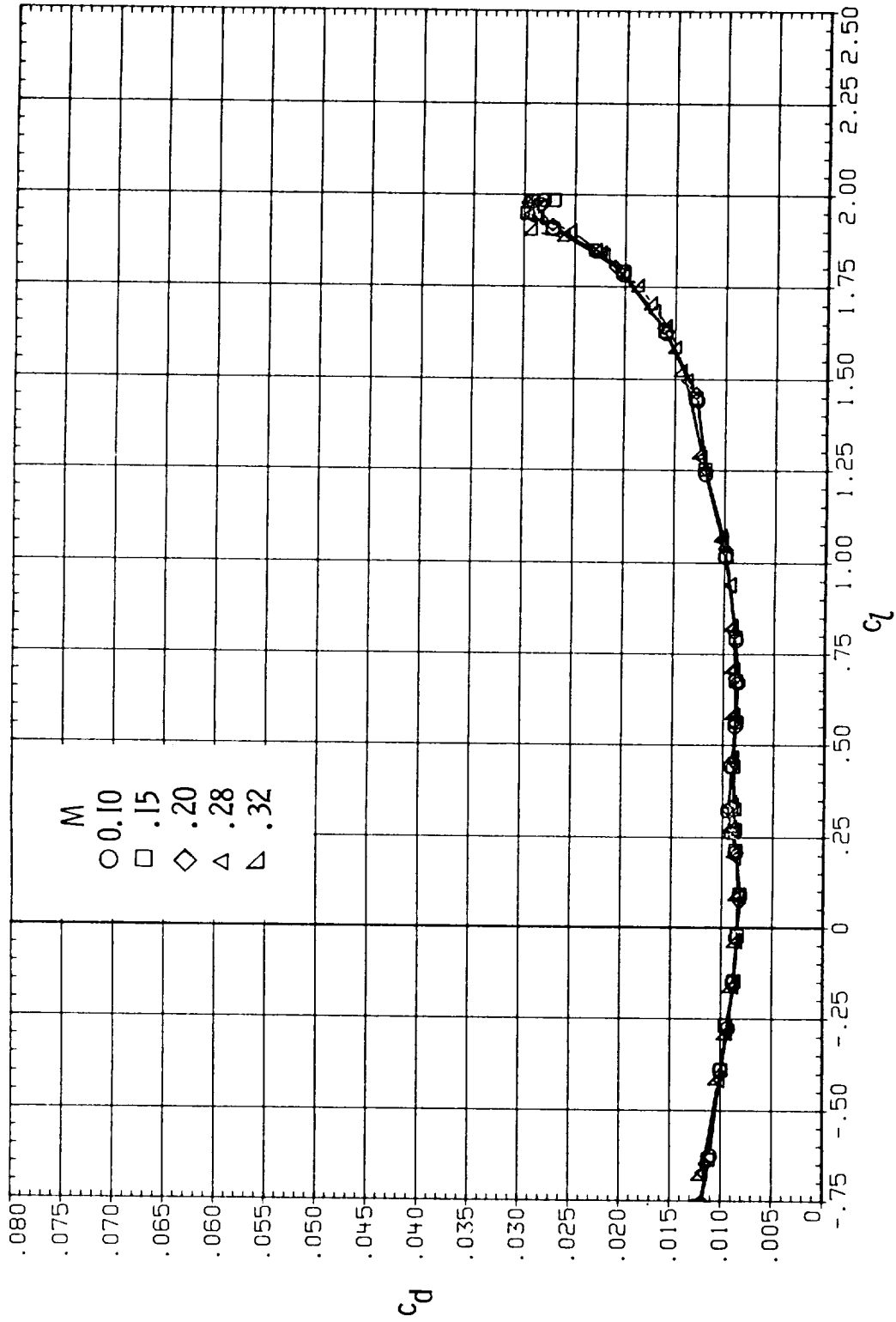


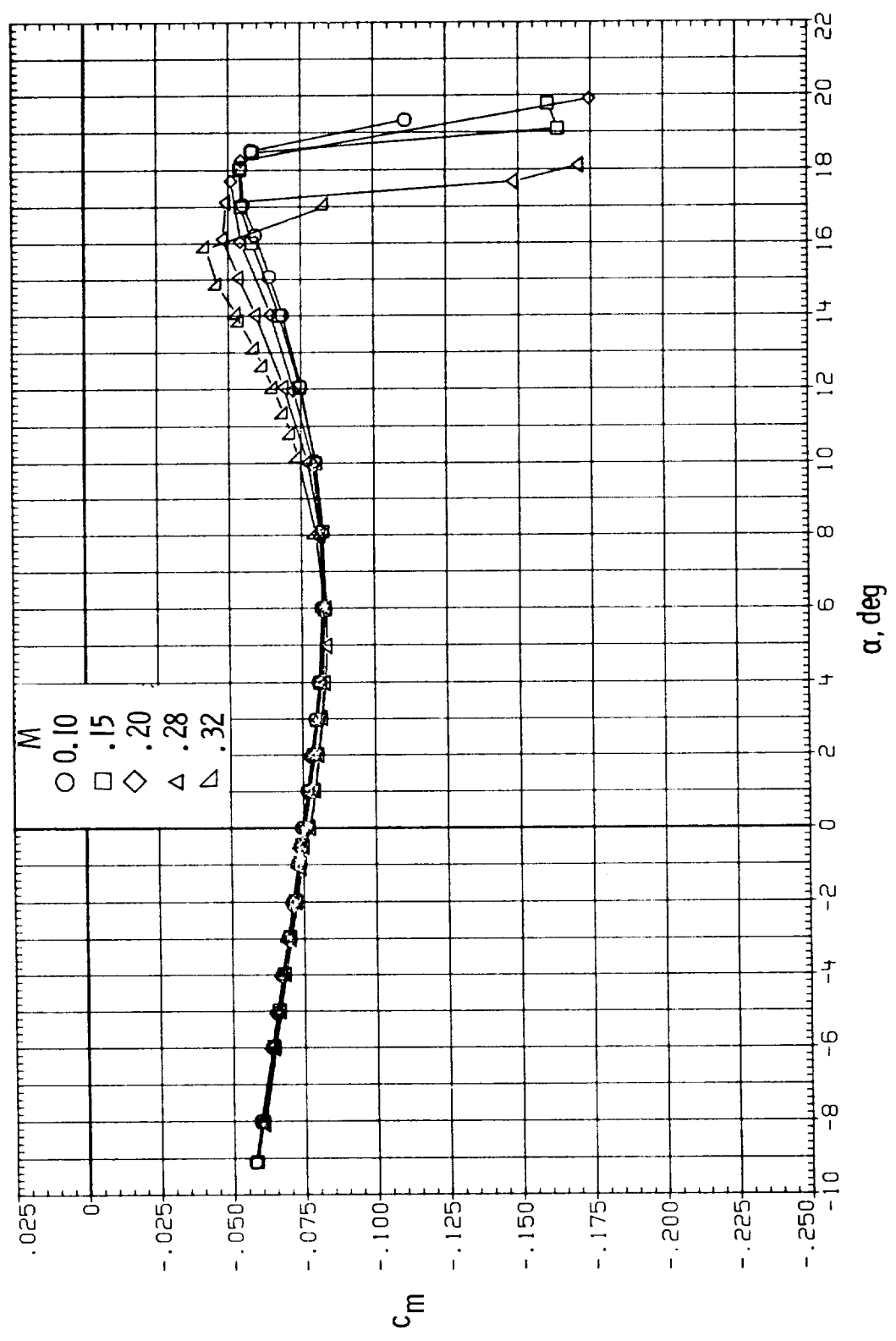
Figure 11.- Effect of Mach number on section characteristics. Roughness located at 0.075c; $R = 6.0 \times 10^6$.

(a) Lift.



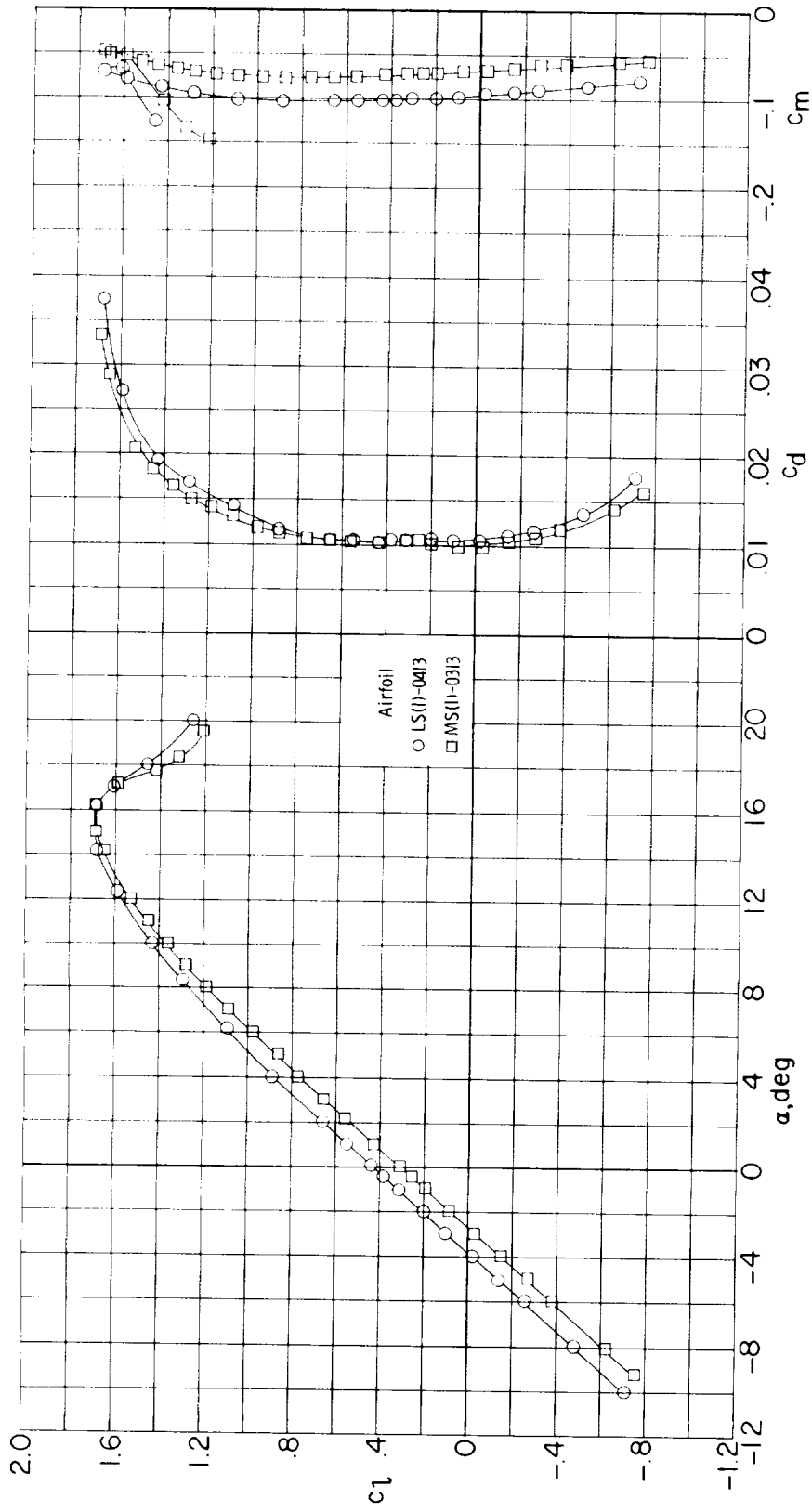
(b) Drag.

Figure 11.- Continued.



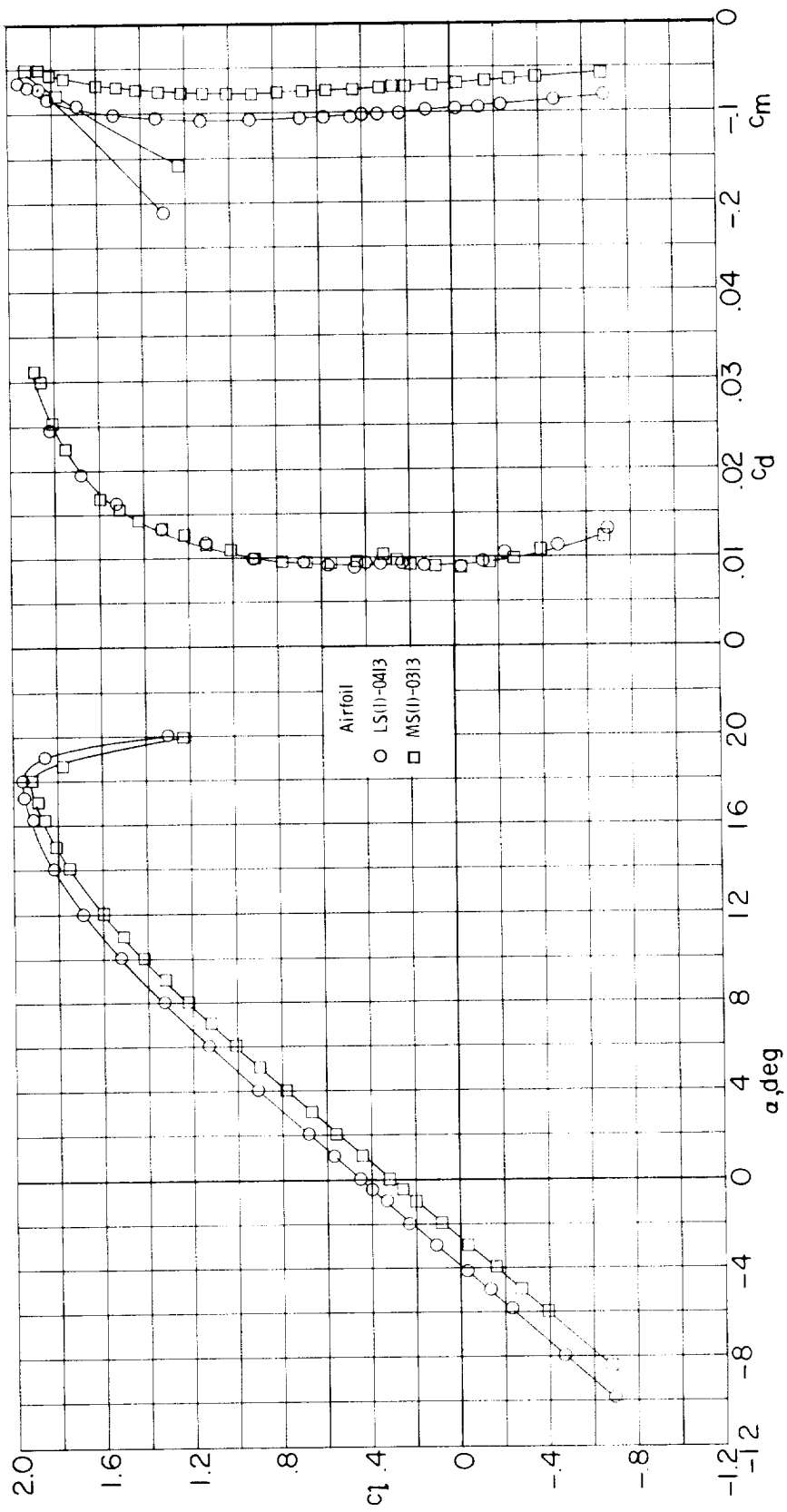
(c) Pitching moment.

Figure 11.- Concluded.



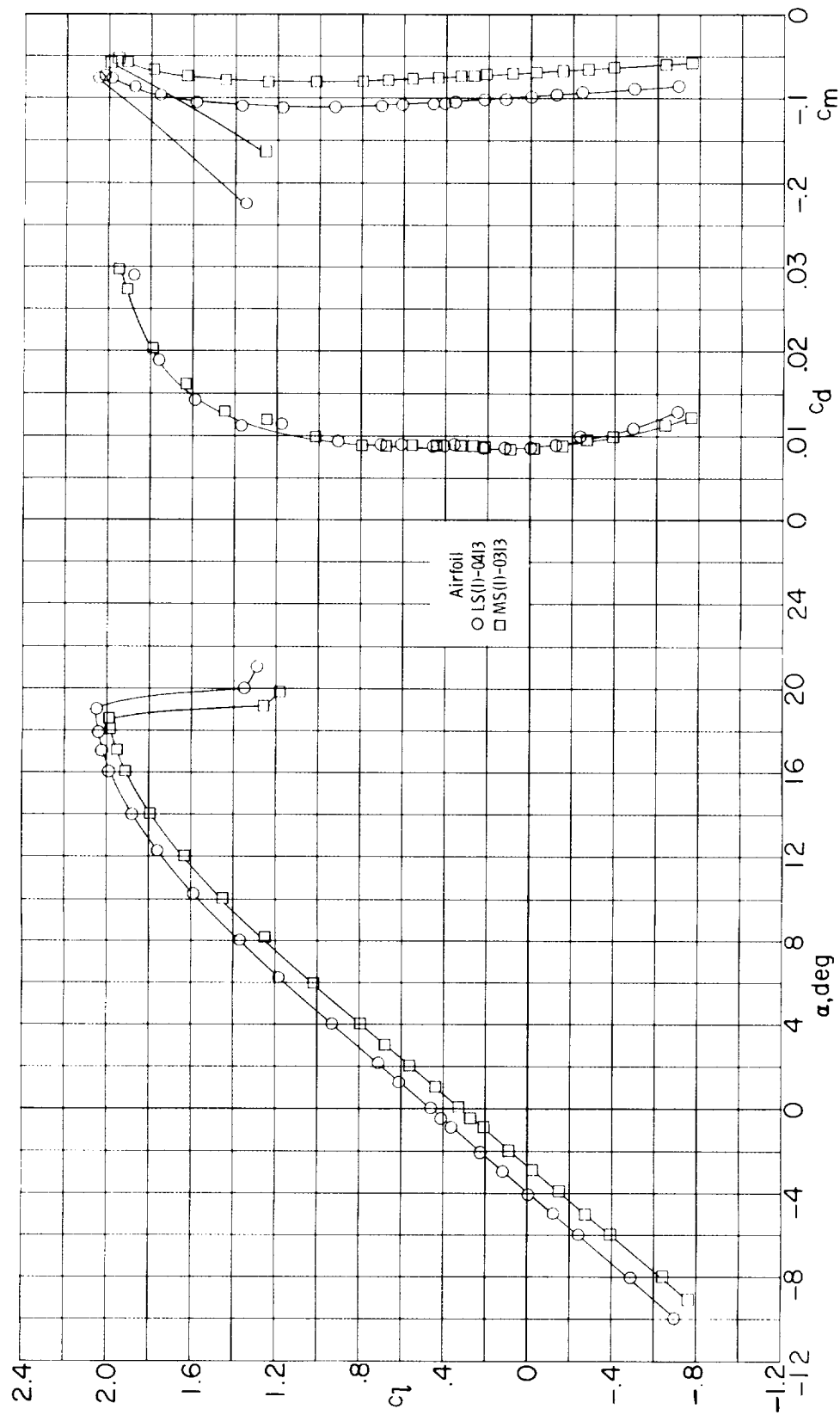
(a) $R = 2.0 \times 10^6$.

Figure 12.- Comparison of section characteristics for LS(1)-0413 and MS(1)-0313 airfoils. Roughness on; $M = 0.15$.

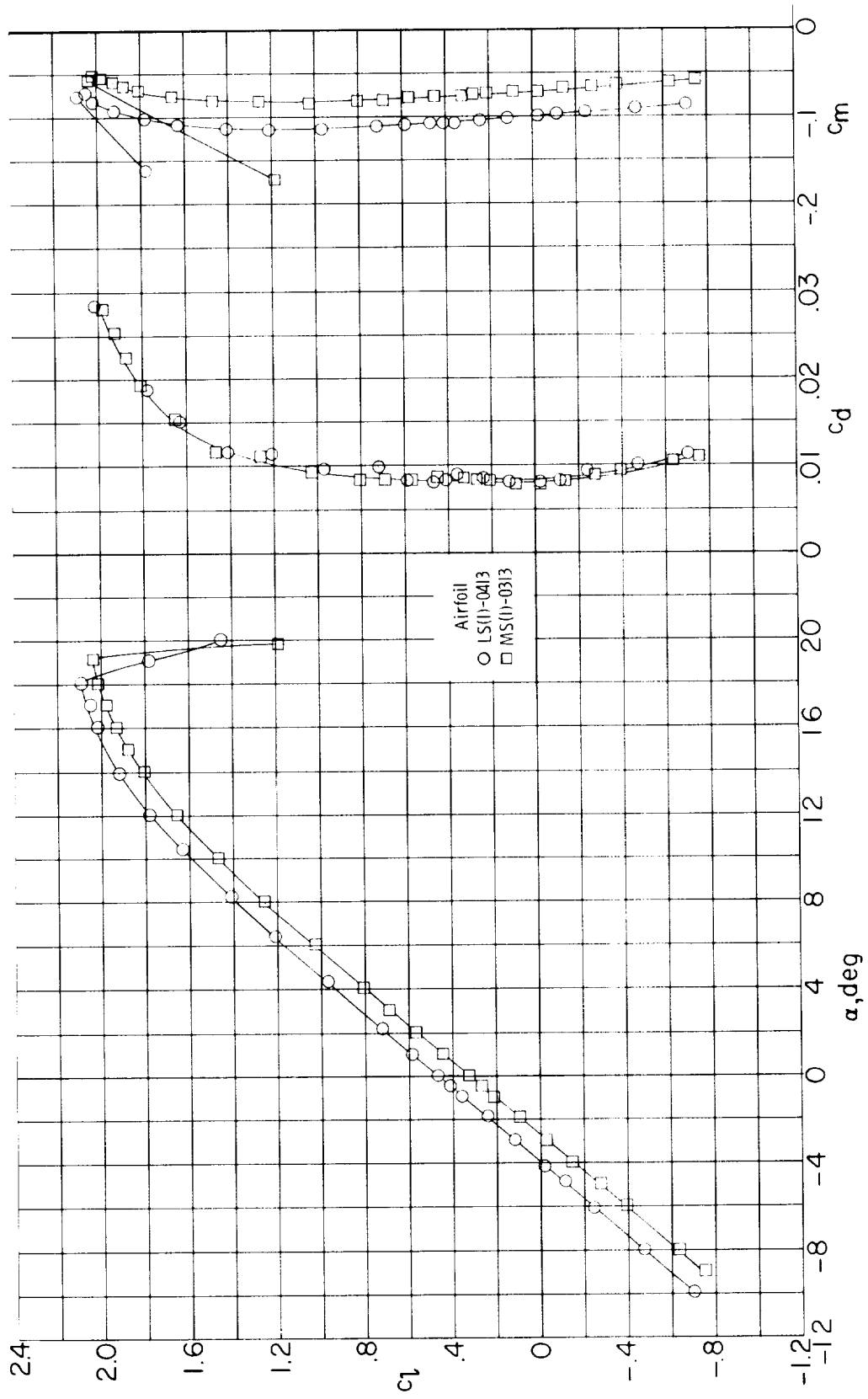


(b) $R = 4.0 \times 10^6$.

Figure 12.- Continued.

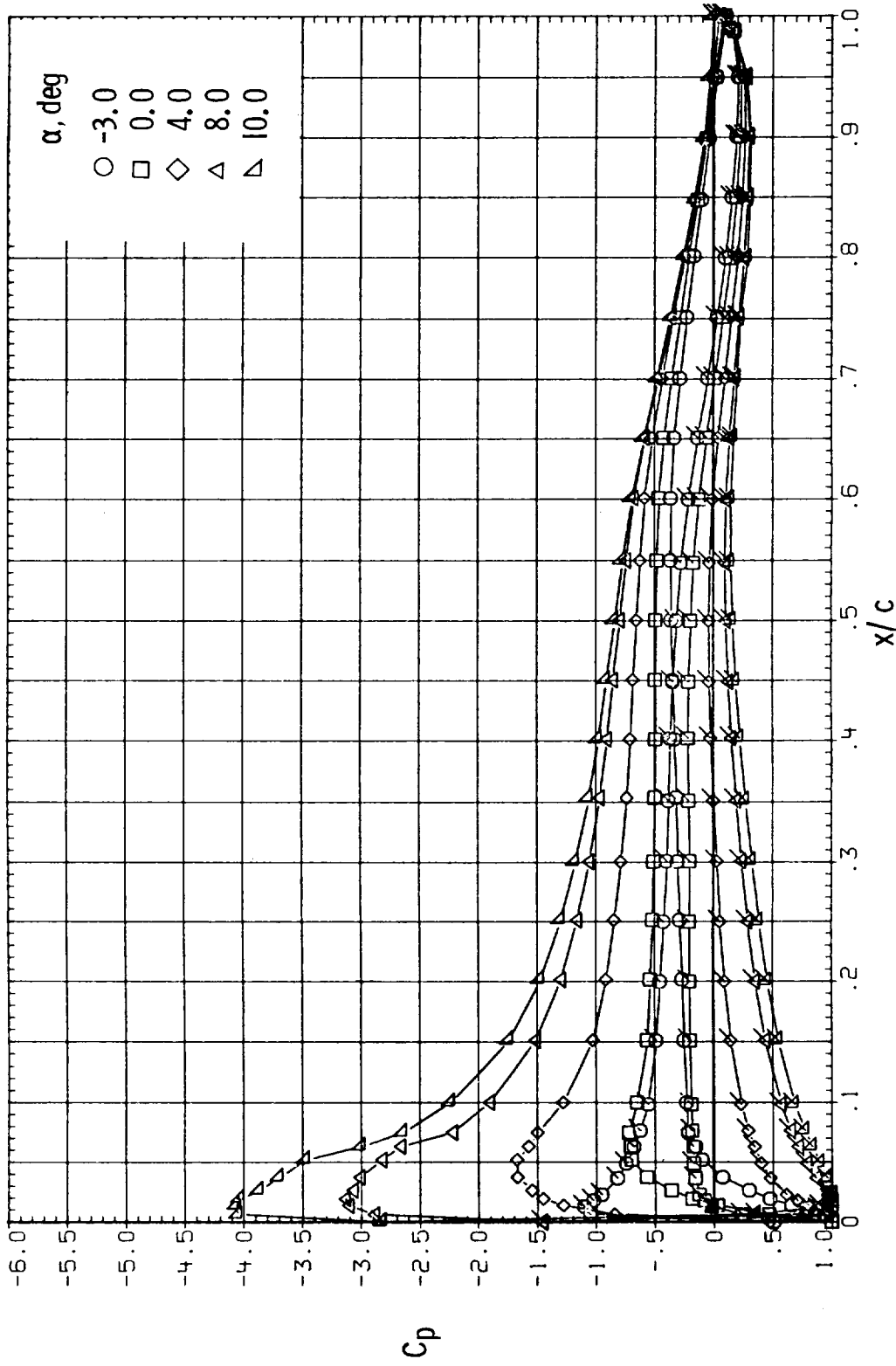


(c) $R = 6.0 \times 10^6$.
 Figure 12.- Continued.



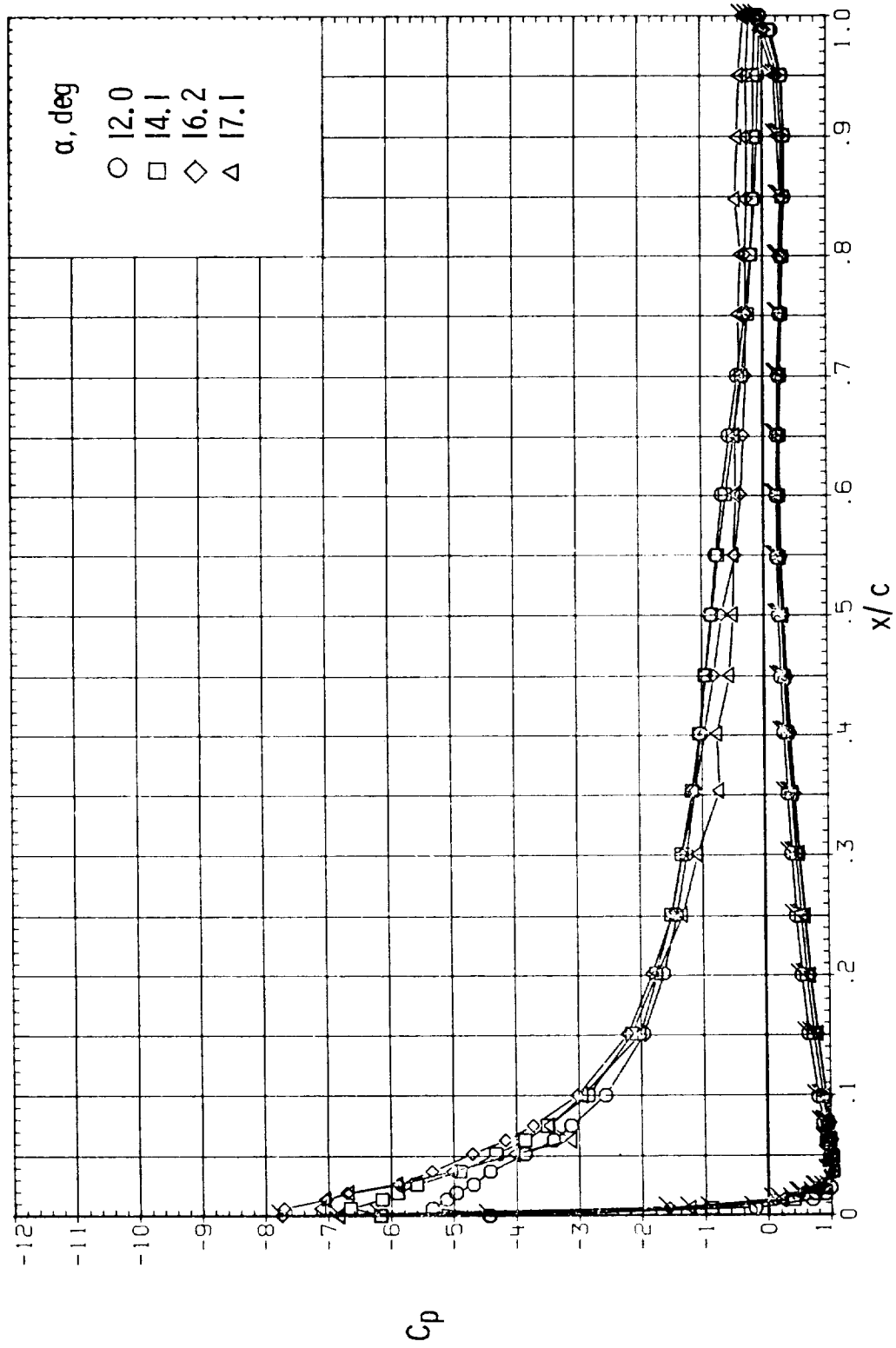
(d) $R = 9.0 \times 10^6$.

Figure 12.- Concluded.



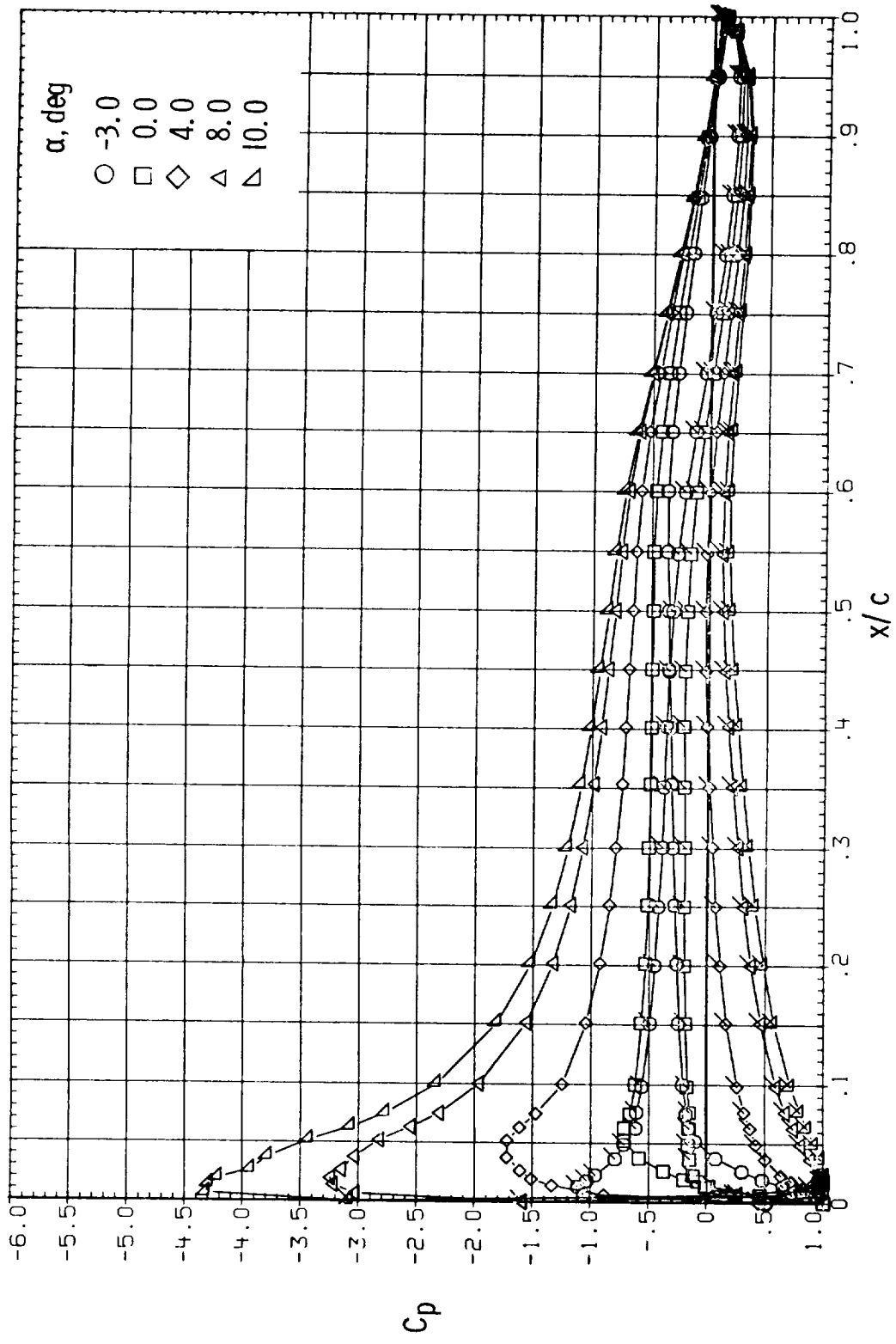
(a) $R = 2.0 \times 10^6$.

Figure 13.- Effect of angle of attack and Reynolds number on chordwise pressure distributions for MS(1)-0313 airfoil. Roughness on; $M = 0.15$. (Flagged symbols designate lower surface.)



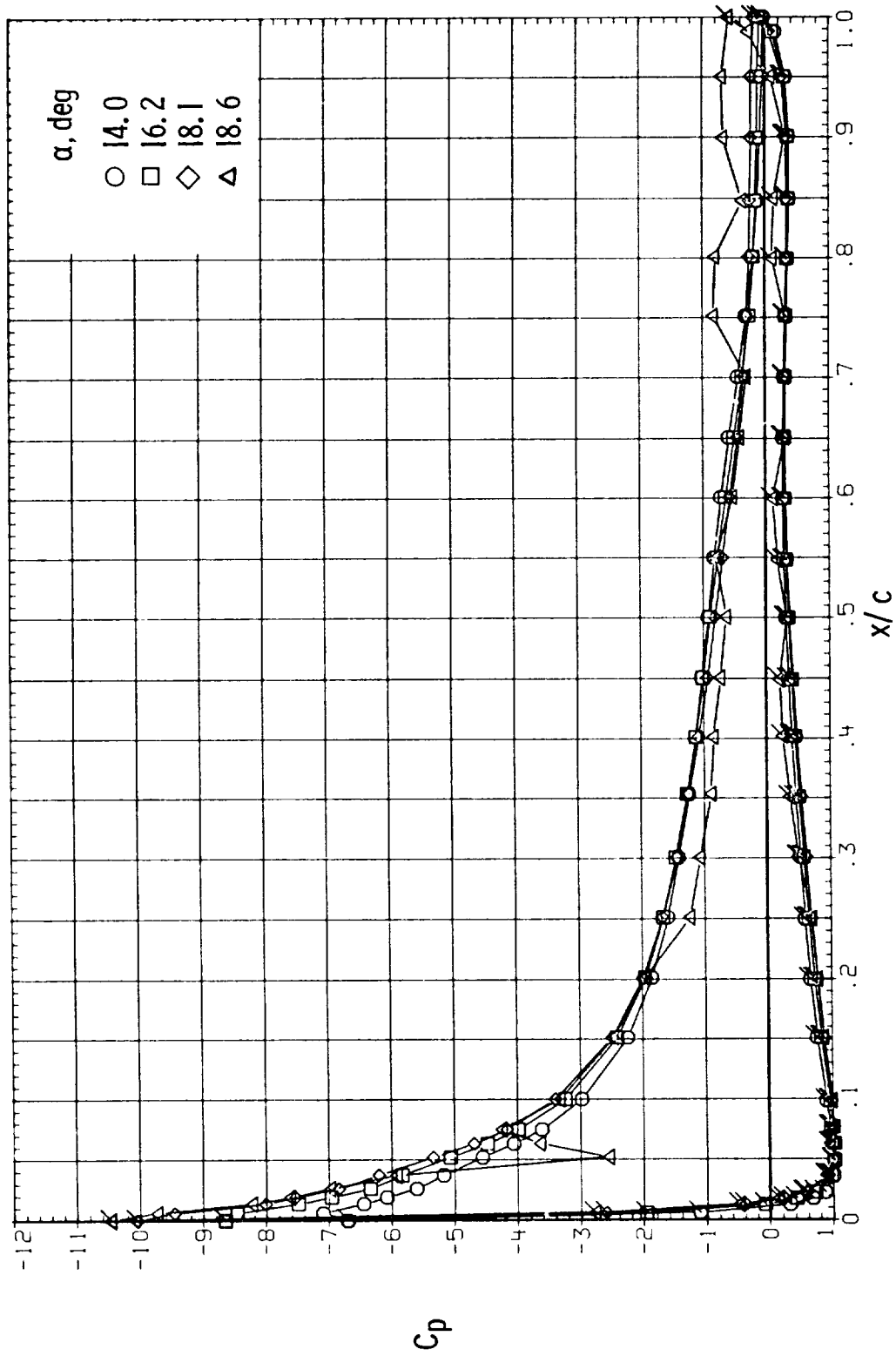
(a) $R = 2.0 \times 10^6$. Concluded.

Figure 13.- Continued.



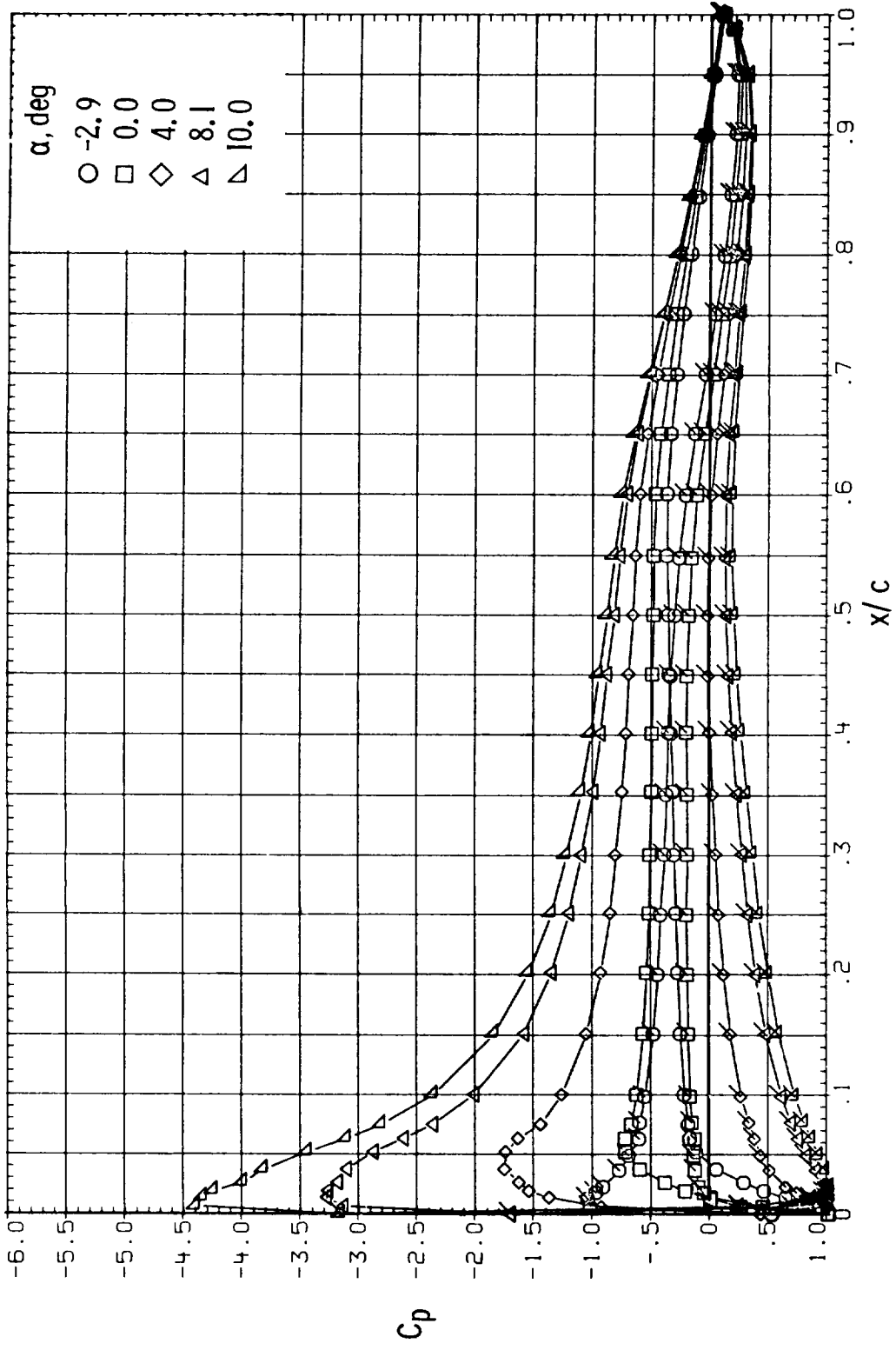
(b) $R = 4.0 \times 10^6$.

Figure 13.- Continued.



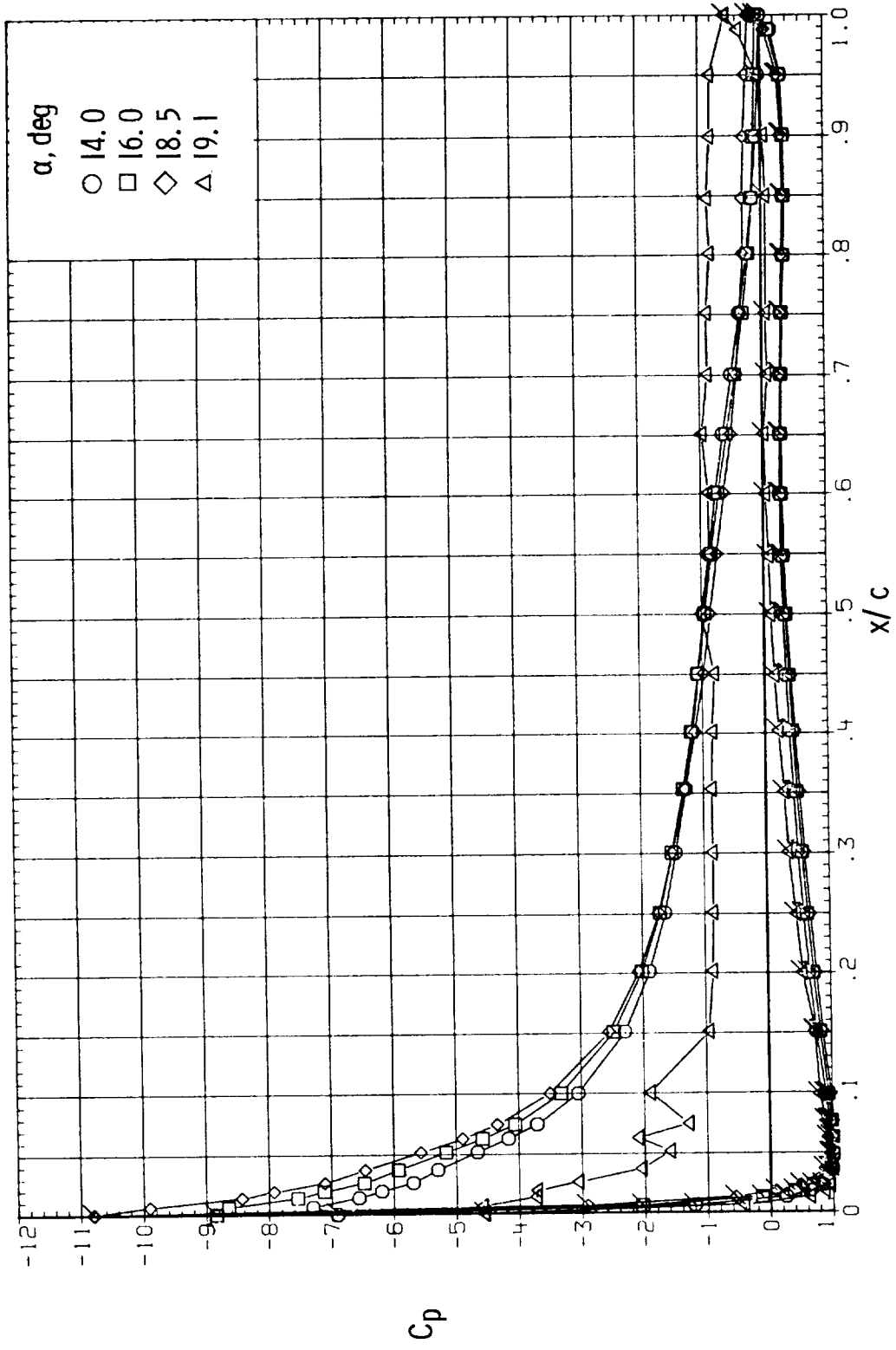
(b) $R = 4.0 \times 10^6$. Concluded.

Figure 13.- Continued.



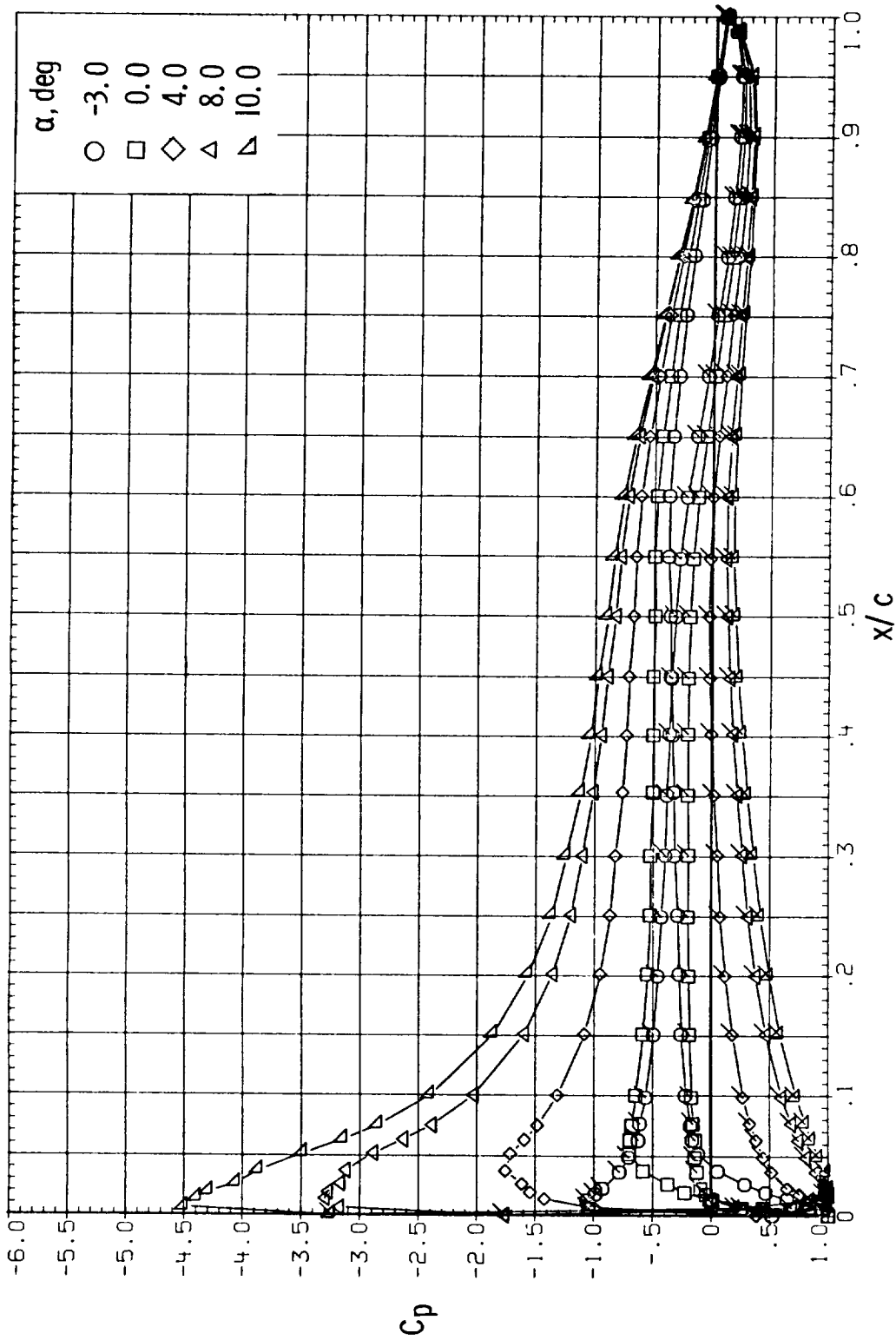
(c) $R = 6.0 \times 10^6$.

Figure 13.- Continued.



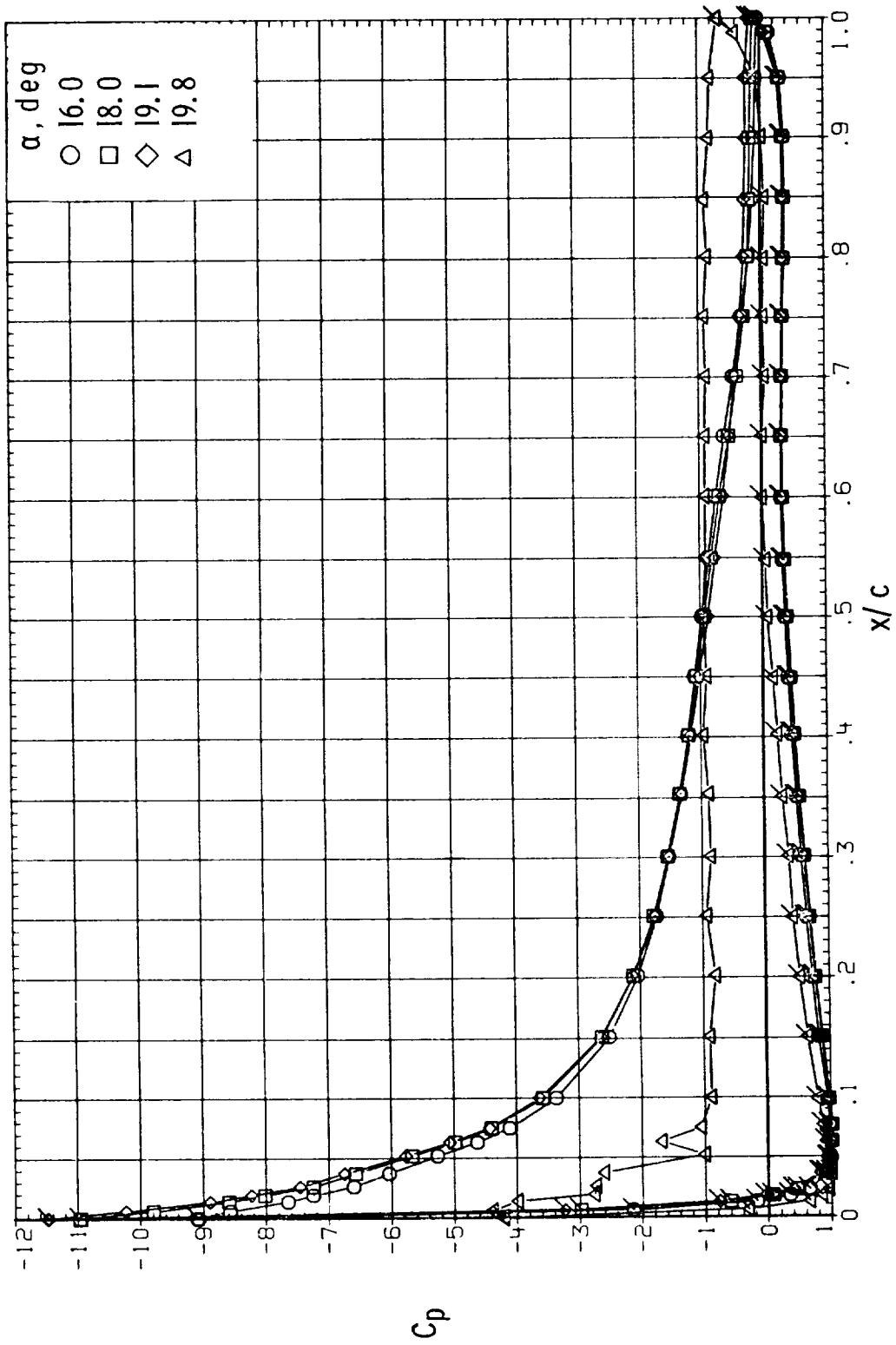
(c) $R = 6.0 \times 10^6$. Concluded.

Figure 13.- Continued.



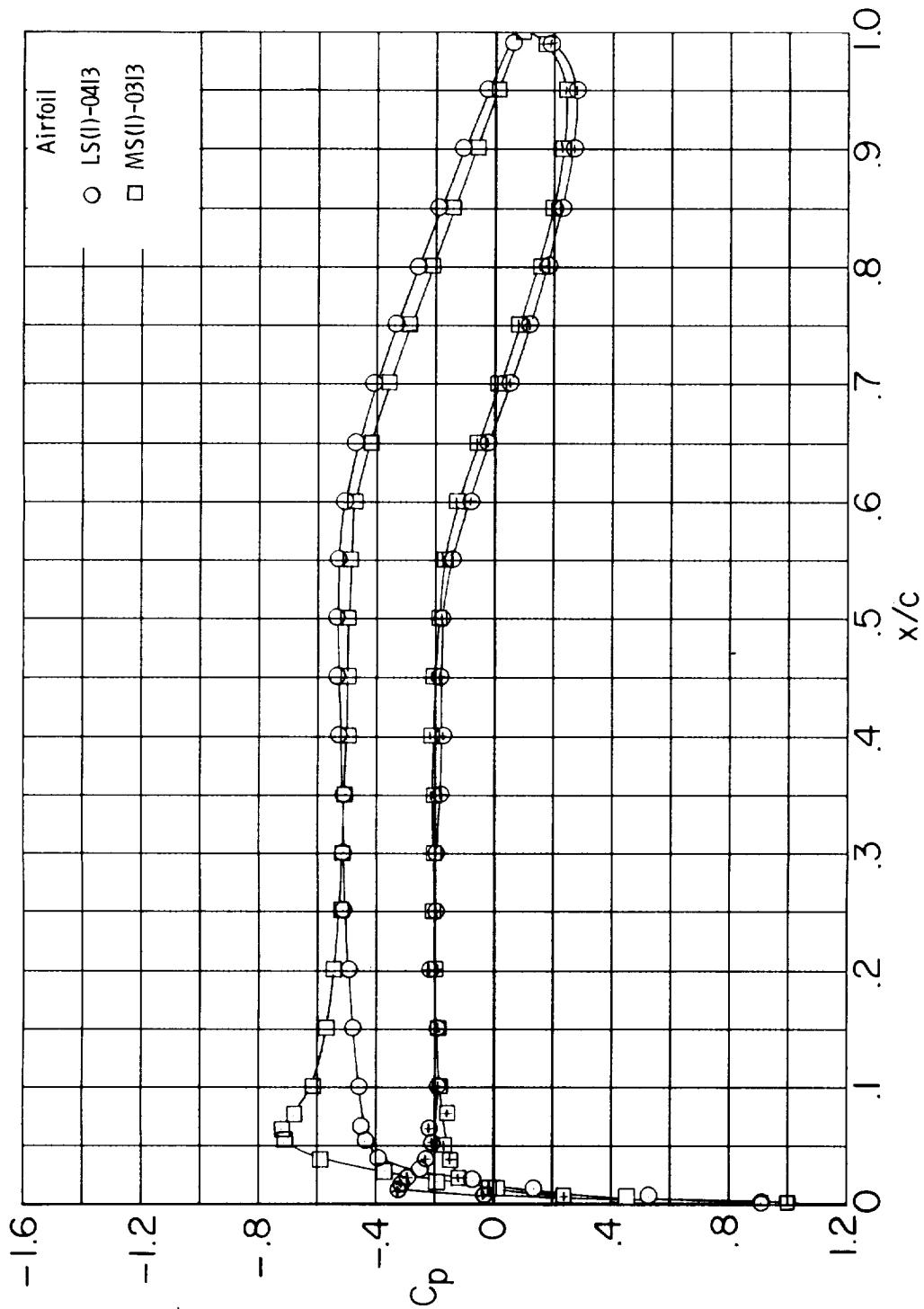
(d) $R = 9.0 \times 10^6$.

Figure 13.- Continued.



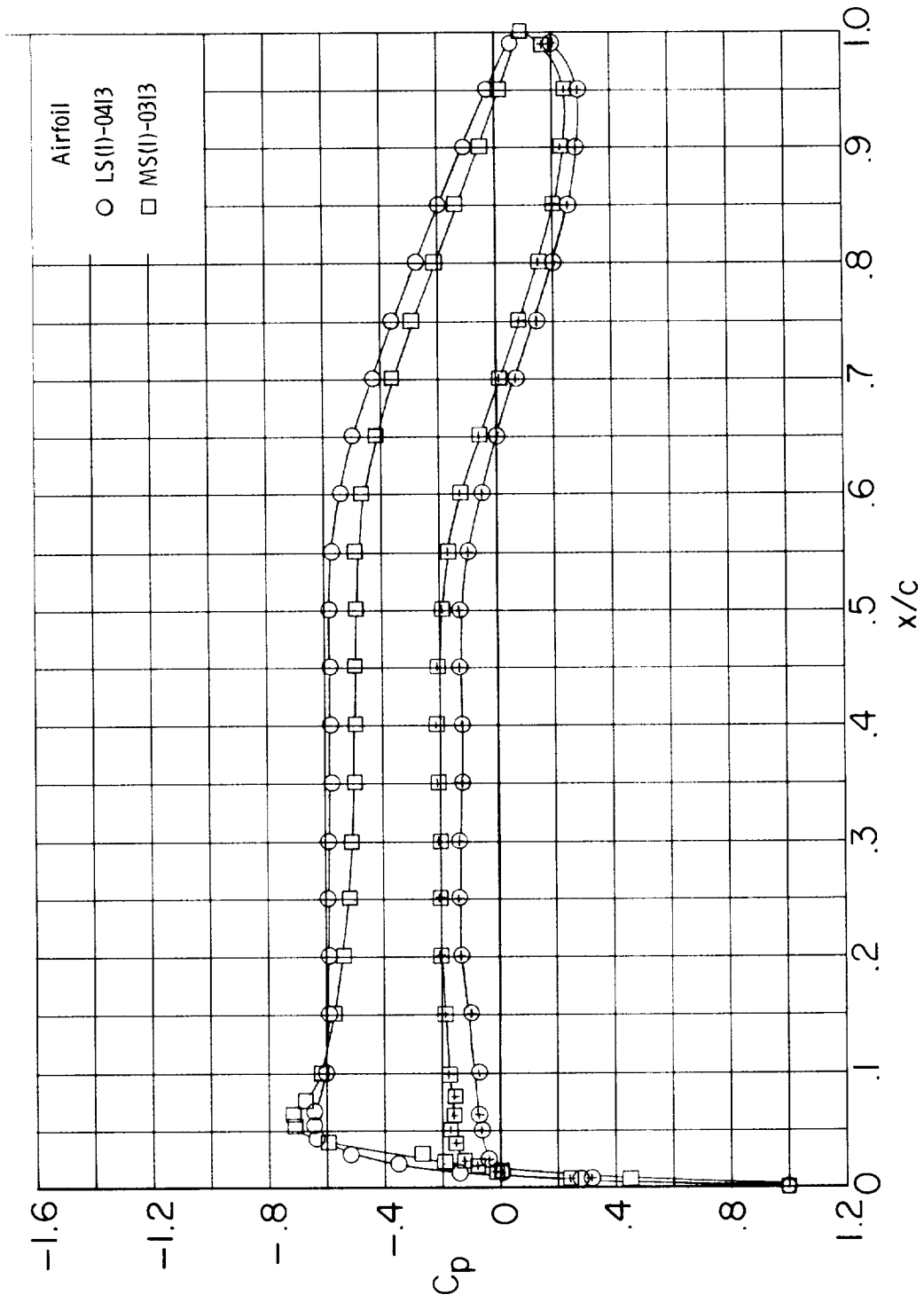
(d) $R = 9.0 \times 10^6$. Concluded.

Figure 13.- Concluded.



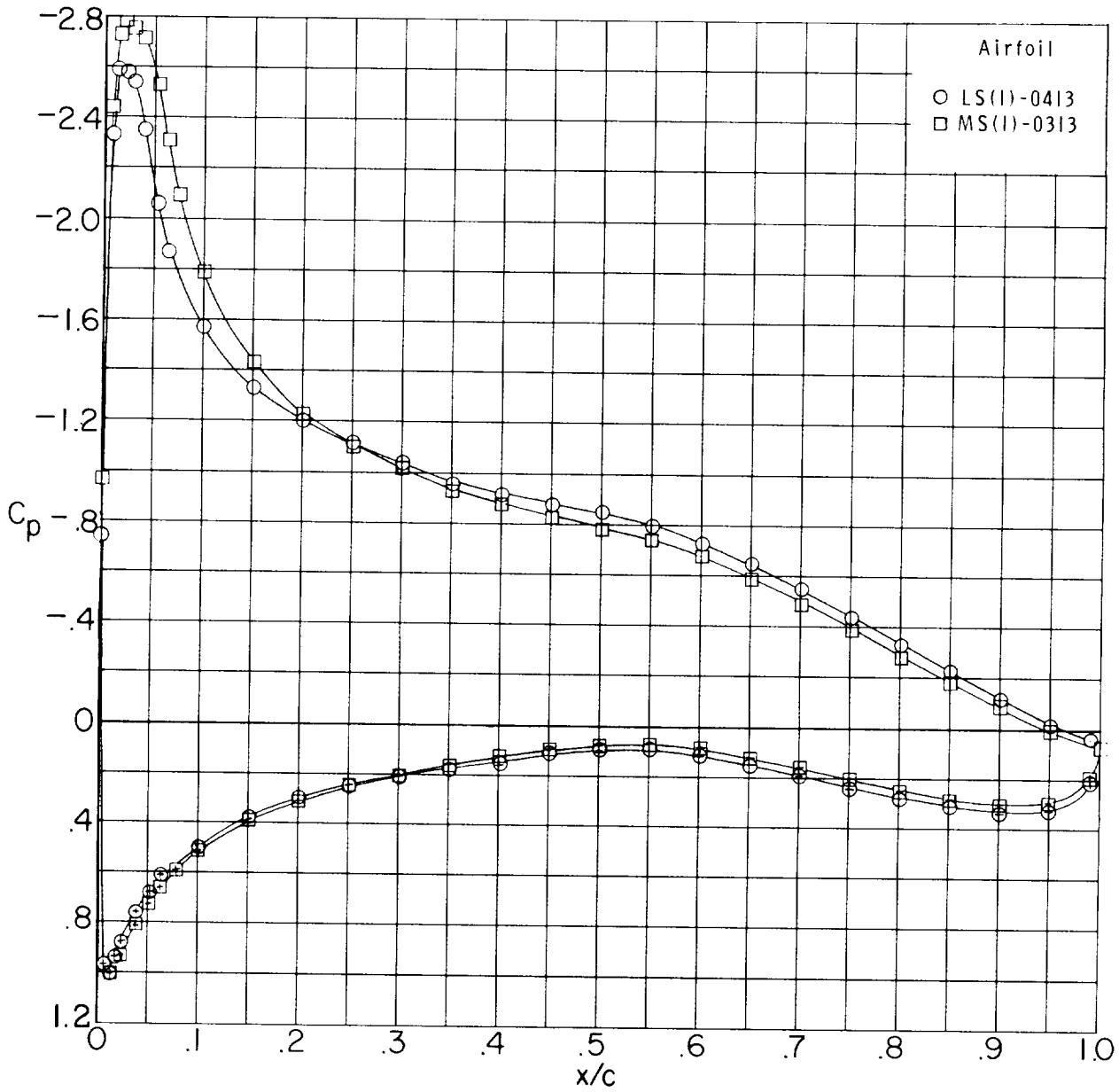
(a) $c_l = 0.3$; $R = 4.0 \times 10^6$.

Figure 14.- Comparison of chordwise pressure distributions for LS(1)-0413 and MS(1)-0313 airfoils. Roughness on; $M = 0.15$. (Symbols with + inside designate lower surface.)



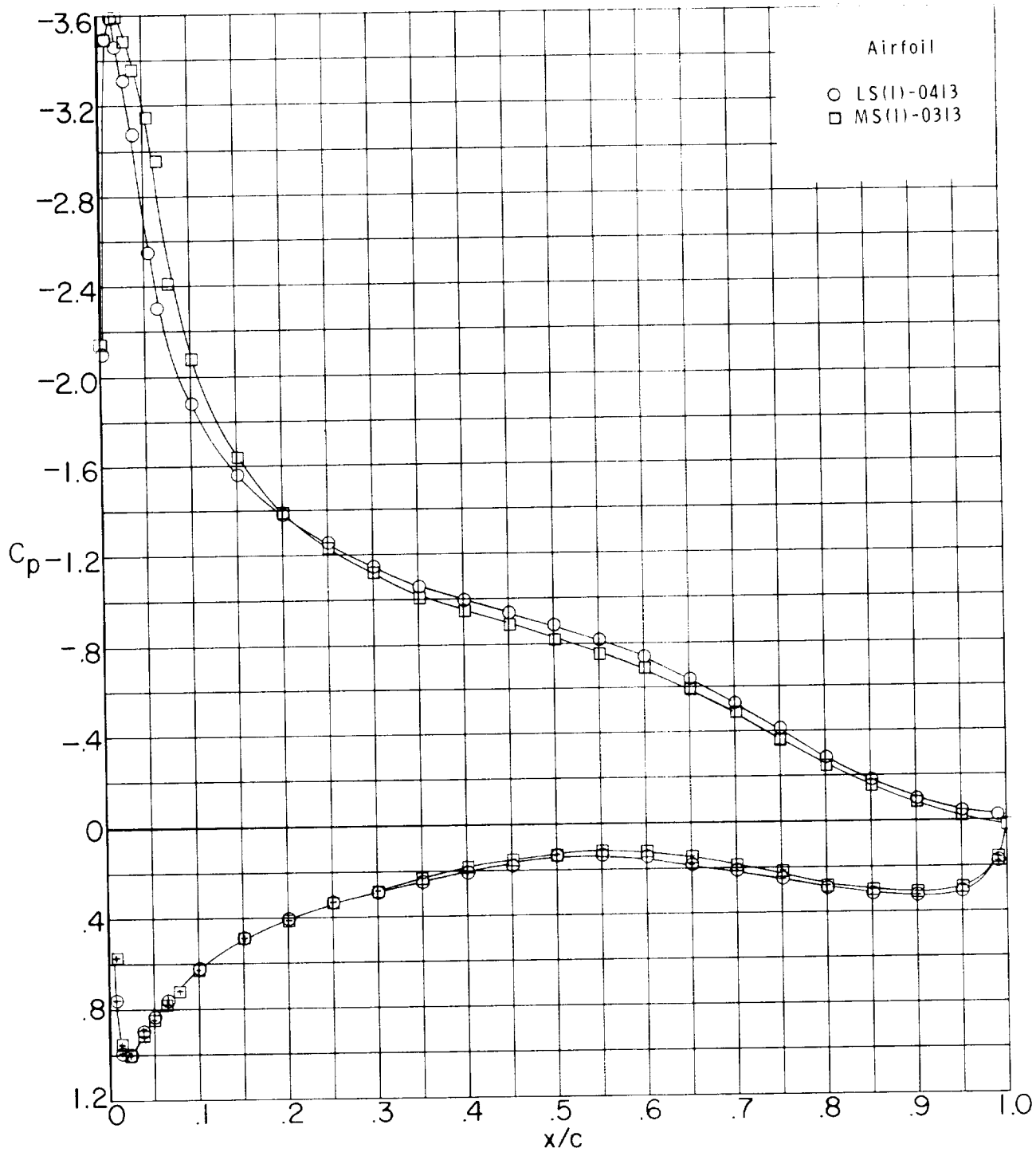
(b) $\alpha = 0^\circ$; $R = 4.0 \times 10^6$.

Figure 14.- Continued.



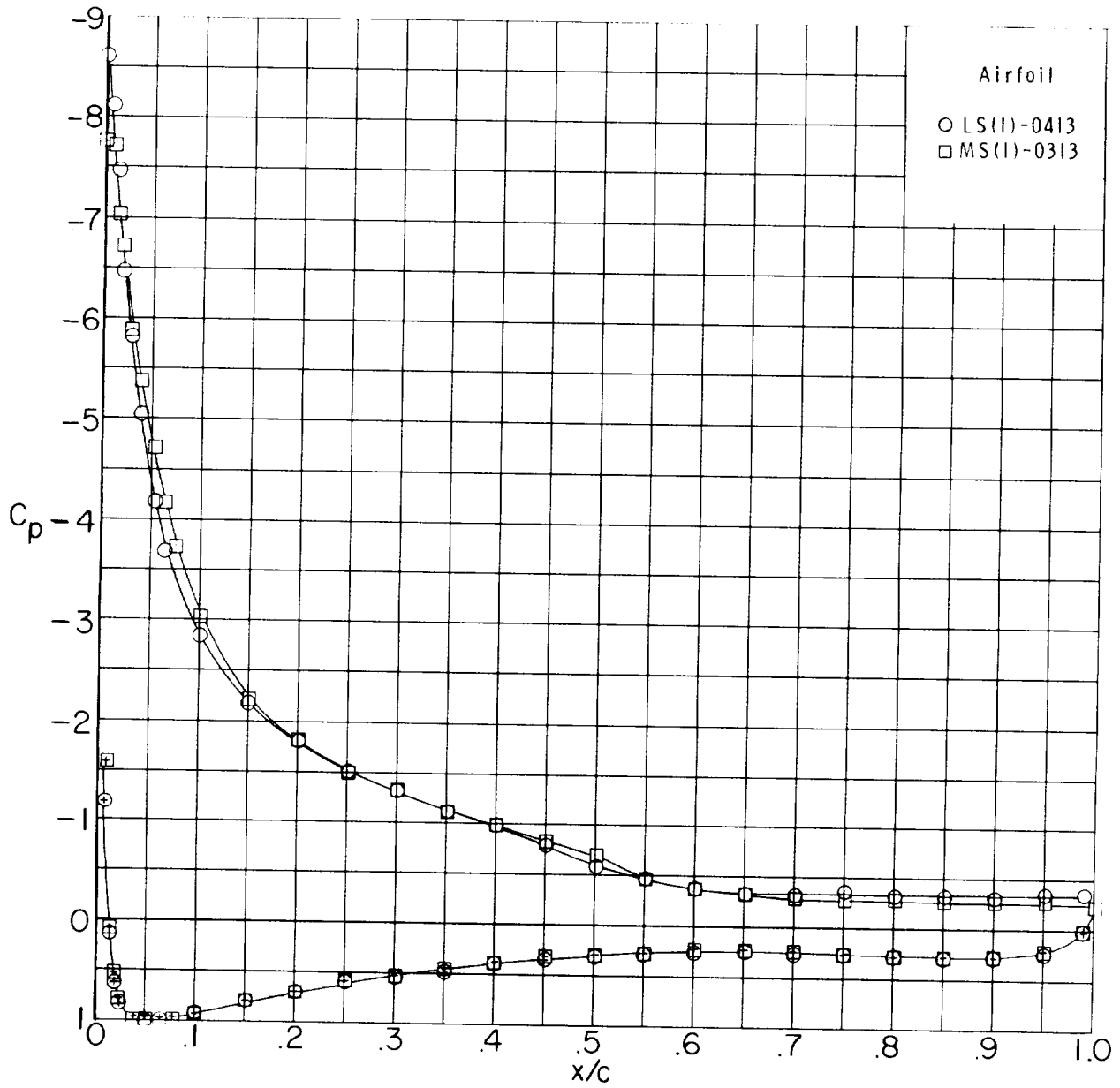
(c) $c_l = 1.1$; $R = 4.0 \times 10^6$.

Figure 14.- Continued.



(d) $c_l = 1.3$; $R = 2.0 \times 10^6$.

Figure 14.- Continued.



(e) $c_l = 1.7$; $R = 2.0 \times 10^6$.

Figure 14.- Concluded.

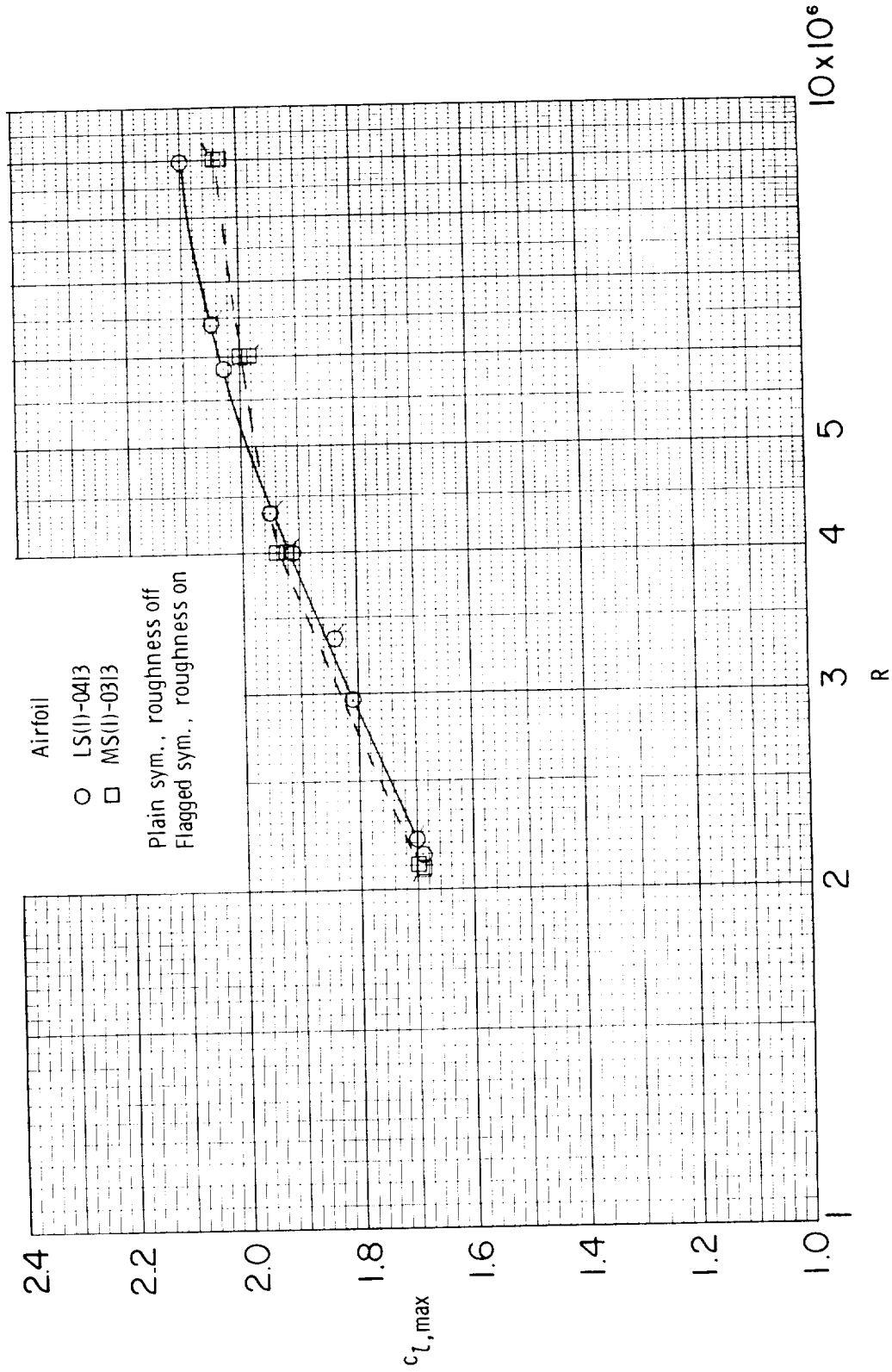


Figure 15.- Variation of maximum lift coefficient with Reynolds number for LS(1)-0413 and MS(1)-0313 airfoils. $M = 0.15$. (Data for LS(1)-0413 airfoil from ref. 3.)

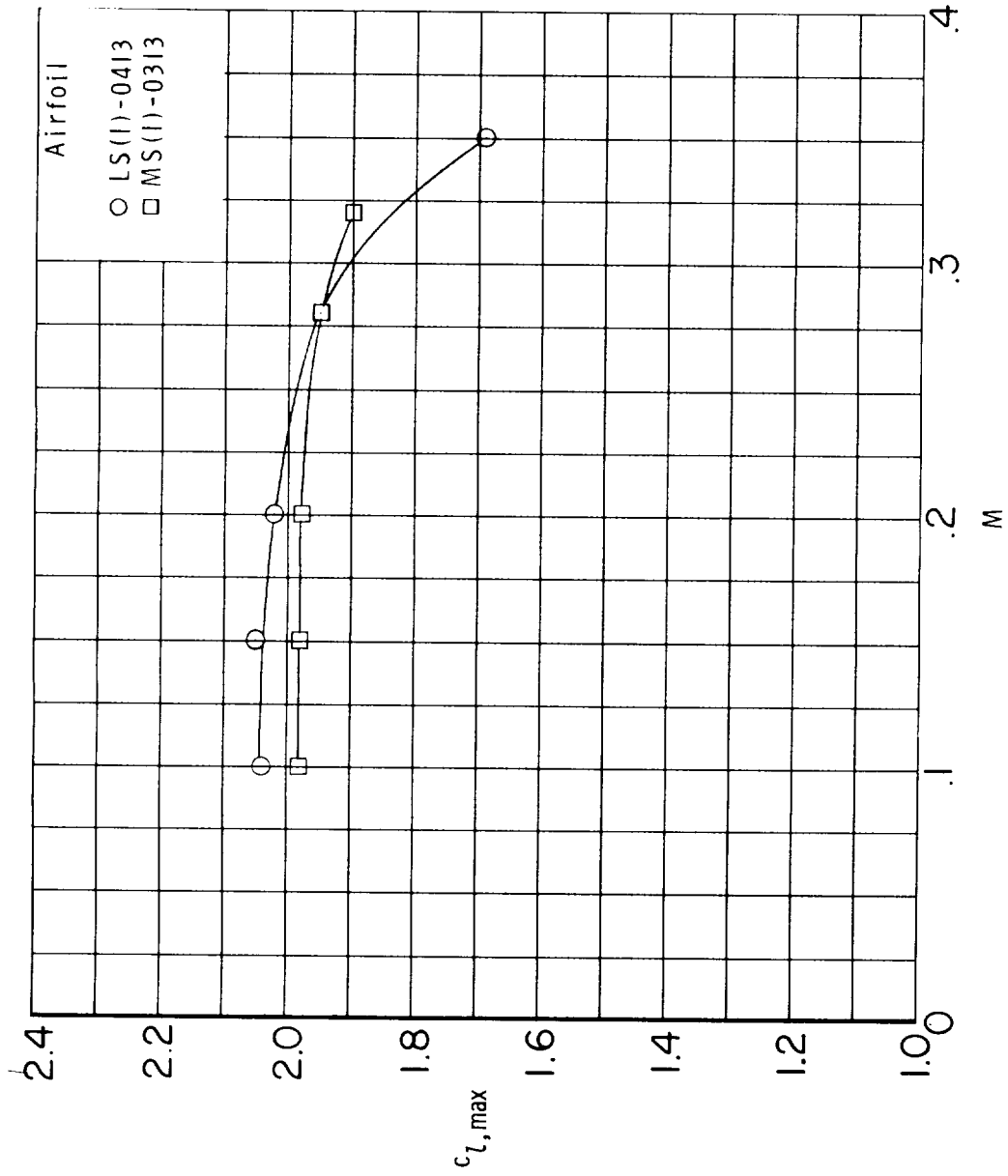


Figure 16.- Variation of maximum lift coefficient with Mach number for LS(1)-0413 and MS(1)-0313 airfoils. Roughness on; $R = 6.0 \times 10^6$. (Data for LS(1)-0413 airfoil from ref. 3.)

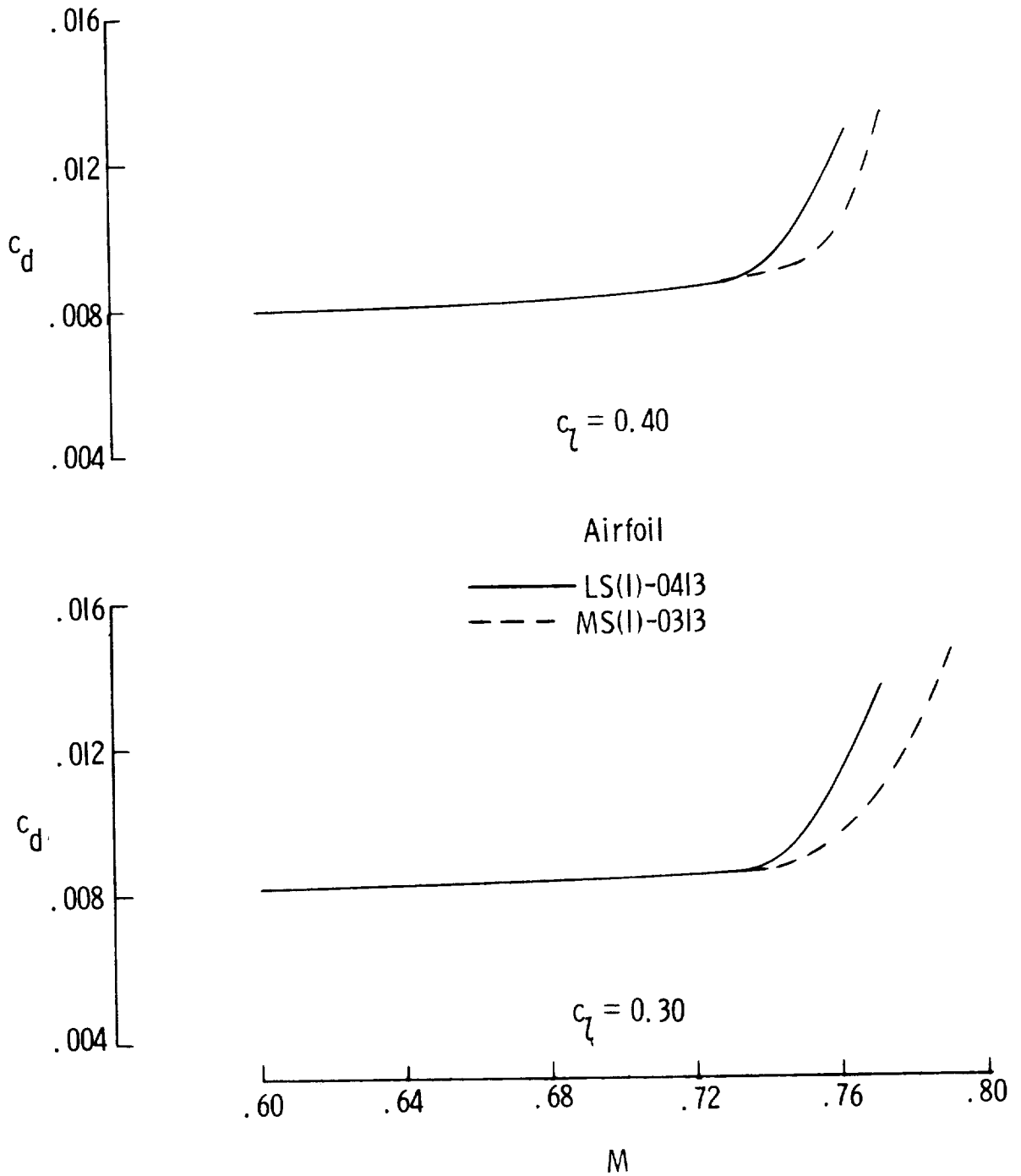


Figure 17.- Calculated drag-rise characteristics for LS(1)-0413 and MS(1)-0313 airfoils. $R = 14.0 \times 10^6$.



1. Report No. NASA TP-1498	2. Government Accession No.	3. Recipient's Catalog No.
4. Title and Subtitle LOW-SPEED AERODYNAMIC CHARACTERISTICS OF A 13-PERCENT-THICK MEDIUM-SPEED AIRFOIL DESIGNED FOR GENERAL AVIATION APPLICATIONS	5. Report Date August 1979	6. Performing Organization Code
	8. Performing Organization Report No. L-12976	10. Work Unit No. 505-06-33-10
7. Author(s) Robert J. McGhee and William D. Beasley	11. Contract or Grant No.	13. Type of Report and Period Covered Technical Paper
9. Performing Organization Name and Address NASA Langley Research Center Hampton, VA 23665	14. Sponsoring Agency Code	
	12. Sponsoring Agency Name and Address National Aeronautics and Space Administration Washington, DC 20546	
15. Supplementary Notes		
16. Abstract Wind-tunnel tests have been conducted to determine the low-speed two-dimensional aerodynamic characteristics of a 13-percent-thick medium-speed airfoil (MS(1)-0313) designed for general aviation applications. The results were compared with data for the 13-percent-thick low-speed airfoil (LS(1)-0413). The tests were conducted over a Mach number range from 0.10 to 0.32, a chord Reynolds number range from 2.0×10^6 to 12.0×10^6 , and an angle-of-attack range from about -8° to 20° . The objective of retaining good high-lift low-speed characteristics for an airfoil designed to have good medium-speed cruise performance was achieved.		
17. Key Words (Suggested by Author(s)) Low-speed characteristics Medium-speed airfoil Reynolds number effects Mach number effects General aviation aircraft	18. Distribution Statement FEDD Distribution Subject Category 02	
19. Security Classif. (of this report) Unclassified	20. Security Classif. (of this page) Unclassified	21. No. of Pages 76
		22. Price*

Available: NASA's Industrial Application Centers

NASA-Langley, 1979